The role of the volume-regulated anion channel VRAC/LRRC8 in myoblast differentiation

Inaugural-Dissertation

to obtain the academic degree

Doctor rerum naturalium (Dr. rer. nat.)

submitted to the Department of Biology, Chemistry, Pharmacy

of Freie Universität Berlin

by

Lingye Chen

from Guangdong, China

Berlin, 2021

This work was prepared under the supervision of Prof. Dr. Tobias Stauber at the Freie Universität Berlin from October 2016 until December 2020.

1st Reviewer: Prof. Dr. Tobias Stauber, BCP Freie Universität Berlin

2nd Reviewer: Prof. Dr. Sigmar Stricker, BCP Freie Universität Berlin

Date of defense: 15.02.2021

Statutory Declaration

I confirm that I have prepared this dissertation entitled "*The role of the volume-regulated anion channel VRAC/LRRC8 in myoblast differentiation*" independently and without impermissible help. All external sources and resources have been specified and properly cited or acknowledged. This dissertation has not been submitted, accepted, rated as insufficient or rejected in any other doctorate procedure.

Berlin, 2021

Lingye Chen

Preface

Part of this work has been published in:

Lingye Chen, Thorsten M. Becker, Ursula Koch, Tobias Stauber,

The LRRC8/VRAC anion channel facilitates myogenic differentiation of murine myoblasts by promoting membrane hyperpolarization.

J. Biol. Chem., 2019. 294: 14279-14288, doi: 10.1074/jbc.RA119.008840

Lingye Chen, Benjamin König, Tobias Stauber,

LRRC8 channel activation and reduction in cytosolic chloride concentration during early differentiation of C2C12 myoblasts.

Biochem. Biophysic. Res. Commun., 2020. 532: 482-488,

doi: 10.1016/j.bbrc.2020.08.080

Electrophysiological measurements shown in this thesis were performed by Dr. Thorsten M. Becker from the AG Koch, BCP Freie Universität Berlin.

Contents

List of Figures

List of Tables

List of Abbreviations

ANOVA	analysis of variance
ARS	Alizarin red S
ATP	adenosine triphosphate
AVD	apoptotic volume decrease
BMP-2	bone morphogenetic protein-2
C3	three-fold rotational symmetry
C6	six-fold rotational symmetry
CaMK	Ca^{2+}-calmodulin-dependent kinase
CaCC	Ca^{2+}-activated Cl^- channel
$[Ca^{2+}]_i$	intracellular Ca^{2+} concentration
CBX	carbenoxolone
cGAMP	cyclic guanosine monophosphate-adenosine monophosphate
cFRET	corrected FRET
$[Cl^-]_i$	intracellular Cl^- concentration
DCPIB	4-(2-butyl-6,7-dichloro-2-cyclopentyl-indan-1-on-5-yl)oxybutyric acid
$DiBAC_4(3)$	bis-(1,3-dibarbituric acid)trimethine oxanol
DM1	myotonic dystrophy type 1
DPBS	Dulbecco's phosphate-buffered saline
EAAs	excitatory amino acids
EAG	*ether-à-go-go* K^+ channel
ER	endoplasmic reticulum
ERG	*ether-à-go-go* related gene K^+ channel
FRET	fluorescence resonance energy transfer
GFP	green-fluorescent protein
GTP	5'-guanosine-triphosphate
IBMX	3-isobutyl-1-methylxanthine
IP_3Rs	inositol 1,4,5 tris-phosphate receptors

K_v7	voltage-gated potassium channel 7
Kir2.1	inward-rectifying K^+ channel 2.1
LRRC8	leucine-rich repeat-containing 8
LRRs	leucine-rich repeats
MEF2	myocyte enhancer factor 2
MRF4	myogenic regulatory factor 4
Myf5	myogenic factor 5
MyHC	myosin heavy chain
MyoD	myoblast determination protein
NFA	niflumic acid
NFAT	nuclear factor of activated T-cells
NFκB	nuclear factor kappa-light-chain-enhancer of activated B cells
NPPB	5-nitro-2-(3-phenylpropylamino)benzoic acid
PCR	polymerase chain reaction
ORO	oil red O
RFP	red-fluorescent protein
ROI	region of interest
RVD	regulatory volume decrease
S.D.	standard deviation
seFRET	sensitized-emission FRET
siRNA	small interfering ribonucleic acid
SOCE	store-operated Ca^{2+} entry
SPQ	6-methoxy-*N*-(3-sulfopropyl)quinolinium
STIM1	stromal interaction molecule 1
TRPCs	transient receptor potential canonical channels
VGCC	voltage-gated Ca^{2+} channel
VRAC	volume-regulated anion channel
VSOAC	volume-stimulated organic osmolyte and anion channel
VSOR	volume expansion-sensing outwardly rectifying anion channel
YFP	yellow-fluorescent protein

Abstract

Myoblast differentiation and fusion are essential for the formation of multinucleated myofibers during skeletal muscle development and regeneration. An elaborate signaling network, including the action of various ion channels and transporters, is involved in myogenesis. Multiple studies have demonstrated the roles of K^+ and Ca^{2+} channels in skeletal myogenesis, but the involvement of Cl^- channels is poorly understood. In this thesis, I determine that the volume-regulated anion channel (VRAC)/leucine-rich repeat containing family 8 (LRRC8) promotes mouse myoblast differentiation.

Immunoblotting showed the expression of all five LRRC8 subunits of heteromeric VRAC during myotube formation of murine C2C12 myoblasts. siRNA-mediated knockdown of the essential VRAC subunit LRRC8A did not affect myoblast proliferation but significantly reduced the expression of the myogenic transcription factor myogenin and inhibited myoblast fusion. Suppression of VRAC activity by either pharmacological VRAC inhibitors or overexpression of LRRC8A also effectively reduced myoblast differentiation and fusion. VRAC inhibition blocked plasma membrane hyperpolarization of myoblasts early during differentiation and prevented the steady-state increase of intracellular Ca^{2+} levels that normally occurs during myogenesis. Consistently, I could show temporary activation of VRAC within the first 2 h of myoblast differentiation by a non-invasive FRET-based sensor, demonstrating that VRAC acts upstream of K^+ channel activation. Myoblast differentiation resulted in a significant decrease in intracellular Cl^- that was abolished by the VRAC inhibitor carbenoxolone. However, as judged by the expression of myogenin in C2C12 cells, lowering the cytosolic Cl^- level by extracellular Cl^- depletion did not enhance differentiation. Instead, it suppressed myosin expression and myotube formation.

This work provides a possible mechanism for the thinning of skeletal muscle bundles observed in LRRC8A-deficient mice and emphasizes the importance of volume-regulated LRRC8 anion channels in cell differentiation.

Zusammenfassung

Die Differenzierung und Fusion von Myoblasten ist für die Bildung mehrkerniger Myofasern während der Entwicklung und Regeneration der Skelettmuskulatur wesentlich. Ein ausgeklügeltes Signalnetzwerk, einschließlich der Wirkung verschiedener Ionenkanäle und Transporter, ist an der Myogenese beteiligt. Mehrere Studien haben die Rolle von K^+- und Ca^{2+}-Kanälen bei der Skelettmyogenese gezeigt, aber die Beteiligung von Cl^--Kanälen ist kaum bekannt. In dieser Arbeit stelle ich fest, dass der volumenregulierte Anionenkanal (VRAC) / Leucin-reiche Wiederholung, der Familie 8 (LRRC8) enthält, die Differenzierung von Maus-Myoblasten fördert.

Immunblotting zeigte die Expression aller fünf LRRC8-Untereinheiten von heteromerem VRAC während der Myotubebildung von murinen C2C12-Myoblasten. siRNA-vermittelter Abbau der essentiellen VRAC-Untereinheit LRRC8A beeinflusste die Myoblastenproliferation nicht, reduzierte jedoch die Expression des myogenen Transkriptionsfaktors Myogenin signifikant und inhibierte die Myoblastenfusion. Die Unterdrückung der VRAC-Aktivität durch entweder pharmakologische VRAC-Inhibitoren oder die Überexpression von LRRC8A reduzierte auch wirksam die Differenzierung und Fusion von Myoblasten. Die VRAC-Hemmung blockierte die Plasmamembran-Hyperpolarisation von Myoblasten früh während der Differenzierung und verhinderte den stationären Anstieg der intrazellulären Ca^{2+}-Spiegel, der normalerweise während der Myogenese auftritt. Konsistent konnte ich eine vorübergehende Aktivierung von VRAC innerhalb der ersten 2 Stunden nach der Myoblastendifferenzierung durch einen nicht-invasiven FRET-basierten Sensor zeigen, was zeigt, dass VRAC vor der K^+-Kanalaktivierung wirkt. Die Differenzierung von Myoblasten führte zu einer signifikanten Abnahme des intrazellulären Cl^-, das durch den VRAC-Inhibitor Carbenoxolon aufgehoben wurde. Gemessen an der Expression von Myogenin in C2C12-Zellen verbesserte eine Verringerung des cytosolischen Cl^- Spiegels durch extrazelluläre Cl^- Depletion jedoch nicht die Differenzierung. Stattdessen unterdrückte es die Myosinexpression und die Myotubebildung.

Diese Arbeit bietet einen möglichen Mechanismus für die Ausdünnung von Skelettmuskelbündeln, die bei Mäusen mit LRRC8A-Mangel beobachtet wurden, und betont die Bedeutung volumenregulierter LRRC8-Anionenkanäle für die Zelldifferenzierung.

1. Introduction

1.1 Ion channels and transporters in skeletal myogenesis

According to differences in morphology, function, and distribution, vertebrate muscle tissue is divided into three types, namely smooth muscle, cardiac muscle, and skeletal muscle. Skeletal muscle formation occurs during the entire lifespan of vertebrates, including embryonic development, postnatal growth and damage repair in the adult (Bentzinger *et al*, 2012; Chal & Pourquié, 2017). The transcriptional mechanisms controlling skeletal muscle development have been studied extensively (Figure 1.1). Among these, the muscle-specific transcription factor myogenin is essential for terminal differentiation of myogenic precursor cells (myoblasts) (Bentzinger *et al.*, 2012; Braun & Gautel, 2011; Buckingham & Rigby, 2014; Chal & Pourquié, 2017; Kang & Krauss, 2010). Myogenin belongs to the basic helix-loop-helix (bHLH) myogenic transcription factor family, which also includes myoblast determination protein (MyoD), myogenic factor 5 (Myf5) and myogenic regulatory factor 4 (MRF4) (Bentzinger *et al.*, 2012; Braun & Gautel, 2011). Myogenesis is generally described to begin with cell cycle withdrawal, followed by myogenin expression and subsequent fusion (Figure 1.1) (Sampath *et al*, 2018; Walsh & Perlman, 1997). Until recently, two muscle-specific fusion factors, Myomaker (Millay *et al*, 2013) and Myomerger–Minion–Myomixer (Bi *et al*, 2017; Quinn *et al*, 2017; Zhang *et al*, 2017a), have been found to govern the fusion of differentiated mononucleated myoblasts (myocytes) either with each other to create new myotubes or with existing multinucleated myotubes (Sampath *et al.*, 2018).

Skeletal myogenesis also involves a complex regulatory system of proteins and signaling molecules (Hindi *et al*, 2013). Myotube formation starts with plasma membrane hyperpolarization of myoblasts, followed by a series of cytosolic Ca^{2+} signals (Figure 1.2) (Fennelly & Soker, 2019; Konig *et al*, 2006). These processes occur through the action of ion transport proteins, such as Kir2.1 K^+ channels and voltage-gated T-type Ca^{2+} channels (Bernheim & Bader, 2002; Fennelly & Soker, 2019).

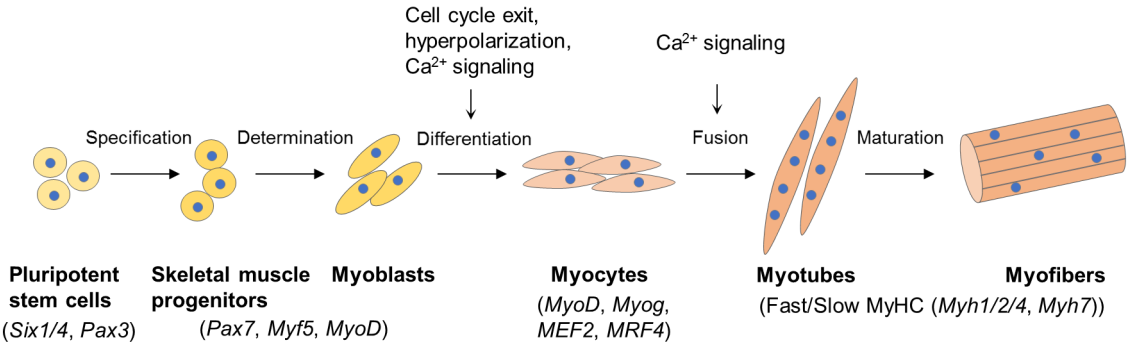

Figure 1.1: Schematic diagram of the development of pluripotent stem cells into skeletal muscle. From left to right, the intermediate cell types and their marker genes are noted along the bottom. *Myog*, myogenin. Major molecular mechanisms recruiting the action of ion channels and transporters during myoblast differentiation and fusion are depicted along the top.

1.1.1 Membrane hyperpolarization

Hyperpolarization of the resting membrane potential is a prerequisite for myoblast differentiation. Primary muscle progenitor cells derived from single satellite cells maintain their stem cell identity rather than express transcription factors of terminal differentiation when hyperpolarization is impaired with high external K^+ or sodium-potassium pump inhibitor ouabain (Fennelly *et al*, 2016; Konig *et al.*, 2006; Konig *et al*, 2004). More specifically, when human myoblasts are induced to differentiate, the activation of an *ether-à-go-go* (EAG) K^+ channel rapidly hyperpolarizes myoblasts from as low as approximately –8 mV to approximately –32 mV (Bernheim *et al*, 1996; Bijlenga *et al*, 1998; Liu *et al*, 1998). Shortly thereafter, the resting membrane potential of myoblasts drops further to approximately –74 mV, due to the activation of the inward-rectifying K^+ channel Kir2.1 (Fischer-Lougheed *et al*, 2001; Liu *et al.*, 1998; Liu *et al*, 2003). The human EAG K^+ current density is low in proliferating myoblasts, increases in fusion-competent myoblasts and declines in myotubes (Liu *et al.*, 1998). By contrast, the Kir2.1 current has been found to be expressed in 40-50% of differentiating myoblasts and in all myotubes (Konig *et al.*, 2004; Liu *et al.*, 1998). Notably, Kir2.1 channels that are already present at the plasma membrane during human myoblast proliferation (Fischer-Lougheed *et al.*, 2001) are activated by dephosphorylation of Kir2.1 at tyrosine 242 within the first 6 hours of differentiation, which is several hours earlier than the expression of two myogenic transcription factors, myogenin and myocyte enhancer factor

2 (MEF2) (Hinard *et al*, 2008; Konig *et al.*, 2004). Thus, plasma membrane hyperpolarization is considered to be the earliest detectable event during myoblast differentiation.

In addition to these contributors of hyperpolarization, *ether-à-go-go* related gene (ERG) K^+ channels (Liu *et al.*, 2003) and store-operated Ca^{2+} entry (SOCE) channels (Darbellay *et al*, 2009) have been shown to regulate the resting membrane potential of fusion-competent myoblasts. Inhibition of the human ERG K^+ channel activity depolarized myoblasts by approximately 10 mV (Liu *et al.*, 2003), whereas knockdown of stromal interaction molecule 1 (STIM1) or Orai1 reduced SOCE amplitude, impaired hyperpolarization and consequently inhibited myoblast differentiation (Darbellay *et al.*, 2009). Furthermore, it has been reported that by activating the intermediate-conductance Ca^{2+}-activated K^+ channel (IK_{Ca}), extracellular 5'-guanosine-triphosphate (GTP) hyperpolarizes C2C12 (a mouse skeletal muscle myoblast cell line) cells from a mean value of −15 mV to approximately −75 mV and increases myosin heavy chain (MyHC) expression (Fioretti *et al*, 2005; Pietrangelo *et al*, 2006; Tanaka *et al*, 2017).

1.1.2 Ca^{2+} signals during myoblast differentiation and fusion

Ca^{2+} acts as an intracellular second messenger, triggering responses in various cell types in response to extracellular stimuli. A good example comes from skeletal muscle, where Ca^{2+} signaling plays a fundamental role in many cellular processes from cell growth to muscle fiber excitation-contraction coupling and metabolism (Choi *et al*, 2020; Stiber & Rosenberg, 2011; Tu *et al*, 2016). In terms of skeletal myogenesis, a cytoplasmic free Ca^{2+} increase is essential for the expression of myogenic transcription factors and the formation of normal-sized myotubes (Bijlenga *et al*, 2000; Constantin *et al*, 1996; Konig *et al.*, 2006; Przybylski *et al*, 1989; Przybylski *et al*, 1994). More specifically, the hyperpolarization of human myoblasts induced by the sequential activation of EAG and Kir2.1 triggers a small but sustained influx of Ca^{2+} through α1H T-type voltage-gated Ca^{2+} channels (VGCCs), sufficient to cause a significant increase in resting intracellular Ca^{2+} concentration (Bijlenga *et al.*, 2000; Liu *et al.*, 2003). This cytosolic Ca^{2+} signal

activates the calcineurin/NFAT pathway, thereby inducing the expression of myogenin and MEF2 (Konig *et al.*, 2006). Another well-known Ca^{2+}-dependent pathway, Ca^{2+}-calmodulin-dependent kinase (CaMK), is required for intact myogenin expression (Xu *et al*, 2002) but does not link to Kir2.1-induced hyperpolarization (Konig *et al.*, 2006). Interestingly, a 10-mV depolarization of the resting potential increased the T-type Ca^{2+} current and raised the intracellular free Ca^{2+} concentration, thus triggering a ten-fold acceleration of human myoblast fusion (Liu *et al.*, 2003). However, the involvement of T-type VGCCs as a primary Ca^{2+} entry mechanism in myoblast differentiation seems to be species-dependent, as it was shown that L-type rather than T-type Ca^{2+} currents can regulate the expression of myogenin and MyHC in C2C12 cells (Bidaud *et al*, 2006; Porter *et al*, 2002). A link between L-type VGCCs and calcineurin activity has also been suggested (Spangenburg *et al*, 2004).

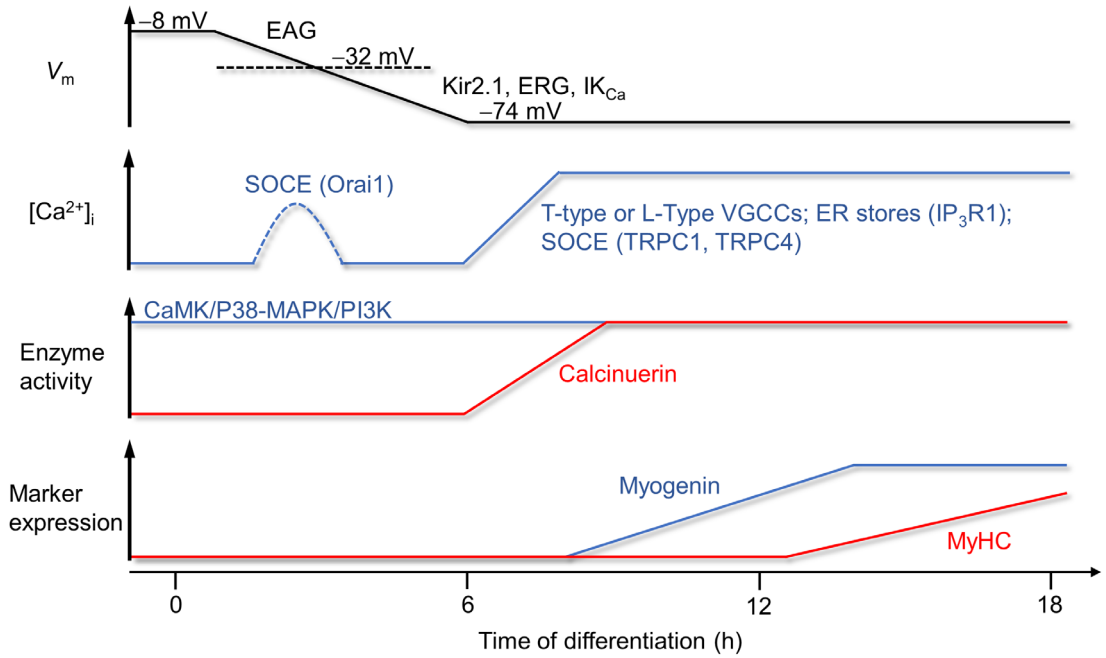

Figure 1.2: Chronological illustration of the roles of membrane hyperpolarization and Ca^{2+} signals during myoblast differentiation. The expression profile of ion channels and transporters involved at different stages of differentiation is depicted. IK_{Ca}, intermediate-conductance Ca^{2+}-activated K^+ channels; MAPK, mitogen-activated protein kinase; PI3K, phosphoinositide 3-kinase. Figure modified from (Konig *et al.*, 2006).

Another Ca^{2+} source of intracellular Ca^{2+} elevation upon myoblast differentiation is Ca^{2+} release from the endoplasmic reticulum (ER) through inositol 1,4,5 tris-phosphate receptors (IP_3Rs), followed by Ca^{2+} entry through SOCE channels (Araya *et al*, 2004; Arnaudeau *et al*, 2006; Nakanishi *et al*, 2015; Seigneurin-Venin *et al*, 1996). Knockdown of IP_3R1 in human myoblasts impaired both endogenous spontaneous Ca^{2+} oscillations and SOCE, which in turn greatly reduced the activity of two key enzymes of muscle differentiation, calcineurin and CamKII (Antigny *et al*, 2014). In contrast, the overexpression of IP_3R1 not only rescued normal differentiation of IP_3R1-silenced myoblasts, but also increased the percentage of MEF2-positive nuclei after one day of differentiation (Antigny *et al.*, 2014). Upon Ca^{2+} store depletion, STIM1 (an ER Ca^{2+} sensor) forms cluster and triggers a Ca^{2+} influx (also called SOCE) through SOCE-mediating channels located at the ER-plasma membrane junction, thereby efficiently restoring the ER Ca^{2+} content (Jousset *et al*, 2007; Luik *et al*, 2006; Wu *et al*, 2006). SOCE-mediating channels are divided into two groups (Choi *et al.*, 2020): Orai channels (Luik *et al.*, 2006; Xu *et al*, 2006) and transient receptor potential canonical channels (TRPCs) (López *et al*, 2006; Yuan *et al*, 2007). The important roles of STIM1 (Darbellay *et al*, 2010; Darbellay *et al.*, 2009; Li *et al*, 2012; Stiber *et al*, 2008), Orai1 (Darbellay *et al.*, 2009; Wei-Lapierre *et al*, 2013), TRPC1 (Formigli *et al*, 2009; Louis *et al*, 2008; Meacci *et al*, 2010; Zanou *et al*, 2012), and TRPC4 (Antigny *et al*, 2013; Antigny *et al*, 2017) during myogenesis in mouse and human have been established. Silencing any of them reduced SOCE and myoblast differentiation, whereas forced expression of STIM1 with Orai1, TRPC1 or TRPC4 in human myoblasts increased SOCE, accelerated myoblast fusion, and produced hypertrophic myotubes (Antigny *et al.*, 2013; Darbellay *et al.*, 2009).

Furthermore, the *N*-methyl-*D*-aspartate (NMDA) receptor, a subtype of ionotropic glutamate receptor, was shown to mediate Ca^{2+} influx and promote C2C12 myoblast fusion (Lee *et al*, 2004). It is worth recalling that the graded Ca^{2+} signal involved in skeletal muscle formation depends on Ca^{2+} release from intracellular stores as well as on Ca^{2+} influx from extracellular medium (Arnaudeau *et al.*, 2006; Liu *et al.*, 2003). However, all these Ca^{2+} signals are inhibited when the hyperpolarization process that

increases the driving force for Ca^{2+} is blocked (Constantin *et al.*, 1996; Konig *et al.*, 2006; Pietrangelo *et al.*, 2006).

1.1.3 Further molecular mechanisms of myogenesis

The failure of myoblasts to exit the cell cycle leads to defective myotube formation (Timchenko *et al*, 2001; Walsh & Perlman, 1997). It has been shown that blocking the Ca^{2+}- and voltage-dependent K^+ channel KCa1.1 in human primary myoblasts induces increased levels of cytosolic Ca^{2+} and of active NFκB, resulting in enhanced proliferation and reduced fusion (Tajhya *et al*, 2016). Interestingly, KCa1.1 expression in myotonic dystrophy type 1 (DM1) (Meola & Cardani, 2015) myoblasts was found to be significantly decreased, whereas introducing functional KCa1.1 α-subunits into DM1 myoblasts reduced their proliferation to normal levels and rescued expression of MEF2 and myogenin (Tajhya *et al.*, 2016). Similarly, constitutive overexpression of the chloride intracellular channel 5 (CLIC5) partly shifted C2C12 cells from G2/M phase to G0/G1 phase, resulting in decreased cell proliferation and increased expression levels of myogenin and MyHC (Li *et al*, 2010). Activation of K_v7 channels in C2C12 myoblasts reduced proliferation and stimulated differentiation (Iannotti *et al*, 2010). In particular, it was reported that the endocannabinoid 2-arachidonoylglycerol inhibits skeletal muscle differentiation via cannabinoid type 1 receptor-mediated inhibition of $K_v7.4$ channels (Iannotti *et al*, 2014). Knockdown of $K_v7.4$ reduced the expression levels of several differentiation markers, but overexpression of $K_v7.4$ did not enhance myoblast differentiation (Iannotti *et al*, 2013).

Inhibition of mechanosensitive (or stretch-activated) cation channels by pharmacological blockers leads to impaired phenotypic maturation of C2C12 myoblasts, including reduced expression of sarcomeric proteins and MyHC and decreased creatine kinase activity (Formigli *et al*, 2007; Wedhas *et al*, 2005), with contradicting findings on the inhibitory effect on myogenin expression. Several further ion transport proteins have been implicated in skeletal myogenesis, including TRPC3 (Woo *et al*, 2010), Pannexin1 and Pannexin3 (Langlois *et al*, 2014), connexin43 (Araya *et al*, 2005; Araya *et al*, 2003;

Meacci *et al.*, 2010), two-pore domain potassium channels TASK2 and TREK1 (Afzali *et al*, 2016), nicotinic acetylcholine receptors (Constantin *et al.*, 1996; Krause *et al*, 1995), transient receptor potential vanilloid 1 (Kurosaka *et al*, 2016; Obi *et al*, 2019) and Na^+-K^+-$2Cl^-$ cotransporter 1 (Mandai *et al*, 2017). However, the specific working mechanism of these proteins has not been elucidated yet.

1.2 The volume-regulated anion channel (VRAC)

Vertebrate cells adjust their volume in response to external osmolarity changes or during the execution of various cellular functions (Hoffmann *et al*, 2009). Cell volume regulation usually involves the transport of Cl^-, K^+, Na^+ and small organic osmolytes, which is carried out by various ion channels and transporters in the plasma membrane (Hoffmann *et al.*, 2009; Jentsch, 2016). Osmotic gradients generated from this process subsequently drive water in and out of cells. Specifically, the volume-regulated anion channel (VRAC) opens upon osmotic cell swelling and facilitates regulatory volume decrease (RVD) by mediating the efflux of Cl^- and organic substances (Chen *et al*, 2019b; Jentsch, 2016; Jentsch *et al*, 2016; Osei-Owusu *et al*, 2018; Pedersen *et al*, 2015; Pedersen *et al*, 2016; Stauber, 2015; Strange *et al*, 2019). VRAC-mediated Cl^- currents were first reported in the 1980s (Grinstein *et al*, 1982; Hazama & Okada, 1988; Hoffmann *et al*, 1984). Since then, the biophysical properties and cell physiology of VRAC have been extensively studied (Nilius *et al*, 1997; Okada, 1997; Okada *et al*, 2009; Pedersen *et al.*, 2015). The channel was also referred to as VSOR (the volume expansion-sensing outwardly rectifying anion channel) (Okada, 1997) or VSOAC (the volume-stimulated organic osmolyte and anion channel) (Jackson *et al*, 1994). Many molecular candidates, including P-glycoprotein, pI_{Cln}, and ClC-3, were proposed to form VRAC, but all were disproved (Okada, 1997; Pedersen *et al.*, 2015). In 2014, two independent studies simultaneously identified leucine-rich repeat-containing 8A (LRRC8A) as an essential component of VRAC (Qiu *et al*, 2014; Voss *et al*, 2014).

1.2.1 LRRC8 proteins and VRAC structure

VRAC is a heteromeric channel formed by LRRC8 family proteins, which consist of five members, LRRC8A-E (Abascal & Zardoya, 2012; Kubota *et al*, 2004). LRRC8A is the only obligatory subunit (Qiu *et al.*, 2014; Voss *et al.*, 2014) and requires conjugation with at least one other LRRC8 isoform (LRRC8B, C, D or E) to reconstitute physiological VRAC activity (Voss *et al.*, 2014). Whereas LRRC8A is targeted to the plasma membrane both in native cells and when overexpressed on its own (Qiu *et al.*, 2014; Voss *et al.*, 2014), LRRC8B-LRRC8E must be co-expressed with LRRC8A to reach the plasma membrane (Voss *et al.*, 2014). However, heterologous co-expression of LRRC8 proteins did not significantly increase VRAC currents above endogenous levels (Voss *et al.*, 2014). Conversely, overexpression of LRRC8A alone was found to suppress endogenous VRAC currents, which may be due to a stoichiometric imbalance in the heteromeric channel (Qiu *et al.*, 2014; Voss *et al.*, 2014).

The LRRC8 paralogs consist of approximately 800 amino acid residues, with an average sequence similarity of 45.92% and a molecular weight of approximately 95 kDa (Abascal & Zardoya, 2012; Kubota *et al.*, 2004). Four groups recently described the structure of LRRC8A homomeric complex determined by cryo-electron microscopy (Deneka *et al*, 2018; Kasuya *et al*, 2018; Kefauver *et al*, 2018; Kern *et al*, 2019). As shown in Figure 1.3*A*, LRRC8A comprises four transmembrane domains, with its N- and C-termini located in the cytoplasm. The cytosolic amino terminal stretch is 23 amino acids long and it seems to have essentially no fixed structure (Deneka *et al.*, 2018; Kasuya *et al.*, 2018; Kefauver *et al.*, 2018) except for a short N-terminal coil that protrudes into the channel pore (Kefauver *et al.*, 2018). The carboxyl terminal half contains 15-16 leucine-rich repeats (LRRs), forming a crescent-shaped structure common to many LRR-containing proteins (Abascal & Zardoya, 2012; Bella *et al*, 2008).

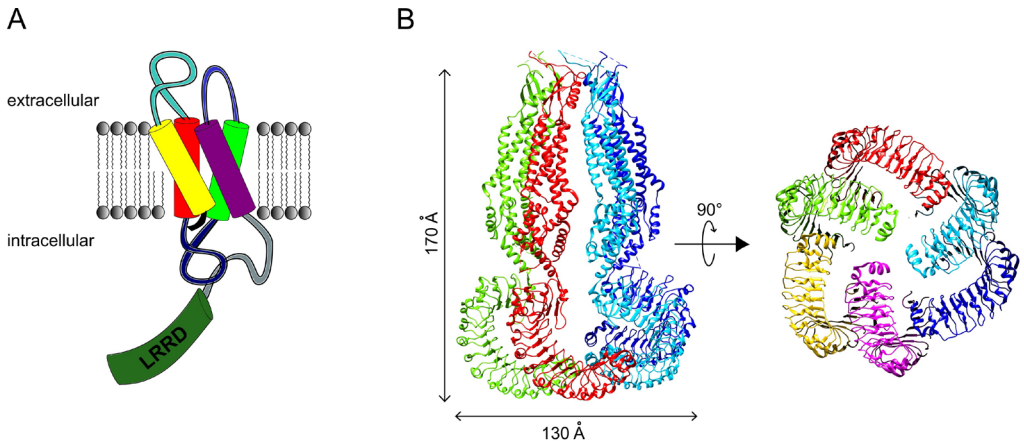

Figure 1.3: Structure of VRAC. ***A***, Schematic diagram of the structure of a single LRRC8 subunit within a hexamer. ***B***, Ribbon representation of the hexameric LRRC8A channel structure (PDB 5ZSU (Kasuya *et al.*, 2018)) viewed from within the plasma membrane (two subunits in the back not shown for clarity, left) and from the intracellular side (right). Loop regions of unsolved structure are depicted as dashed lines. Figure from (Chen *et al.*, 2019b).

LRRC8A homomers, although not exhibiting normal VRAC properties (Deneka *et al.*, 2018; Kasuya *et al.*, 2018; Kefauver *et al.*, 2018; Syeda *et al*, 2016), show a pore-forming hexameric structure (Figure 1.3*B*). Importantly, the hexameric structure was also observed for LRRC8A/C heteromers (Deneka *et al.*, 2018), which confirms that VRACs share topology and channel structure with pannexins/innexins and connexins (Abascal & Zardoya, 2012). However, the precise arrangement of the six LRRC8 subunits is still a matter of debate. For the extracellular, transmembrane, and intracellular loop regions, three studies described a six-fold rotational symmetry (i.e. C6 symmetry) (Deneka *et al.*, 2018; Kefauver *et al.*, 2018; Kern *et al.*, 2019) while one showed a C3 symmetry (Figure 1.3*B*) (Kasuya *et al.*, 2018). Regarding the LRR regions, both C3 symmetry (a trimer of dimers) (Figure 1.3*B*) (Deneka *et al.*, 2018; Kasuya *et al.*, 2018; Kefauver *et al.*, 2018) and disordered heterogeneous arrangement (Kern *et al.*, 2019) have been proposed. The pore structure of LRRC8A homo-hexamer consists of a central transmembrane domain and two flanking subdomains which protrude from the membrane towards the extracellular and the cytoplasmic side. Hydrophilic and positively charged residues are distributed along the pore (Deneka *et al.*, 2018; Kasuya *et al.*, 2018; Kefauver *et al.*, 2018; Kern *et al.*, 2019). During permeation, the extracellular constriction containing a ring of six positively charged arginine residues, R103, acts as a size and charge selectivity filter

(Deneka *et al.*, 2018; Kefauver *et al.*, 2018; Kern *et al.*, 2019). Notably, the equivalent position (R103) in LRRC8C or LRRC8E is a leucine residue, and in LRRC8D is a phenylalanine residue.

1.2.2 LRRC8 subunit composition and VRAC properties

The biophysical characteristics of VRAC have been described in multiple vertebrate cell types (Akita & Okada, 2014; Nilius *et al.*, 1997; Nilius *et al*, 1994; Strange *et al.*, 2019). Upon extracellular osmolarity reduction, VRAC-mediated currents develop over a few minutes and exhibit moderate outward rectification (larger currents at inside-positive than at inside-negative voltages, and hence the alternative name the volume expansion-sensing outwardly rectifying anion channel, VSOR (Okada, 1997)), with the relative anion selectivity as follow: $I^- > NO_3^- > Br^- > Cl^- > F^-$. In addition, VRAC exhibits channel inactivation at high positive voltages (currents decrease with time at a constant voltage).

Importantly, differences in the LRRC8 subunit composition give rise to the variability of functional VRAC properties (Jentsch, 2016; Strange *et al.*, 2019; Syeda *et al.*, 2016; Voss *et al.*, 2014). For instance, constitutive currents of LRRC8A/E heteromers were dramatically potentiated by intracellular oxidizing agents, while that of LRRC8A/C and LRRC8A/D were inhibited by oxidation (Gradogna *et al*, 2017b). On the other hand, LRRC8A/E heteromers exhibit faster inactivation at less positive membrane potentials than LRRC8A/C and LRRC8A/D (Lutter *et al*, 2017; Voss *et al.*, 2014). Moreover, LRRC8D increases the permeability of cells to all organic substrates such as glutamate, *myo*-inositol, taurine, and γ-aminobutyric acid (Gaitán-Peñas *et al*, 2016; Lutter *et al.*, 2017; Schober *et al*, 2017), which probably explains the existence of VRACs as "VSOACs" (volume-stimulated organic osmolyte and anion channels) (Jackson *et al.*, 1994). LRRC8D was also crucial for the transport of the anticancer drug cisplatin (Planells-Cases *et al*, 2015) and the antibiotic blasticidin (Lee *et al*, 2014). Interestingly, the increased permeability of LRRC8A/D heteromers to large organic solutes may be due to the bulky phenylalanine residue in LRRC8D that may widen the channel pore (Deneka *et al.*, 2018). LRRC8E rather specifically makes VRAC more permeable to negatively

charged glutamate and aspartate (Lutter *et al.*, 2017) and cyclic dinucleotide 2'3'-cGAMP (Zhou *et al*, 2020). These observations strongly suggest that cell- and tissue-specific LRRC8 subunit composition correlates with the physiological roles of VRAC in these tissues (Gradogna *et al.*, 2017b; Stuhlmann *et al*, 2018; Voss *et al.*, 2014).

The mechanism by which cell swelling activates VRAC remains obscure. A widely studied but still controversial activation pathway is the reduction of intracellular ionic strength (Best & Brown, 2009; Cannon *et al*, 1998; Emma *et al*, 1997; König *et al*, 2019; Sabirov *et al*, 2000; Syeda *et al.*, 2016; Voets *et al*, 1999; Zhang & Lieberman, 1996). Multiple parameters altered by changes in cell volume have been proposed to activate VRAC, such as membrane tension, alterations in cytoskeleton or plasma membrane domains, and changes in macromolecule crowding (Akita & Okada, 2014; Chen *et al.*, 2019b; Hoffmann *et al.*, 2009; Mongin & Orlov, 2001). Moreover, there are many contradictory reports on the involvement of second-messenger pathways, including kinases and phosphatases (Hoffmann *et al.*, 2009; König *et al.*, 2019; Pedersen *et al.*, 2015). On the other hand, VRAC can be opened iso-volumetrically in various contexts. For instance, VRAC can be activated without cell swelling by pro-apoptotic drugs (involving apoptotic volume decrease) (Gradogna *et al*, 2017a; Ise *et al*, 2005; Planells-Cases *et al.*, 2015; Shimizu *et al*, 2004) in cancer cells, ATP (involving Ca^{2+} signaling and protein phosphorylation events) (Akita *et al*, 2011; Hyzinski-García *et al*, 2014; Rudkouskaya *et al*, 2008; Yang *et al*, 2019) in astrocytes, sphingosine-1-phosphate (Burow *et al*, 2015) in macrophages, and reactive oxygen species generated by the stimulation of certain plasma membrane receptors (Deng *et al*, 2010; Friard *et al*, 2019; Liu *et al*, 2009; Shimizu *et al.*, 2004; Varela *et al*, 2004; Wang *et al*, 2017) in several cell types. Furthermore, VRAC activity was reported to be modulated by diverse G-proteins, G-protein-coupled receptors, phosphatidylinositol-3,4,5-trisphosphate, intracellular ATP levels, Ca^{2+} concentrations, tumor necrosis factor-α, and PI3K-AKT signaling among others (Akita & Okada, 2014; Chen *et al.*, 2019b; Okada *et al*, 2019; Pedersen *et al.*, 2015; Pedersen *et al.*, 2016). As mentioned above, the diverse and confusing data regarding VRAC activation and/or regulation may also be attributed to cell- and tissue-specific LRRC8 subunit composition.

1.2.3 Assessment of VRAC activity

There are several techniques commonly used to study VRAC activation. As the gold standard for evaluating ion channel activity, electrophysiology has been extensively used to measure VRAC currents at the single-channel level or the whole-cell level (Akita & Okada, 2014; Nilius *et al.*, 1997; Nilius *et al.*, 1994; Strange *et al.*, 2019). Generally, there are three main steps to set up a whole-cell patch-clamp configuration (Liem *et al*, 1995). First, approach an isolated cell attached to a coverslip with a polished glass pipette containing an electrode. Second, establish a tight seal with the cell membrane via negative pressure of the pipette solution. Third, rupture the sealed membrane patch by a further suction pulse, thereby establishing electrical access to the cell interior.

Fluorescence resonance energy transfer (FRET) is a physical process in which energy is transferred from an excited fluorophore (the donor) to another molecular fluorophore (the acceptor) in a non-radiative manner (Sekar & Periasamy, 2003). FRET only occurs between closely spaced fluorophores (< 10 nm) and has been used to study various biological phenomena, such as protein-protein interactions and conformational changes of proteins (Bykova *et al*, 2006; Miranda *et al*, 2013; Sekar & Periasamy, 2003; Zachariassen *et al*, 2016). The Stauber lab has recently developed a FRET sensor of C-terminal rearrangement to monitor VRAC activity in living cells (König *et al.*, 2019). The FRET efficiency between fluorophores fused to the C-termini of LRRC8 subunits decreased upon osmotic swelling-induced VRAC activation; and patch-clamp fluorometry further confirmed that FRET changes reflect channel gating (König *et al.*, 2019). This novel optical sensor for VRAC activity has several advantages over electrophysiological methods: 1) it enables subcellular monitoring of VRAC activity; 2) it provides spatio-temporal information about the channels; 3) it is non-invasive and thus allows long-term live-cell experiments (König *et al.*, 2019).

Since VRAC is activated upon osmotic swelling and contributes to subsequent RVD, a direct way to assess its action is to measure cell volume. Various methods have been developed for cell volume measurements (Model, 2018). Currently, Coulter electronic sizing of cell suspensions is considered to be the most reliable method (Model, 2018) and

was used to determine the role of VRAC in RVD (Qiu *et al.*, 2014). The influence of VRAC on RVD was also evaluated by the calcein fluorescence method (Capó-Aponte *et al*, 2005; Planells-Cases *et al.*, 2015; Stuhlmann *et al.*, 2018; Voss *et al.*, 2014), optical bright field cross-sectioning (Kang *et al*, 2018), and flow cytometry (by measuring cell size-dependent light scattering) (Sirianant *et al*, 2016).

The radiotracer assay is usually applied to determine the permeability of VRAC to various organic substances (Hyzinski-García *et al.*, 2014; Lutter *et al.*, 2017; Planells-Cases *et al.*, 2015; Qiu *et al.*, 2014; Schober *et al.*, 2017; Voss *et al.*, 2014; Wilson *et al*, 2019). ^{3}H and ^{14}C are two commonly used radioactive elements. Additionally, the high permeability of VRAC to I^- was exploited in the determination of its molecular correlate (the LRRC8 protein family) (Qiu *et al.*, 2014; Voss *et al.*, 2014). The application of high extracellular I^- causes I^- to flow into cells expressing the halide-sensitive yellow-fluorescent protein (YFP) (Galietta *et al*, 2001) through activated VRAC, thereby quenching the fluorescence of YFP (Ghosh *et al*, 2017; Planells-Cases *et al.*, 2015; Qiu *et al.*, 2014; Voss *et al.*, 2014). Furthermore, cellular uptake of the anticancer drug cisplatin through VRAC can be measured by inductively coupled plasma mass spectrometry (ICP-MS) (Brouwers *et al*, 2006; Planells-Cases *et al.*, 2015).

1.2.4 Physiological roles of VRAC in volume regulation and beyond

Generally, VRAC can fulfill its proposed functions by three distinct basic mechanisms (Figure 1.4) (Chen *et al.*, 2019b). First of all, VRAC is a well-known key player in RVD by its extrusion of Cl^- and osmolytes (Hoffmann *et al.*, 2009; Jentsch, 2016). Consistently, RVD was strongly reduced in HeLa cells (Qiu *et al.*, 2014) and astrocytes (Formaggio *et al*, 2019) upon knockdown of the essential VRAC subunit LRRC8A and a complete loss of RVD was seen in *LRRC8A*$^{-/-}$ or *LRRC8(B/C/D/E)*$^{-/-}$ HEK cells (Planells-Cases *et al.*, 2015; Voss *et al.*, 2014).

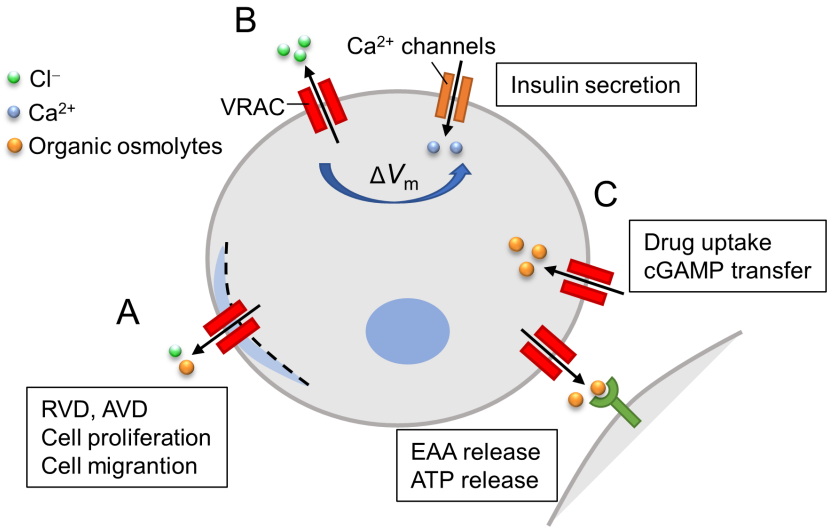

Figure 1.4: Schematic overview of three distinct mechanisms by which VRAC can exert its proposed physiological tasks. ***A***, The release of chloride and organic osmolytes leads to osmotic efflux of water, resulting in a volume decrease. ***B***, Opening of VRAC shifts the plasma membrane potential (V_m) towards the equilibrium potential of chloride, affecting the activity of other ion channels. ***C***, Substances conducted by VRAC can act as signaling molecules. Figure modified from (Chen *et al.*, 2019b).

During spermatogenesis, male germ cells encounter large alterations in extracellular osmolarity from ~350 mOsm in the seminiferous tubules to ~290 mOsm in the rete testis, and finally up to ~410 mOsm in the cauda epididymis (Cooper *et al*, 2004; Petrunkina *et al*, 2004; Yeung *et al*, 2006). Therefore, the ability of male germ cells to maintain a near-constant cell volume is particularly important for their proper development and maturation (Yeung *et al.*, 2006). Indeed, the spontaneous mouse mutant *ébouriffé* (Lalouette *et al*, 1996), which was found to carry a mutation that truncates the C-terminal LRRs of LRRC8A and markedly diminishes VRAC activity (Platt *et al*, 2017), and mice lacking LRRC8A specifically in germ cells both exhibit abnormal sperm development and male infertility (Bao *et al*, 2018; Lück *et al*, 2018). Consistent with impaired volume regulation, late-stage spermatids (in testis) from these mice present round, swollen cytoplasm. Further developed spermatozoa (in epididymis) display enlarged cytoplasm, disorganized mitochondrial sheaths, and flagellar coiling, resulting in reduced motility (Bao *et al.*, 2018; Lück *et al.*, 2018). Additionally, a heterozygous R545H missense point mutation in LRRC8A was identified in a male patient with fertility disorder termed Sertoli cell-only syndrome (Bao *et al.*, 2018). However, when co-expressed with LRRC8C or

LRRC8D in *Xenopus* oocytes, the mutation only decreased VRAC currents by 25-30% (Bao *et al.*, 2018), while heterozygous *Lrrc8a*$^{+/-}$ mice showed normal fertility (Kumar *et al*, 2014). Therefore, it is still doubtful whether the mutation causes infertility.

A hallmark of programmed cell death is the reduction of cellular volume (apoptotic volume decrease, AVD) (Bortner & Cidlowski, 1998; Lang & Hoffmann, 2012). Similar to RVD, VRAC was proposed to be involved in AVD (Akita & Okada, 2014; Kunzelmann, 2016; Okada *et al*, 2006). As noted earlier, apoptosis inducers such as staurosporine and Fas ligand (Okada *et al.*, 2006; Planells-Cases *et al.*, 2015; Shimizu *et al.*, 2004) or platinum-based anticancer drugs such as cisplatin (Gradogna *et al.*, 2017a; Ise *et al.*, 2005; Planells-Cases *et al.*, 2015) can induce VRAC currents independent of cell swelling. Disruption of LRRC8A in HCT116 cells suppressed cisplatin- or staurosporine-induced transport of anion and taurine and activation of caspase-3 (Planells-Cases *et al.*, 2015). It is notable that LRRC8A and LRRC8D were identified in a genome-wide screen for carboplatin resistance (Planells-Cases *et al.*, 2015). Disruption of LRRC8A or LRRC8D strongly reduced cellular uptake of cisplatin and carboplatin under isotonic conditions, whereas cell swelling enhanced LRRC8 subunit-dependent cisplatin uptake (Planells-Cases *et al.*, 2015). Importantly, low expression of LRRC8D correlated with a significant reduction in the survival rate of ovarian cancer patients treated with platinum-based drugs (Planells-Cases *et al.*, 2015). Thus, it has been suggested that VRAC contributes to cellular drug response by both mediating cisplatin uptake and promoting AVD-dependent apoptosis.

VRAC has also been implicated in cell proliferation and migration, fundamental physiological processes that are directly related to cell volume regulation (Hoffmann *et al.*, 2009; Schwab *et al*, 2012; Stroka *et al*, 2014). Various non-specific blockers of VRAC were reported to inhibit the proliferation and migration of diverse cell types (Klausen *et al*, 2007; Liang *et al*, 2014; Nilius *et al.*, 1997; Wondergem *et al*, 2001; Wong *et al*, 2018; Xue *et al*, 2018). However, LRRC8A deficiency did not affect normal proliferation or migration of HeLa cells (Sirianant *et al.*, 2016), vascular smooth muscle cells (Choi *et al*, 2016), C2C12 myoblasts and HCT116 cells (Liu & Stauber, 2019). siRNA against LRRC8A was reported to inhibit proliferation of glioblastoma cells in one study (Rubino

et al, 2018) but not in another (Liu & Stauber, 2019). On the other hand, knockdown of LRRC8A was shown to suppress the growth and metastasis of hepatocellular carcinoma cells (Lu *et al*, 2019) and the tumorigenesis of human colon cancer HCT116 cells (Zhang *et al*, 2018) *in vivo*. Overall, the role of VRAC in cell proliferation and migration is at present questionable.

As mentioned above, VRAC can be activated under isovolumetric conditions and is permeable not only to Cl^- but also to various organic osmolytes, for which the central nervous system provides good examples (Akita & Okada, 2014; Elorza-Vidal *et al*, 2019; Mongin, 2016). During normal brain functioning, astrocytes release excitatory amino acids (EAAs), such as glutamate, and regulate astrocyte-neuron communication, including neuronal excitability, synaptic transmission and plasticity. However, excessive release of EAAs from swollen astrocytes during ischemic brain injury leads to excitotoxic neuronal death. VRAC has long been suggested as a major pathway for EAA release in the brain based on non-specific pharmacological hints (Akita & Okada, 2014; Elorza-Vidal *et al.*, 2019; Mongin, 2016). Indeed, the role of the essential VRAC subunit LRRC8A in swelling- and ATP-activated EAA release from astrocytes has been confirmed (Hyzinski-García *et al.*, 2014; Schober *et al.*, 2017; Yang *et al.*, 2019). Combined siRNA knockdown of LRRC8C and LRRC8E also suppressed release of aspartate and glutamate (Schober *et al.*, 2017). Importantly, due to impaired glutamatergic transmission, mice with astrocyte-specific LRRC8A deletion exhibited hippocampal-dependent learning and memory deficits (Yang *et al.*, 2019). During pathological cell swelling, the loss of astrocytic LRRC8A attenuated glutamate-dependent neuronal excitability, thus providing neuroprotection after ischemic stroke (Yang *et al.*, 2019). Notably, a recent study presented both pharmacological and molecular biological evidence that cerebellar granule neurons conduct hypotonicity-induced ATP release through LRRC8/VRAC channels (Dunn *et al*, 2020).

A further role has been shown for VRAC in pancreatic insulin secretion. Pancreatic β-cells secrete insulin in response to serum glucose stimulation. Cellular uptake and metabolism of glucose raises intracellular ATP levels and thereby inhibits ATP-sensitive K^+ channels, resulting in cell membrane depolarization and activation of voltage-

dependent Ca^{2+} channels. Transient Ca^{2+} influx in turn triggers exocytosis of insulin-containing granules (Ashcroft & Rorsman, 2013; Rorsman & Braun, 2013; Yang *et al*, 2014). Consistent with a longstanding hypothesis (Best *et al*, 2010), two independent studies simultaneously showed that glucose-induced cell swelling (intracellular hypertonicity) in pancreatic β-cells activates LRRC8A-dependent VRAC currents (Kang *et al.*, 2018; Stuhlmann *et al.*, 2018). VRAC mediates the efflux of Cl^-, leading to membrane potential depolarization and subsequent electrical excitation (Kang *et al.*, 2018; Stuhlmann *et al.*, 2018). Nevertheless, β-cell-specific LRRC8A knock-out mice exhibited normal resting serum glucose levels but reduced glucose tolerance in both studies (Kang *et al.*, 2018; Stuhlmann *et al.*, 2018).

Both LRRC8A protein expression and VRAC currents were found to be increased in hypertrophic adipocytes from obese mice and humans (Xie *et al*, 2017; Zhang *et al*, 2017b). Even though *Lrrc8a* ablation reduced lipogenesis of 3T3-F442A cells and primary adipocytes *in vitro*, postnatal adipocyte development under basal conditions *in vivo* was not affected by adipocyte-restricted *Lrrc8a* deletion (Zhang *et al.*, 2017b). On the other hand, adipocyte-specific *Lrrc8a*-knockout reduced adipocyte size, adiposity, and body weight whereas increased systemic glucose intolerance and insulin resistance in obese mice (Zhang *et al.*, 2017b). Notably, it was also shown that LRRC8C (also named factor of adipocyte differentiation 158, FAD158) is required for adipocyte differentiation (Tominaga *et al*, 2004) and high-fat diet-induced obesity (Hayashi *et al*, 2011). Interestingly, the role of LRRC8A in adipocyte glucose uptake and lipogenesis was ascribed to the regulation of insulin-PI3K-AKT2 signaling through physical interactions between C-terminal LRR domain and growth factor receptor-bound 2 (GRB2, an adaptor protein) and caveolin-1 (Zhang *et al.*, 2017b). It remains unclear what the role of VRAC channel function itself is and what the mechanism of VRAC activation may be.

Besides the physiological roles discussed above, the overall biological importance of LRRC8/VRAC channels is demonstrated by the severe phenotypes of *Lrrc8a*$^{-/-}$ mice (Kumar *et al.*, 2014). They showed high prenatal and postnatal lethality with a maximum life span of approximately 100 days. Born *Lrrc8a*$^{-/-}$ mice exhibited severe growth retardation and defective developments in many organs, such as thinning of skeletal

muscle bundles and impairment of T-cell expansion and function (Kumar *et al.*, 2014). Owing to the ubiquitous expression of VRAC in vertebrate cells and its diverse composition and function, many discoveries regarding the cellular and systemic roles of VRAC and individual LRRC8 subunits may emerge in the future.

2. Aim of this work

Skeletal muscle arises from the differentiation and fusion of myoblasts into large multinucleated myotubes. Various ion channels and transporters play a pivotal role in skeletal myogenesis. For example, the action of potassium channels causes membrane hyperpolarization of differentiating myoblasts, thereby promoting the activation of intracellular calcium signals. Correspondingly, a tightly regulated transmembrane movement of the cations K^+ and Ca^{2+} is involved. Whilst the role of K^+ and Ca^{2+} ions and their channels/transporters during skeletal myogenesis have been extensively studied, little is known about the functions of the anion Cl^- and Cl^- channels in this process.

The volume-regulated anion channel (VRAC) formed by LRRC8 hetero-hexamers is a plasma membrane channel that conducts Cl^- and organic osmolytes when activated. Besides a key role in regulatory volume decrease, numerous physiological functions of VRAC have been described, including apoptosis, insulin secretion, and auto/paracrine signaling. Importantly, the thinned skeletal muscle bundles observed in mice lacking the essential VRAC subunit LRRC8A implicate LRRC8/VRAC channels in muscle formation.

Therefore, in this thesis I aim to investigate the role of LRRC8/VRAC channels in skeletal myogenesis by using mouse C2C12 myoblasts. First, I test the significance of both the essential subunit LRRC8A and VRAC channel function itself in myoblast differentiation and fusion. I next explore the mechanism by which VRAC participates in myoblast differentiation. Finally, I determine the timing of VRAC activity during myogenesis and the osmolytes it conducts upon activation. In addition, I test the possible role of VRAC in osteoblast and adipocyte differentiation.

3. Materials and Methods

3.1 Materials

3.1.1 Cell lines

Table 3.1: Cell lines

Name	Cell types	Source
C2C12	mouse myoblast	ATCC: CRL-1772; Kindly provided by P. Knaus (Freie Universität Berlin, Germany)
HeLa	human cervix epithelioid carcinoma	RRID: CVCL_0030; Obtained from Leibniz Forschungsinstitut DSMZ, Germany
3T3-L1	mouse embryonic fibroblast	ATCC: CL-173; Kindly provided by P. Knaus (Freie Universität Berlin, Germany)

3.1.2 Cell culture media and reagents

Table 3.2: Cell culture media and reagents

Name	Company	Product number
Dulbecco's modified eagle medium (DMEM)	PAN-Biotech	P04-03550
Chloride-reduced DMEM (w/o: KCl or NaCl; w: potassium gluconate and sodium gluconate)	PAN-Biotech	Customer’s formula
Opti-MEM	Gibco	31985070
Fetal bovine serum (FBS)	PAN-Biotech	P30-3302
Horse serum	PAN-Biotech	P30-0712
Recombinant human bone morphogenetic protein-2 (BMP-2)	Kindly provided by P. Knaus (Freie Universität Berlin, Germany)	
Recombinant insulin		

Dexamethasone	Sigma-Aldrich	D4902
3-isobutyl-1-methylxanthine (IBMX)	Sigma-Aldrich	I7018
Penicillin-Streptomycin	PAN-Biotech	P06-07100
Trypsin/EDTA	PAN-Biotech	P10-029500
Dulbecco's phosphate-buffered saline (DPBS)	PAN-Biotech	P04-36500

3.1.3 Chemicals and drugs

All chemicals used in this thesis were purchased from Sigma-Aldrich or Carl Roth, unless stated otherwise. The drugs shown in Table 3.3 are pharmacological inhibitors of VRAC.

Table 3.3: Drugs and chemicals

Name	**Company**	**Product number**
Carbenoxolone (CBX)	Sigma-Aldrich	C4790
Niflumic acid (NFA)	Sigma-Aldrich	N0630
5-nitro-2-(3-phenylpropylamino)benzoic acid (NPPB)	Tocris Bioscience	0593
4-(2-butyl-6,7-dichloro-2-cyclopentyl-indan-1-on-5-yl)oxybutyric acid (DCPIB)	Tocris Bioscience	1540
Dimethyl sulfoxide (DMSO)	PAN-Biotech	P60-36720100

3.1.4 siRNAs

Table 3.4: siRNAs

Name	**Species**	**Sequence**	**Company and Product number**
Lrrc8a siRNA1	mouse	sense-CCUUGUAAGUGGGUCACCATT	Thermo Fisher Scientific (s109501)
		antisense-UGGUGACCCACUUACAAGGTA	
Lrrc8a	mouse	sense-	Thermo Fisher

siRNA2		GAUCGACACCAGUACAACUTT	Scientific (s109502)
		antisense-AGUUGUACUGGUGUCGAUCTA	
scrambled siRNA		a non-targeting negative control siRNA	Thermo Fisher Scientific (4390844)

3.1.5 Plasmids

Table 3.5: Plasmids

Name	**Number in internal database**	**Expression vector**	**Supplier/Reference**
pEGFP-N1	23		Clontech
pmRFP-N1	45		Clontech
LRRC8A-GFP	103	pEGFP-N1	Kindly provided by T.J. Jentsch (FMP and MDC, Berlin, Germany) (Voss *et al.*, 2014)
LRRC8A-RFP	104	pmRFP-N1	
LRRC8A-Cerulean	105	pECFP-N1	(König *et al.*, 2019)
LRRC8E-Venus	106	pEYFP-N1	(König *et al.*, 2019)

3.1.6 Primers

Table 3.6: qRT-PCR Primers

Name	**Species**	**Sequence**
Lrrc8c forward	Mouse	5'-TCC TTT TCT GCG GAT ACC CT-3'
Lrrc8c reverse	Mouse	5'-AAC TCG GTC ACC GGA ATC AT-3'
Myogenin forward	Mouse	5'-CCA AGG TCT CCT GTG CTG ATG-3'
Myogenin reverse	Mouse	5'-TTG GCA AAA CCA CAC AAT GC-3'
Gapdh forward	Mouse	5'-TGC GAC TTC AAC AGC AAC TC-3'
Gapdh reverse	Mouse	5'-GCC TCT CTT GCT CAG TGT CC-3'

3.1.7 Antibodies

Table 3.7: Antibodies

Name	Company/Supplier	Product number/Reference
Rabbit anti-LRRC8A (5a)	Kindly provided by T.J. Jentsch (FMP and MDC, Berlin, Germany)	(Planells-Cases *et al.*, 2015; Voss *et al.*, 2014)
Rabbit anti-LRRC8B (5b)		
Rabbit anti-LRRC8C (ct)		
Rabbit anti-LRRC8D (ct)		
Rabbit anti-LRRC8E (ct)		
Mouse anti-myosin	Developmental Studies Hybridoma Bank	clone MF20
Mouse anti-myogenin	Developmental Studies Hybridoma Bank	clone F5D
Rabbit anti-GAPDH	Cell Signaling Technology	clone 14C10
Horseradish peroxidase (HRP)-conjugated goat anti-rabbit	Jackson ImmunoResearch	
HRP-conjugated goat anti-mouse	Jackson ImmunoResearch	
Alexa Fluor 555-labeled goat anti-mouse	Molecular Probes	

3.2 Methods

3.2.1 Cell culture

In general, cells (see Table 3.1) were maintained in growth medium (DMEM supplemented with 10% FBS, 100 units/ml penicillin and 100 µg/ml streptomycin) at 37°C under a humidified atmosphere with 5% CO_2.

3.2.2 Cell differentiation and drug treatment

To induce C2C12 myogenic differentiation, cells at 90-100% confluency were rinsed with DPBS and then switched to differentiation medium (DMEM supplemented with 2% horse serum, 100 units/ml penicillin, and 100 µg/ml streptomycin). Upon induction of differentiation, medium containing drugs or vehicle if applicable was replaced daily. For stock solutions, NFA, NPPB, and DCPIB were dissolved in DMSO, CBX in water.

To induce C2C12 osteogenic differentiation, cells at 90-100% confluency were rinsed with DPBS and then switched to differentiation medium (DMEM supplemented with 2% FBS, 100 units/ml penicillin, 100 µg/ml streptomycin, and 30 nM BMP-2). Upon induction of differentiation, medium containing drugs or vehicle if applicable was replaced every other day.

For induction of adipogenesis, 3T3-L1 preadipocytes at 2 days post-confluence were sequentially incubated with the following media: growth medium supplemented with 250 µM IBMX, 1 µM dexamethasone, and 1 µM insulin (for 2 days); growth medium supplemented with 1 µM insulin (for 2 days) and growth medium (for 4 days). Medium containing drugs or vehicle if applicable was replaced daily during the first 4 days after induction of differentiation.

3.2.3 Cell transfection

For siRNA experiments, C2C12 myoblasts were transfected with 15 nM siRNA using Lipofectamine RNAiMAX (Invitrogen) according to the manufacturer's instructions.

For overexpression, 2 µg/ml of plasmid DNA of pEGFP-N1-LRRC8A, pmRFP-N1-LRRC8A or expression vectors pEGFP-N1, pmRFP-N1 (see Table 3.5) was transfected into C2C12 cells using FuGENE 6 (Promega) according to the manufacturer's instructions. Cells were incubated with transfection complex for 6 h and induced to differentiate one day after transfection.

For co-expression, plasmid constructs of LRRC8A-Cerulean and LRRC8E-Venus (see Table 3.5) were co-transfected into cells plated in 35 mm glass-bottom dishes (MatTek) using FuGENE 6 (Promega) according to the manufacturer's instructions. 500 ng and 2

μg of each plasmid DNA were used on HeLa and C2C12 cells, respectively. C2C12 cells were incubated with transfection complex for 6 h. Both cells were used for FRET experiments one day after transfection.

3.2.4 Cell proliferation assay

C2C12 myoblasts were seeded at a density of 5,000 cells per well in 96-well plates and transfected with siRNA the next day. Cell viability was evaluated with the Cell Counting Kit-8 (Sigma-Aldrich) at 24- and 48-hours post transfection. The absorbance of the water-soluble formazan dye produced from tetrazolium salt WST-8 by cellular dehydrogenase activity was measured at 450 nm using a microplate reader (Biochrom).

3.2.5 Immunofluorescence staining

After the indicated time in myogenic differentiation medium, C2C12 cells growing on coverslips were rinsed with PBS and fixed in 4% paraformaldehyde (PFA)/PBS for 15 min at room temperature. Cells were subsequently permeabilized in 0.2% Triton X-100/PBS for 20 min and blocked in 3% bovine serum albumin/PBS for 1 h. Then, cells were incubated overnight at 4°C with a mouse monoclonal anti-myosin (0.28 μg/ml) or anti-myogenin (1 μg/ml) antibody in blocking buffer. After washing with PBS, cells were incubated with Alexa Fluor 555-labeled anti-mouse Ig (1:1,000) for 1 h at room temperature, stained with DAPI (1:1,000; Sigma-Aldrich) for 10 min, and mounted with Roti-Mount Fluocare (Carl Roth). Images were acquired with a DMi8 fluorescence microscope using a 20× or 40× objective (Leica Microsystems).

3.2.6 Alizarin red S assay

At day 0 or day 8 in osteogenic differentiation medium, C2C12 cells were rinsed with DPBS and fixed in ice-cold 70% ethanol for 1 h. Cellular monolayers were then washed with distilled water and incubated with 2% Alizarin red S (ARS) (Sigma-Aldrich) staining solution (pH 4.2) for 1 h in the dark at room temperature with gentle shaking. After

aspiration of the staining solution, cells were washed five times with distilled water. Quantification of ARS staining was performed as previously described (Gregory *et al*, 2004; Stanford *et al*, 1995). ARS was extracted by incubation of the cellular monolayers with 10% cetylpyridinium chloride (Sigma-Aldrich) in 10 mM Na_2PO_4 (pH 7.0) for 1 h with shaking. Equal aliquots of the extracts were then transferred into a 96-well plate followed by measuring the absorbance at 550 nm on a microplate reader (Biochrom).

3.2.7 Oil red O staining and quantification

At the indicated time after adipogenic induction, 3T3-L1 cells were rinsed with PBS and fixed in 4% PFA/PBS for 30 min at room temperature. Cells were stained with a mixture of 1.5 volumes of oil red O (ORO) (Sigma-Aldrich) stock solution (0.6% in 2-propanol) and 1 volume of distilled water for 15 min at room temperature and subsequently washed five times with distilled water. Differential interference contrast images of ORO staining were acquired with a DMi8 microscope (Leica Microsystems). To quantify ORO staining (Donzelli *et al*, 2011; Martella *et al*, 2014), the dye within stained cells was extracted by incubation with 100% 2-propanol for 15 min at room temperature with shaking. Then, equal aliquots of the extracts were transferred into a 96-well plate and the absorbance at 500 nm was measured using a microplate reader (Biochrom).

3.2.8 Western blotting

C2C12 cells were collected with a cell scraper on ice and lysed in precooled RIPA buffer (150 mM NaCl, 50 mM Tris pH 8.0, 5 mM EDTA pH 8.0, 1% NP-40, 0.5% sodium deoxycholate, 0.1% SDS) containing protease inhibitor cocktails (Roche). Total protein amount was determined using the Pierce BCA Protein Assay Kit (Thermo Fisher Scientific). Equal amounts of protein (20 µg per lane) were separated by 10% SDS-PAGE and transferred onto nitrocellulose membrane (Macherey-Nagel). Blotted membranes were subsequently blocked in 5% skim milk in TBS-T (20 mM Tris pH 7.6, 150 mM NaCl and 0.02% Tween-20) for 1 h at room temperature, incubated with primary antibodies overnight at 4°C, and stained with HRP-conjugated secondary antibodies for

40 min at room temperature. Primary antibodies (see Table 3.7): rabbit anti-LRRC8A-E subunits (1 µg/ml), mouse anti-myogenin (1 µg/ml), mouse anti-myosin (0.28 µg/ml), rabbit anti-GAPDH (1:2,500). Secondary antibodies: goat anti-mouse and goat anti-rabbit (1:5,000). Signals were visualized using an enhanced chemiluminescence reagent (HRP juice; PJK GmbH) and a ChemiSmart5000 digital imaging system (Vilber-Lourmat). Densitometrical quantification was performed with the Fiji software (Schindelin *et al*, 2012).

3.2.9 Quantitative real-time PCR

Total RNA was isolated from C2C12 cells with a NucleoSpin RNA Kit (Macherey-Nagel). SuperScript II Reverse Transcriptase (Invitrogen), Oligo $(dT)_{20}$ Primer (Invitrogen) and 1 µg of total RNA as template were used for cDNA synthesis. To assess gene expression, standard quantitative PCR was conducted with Power SYBR Green PCR Master Mix (Applied Biosystems) on SteponePlus Real-Time PCR System (Applied Biosystems). Results were analyzed with the comparative cycle threshold C_T ($\Delta\Delta C_T$) method by using *Gapdh* as the reference gene. The primer pairs are listed in Table 3.6.

3.2.10 Measurement of plasma membrane potential

Membrane potential measurements using the fluorescent bis-oxonol type plasma membrane potential indicator $DiBAC_4(3)$ were performed as previously described (Dall'Asta *et al*, 1997; Konig *et al.*, 2004). C2C12 myoblasts growing in 8-well chambers (Sarstedt) were washed twice and then incubated at 37°C in imaging buffer (containing in mM: 144 NaCl, 5 KCl, 2 $CaCl_2$, 1 $MgCl_2$, 10 glucose, 10 HEPES pH 7.4) with $DiBAC_4(3)$ (1 µM; Molecular Probes) for 30 min. After incubation, measurements were performed at room temperature on a DMi8 fluorescence microscope (Leica Microsystems) with a 63×/1.40 NA oil-immersion objective. $DiBAC_4(3)$ fluorescence images were acquired at 16-bit, 4×4 binning and 50-msec exposure with a FITC filter set (Ex: 480/40, Dc: 505, Em: 527/30) and an OcraFlash 4.0 camera (Hamamatsu). Calibration for each experiment was performed by adding gramicidin (20 µg/ml; Sigma-Aldrich) to isotonic

imaging buffer containing varying ratios of Na^+ and N-methyl-D-glucamine, maintaining [Na^+] + [N-methyl-D-glucamine] = 144 mM, in individual wells of 8-well chambers. DCPIB or NPPB was included for calibration of DCPIB or NPPB-treated samples. The membrane potential (E_m) was calculated with the Nernst equation:

$$E_m = \frac{RT}{zF} \times ln \frac{[Na^+]_o + [K^+]_o}{[Na^+]_i + [K^+]_i}$$

where R is the universal gas constant, T = 298 K, z = 1, F is the Faraday constant, $[K^+]_o$ = 5 mM; ($[Na^+]_i + [K^+]_i$) is assumed to be 150 mM.

Whole-cell patch-clamp recordings of the resting membrane potential were performed at room temperature with a MultiClamp 700B (Axon Instruments, Molecular Devices) and electrodes with an average resistance of 4 MΩ (range: 3.3-4.8 MΩ) in a submerged chamber containing the external solution containing (in mM): 144 NaCl, 5 KCl, 2 $CaCl_2$, 1 $MgCl_2$, 10 glucose, 10 HEPES, pH 7.4 with NaOH, 329 mOsm. C2C12 myoblasts were visualized using infrared differential interference contrast optics and an infrared video camera (PIKE F-145B; Allied Vision). Recordings were filtered at 10 kHz and sampled at 20 kHz with a Digidata 1550A (Axon Instruments, Molecular Devices). The internal solution consisted of (in mM): 125 K-gluconate, 5 KCl, 1 EGTA, 2 Na_2ATP, 2 MgATP, 0.3 Na_2GTP, 10 Na-phosphocreatine, 10 HEPES, pH 7.25 with KOH, 280 mOsm. Recorded traces were corrected for liquid junction potential. The resting membrane potential was determined from the first 15 s of each recorded trace to avoid membrane potential changes due to cytosol washout. The electrophysiological measurements were performed by Thorsten M. Becker from the AG Koch, FU Berlin.

3.2.11 Sensitized-emission FRET measurements

FRET experiments were in principle performed as previously described (König *et al.*, 2019). 50-70% confluent C2C12 cells were used in experiments with changes in tonicity. Isotonic (340 mOsm) imaging buffer contained (in mM): 150 NaCl, 6 KCl, 1 $MgCl_2$, 1.5 $CaCl_2$, 10 glucose, 10 HEPES, pH 7.4. Hypotonic (250 mOsm) buffer had a decreased

NaCl concentration of 105 mM. 80-100% confluent C2C12 cells were used to measure FRET changes during myogenic differentiation in isotonic differentiation buffer (329 mOsm, containing in mM: 144 NaCl, 5 KCl, 2 $CaCl_2$, 1 $MgCl_2$, 10 glucose, 10 HEPES, pH 7.4). 80-100% confluent HeLa cells were used as control. All FRET experiments were performed at room temperature on a Dmi6000B microscope (Leica Microsystems) equipped with a 63×/1.4 objective and a DFC360 FX camera. Samples were excited with EL6000 light source; emission was recorded with high-speed external Leica filter wheels with Leica FRET set filters (11522073). seFRET images were acquired with the same settings for donor, acceptor and FRET channels (8×8 binning, 100 m-sec exposure, gain 1) every 10 s (for buffer change experiments) or 1 min (for differentiation experiments) with the LAS AF software. Corrected FRET (cFRET) values were calculated according to the following equation (Jiang & Sorkin, 2002):

$$cFRET = \frac{B - A \times \beta - C \times \gamma}{C}$$

where A, B and C correspond to the emission intensities of the donor, FRET and acceptor channels, respectively; β and γ are the correction factors (β = bleed-through of donor emission; γ = cross excitation of acceptor by donor excitation) generated by acceptor- and donor-only references.

3.2.12 Measurement of intracellular Cl^-

Intracellular Cl^- concentration ($[Cl^-]_i$) measurements using the fluorescent indicator 6-methoxy-*N*-(3-sulfopropyl)quinolinium (SPQ; Invitrogen) were performed as previously described (Diaz *et al*, 2010; Pilas & Durack, 1997). C2C12 myoblasts growing in 8-well chambers (Sarstedt) were washed once with Hank's balanced salt solution (HBSS) and then incubated at 37°C in a hypotonic solution (HBSS:H_2O = 1:1) with 5 mM SPQ for 15 min. After that, cells were incubated in HBSS for a further 15 min to allow recovery from the hypotonic shock. For cells cultured in Cl^--reduced medium, an isotonic buffer with 0 mM Cl^- was used (gluconate was used as a substitute for Cl^-). Measurements were

performed at room temperature on a DMi8 microscope (Leica Microsystems) equipped with a 63×/1.40 NA oil-immersion objective and an OcraFlash 4.0 camera (Hamamatsu). SPQ fluorescence images were recorded at 16-bit, 4×4 binning and 100 m-sec exposure with a DAPI filter set (Ex: 360/40, Dc: 400, Em: 425 lp). Calibration for each experiment was achieved using 4 μM nigericin (Sigma-Aldrich) and 5 μM tributyltin (Sigma-Aldrich) to equilibrate intracellular and extracellular Cl^- concentrations ranging from 0 to 100 mM Cl^- in individual wells of 8-well chambers. To set the Cl^- concentrations in the calibration solution, equal molar KNO_3 substituted KCl in the original solution (in mM): 150 KCl, 2 $CaCl_2$, 10 glucose, 10 HEPES, pH 7.2. Ionophores nigericin and tributyltin were added freshly, and CBX was included for calibration of CBX-treated samples. The relationship between fluorescence of SPQ and Cl^- concentration is described by the Stern-Volmer equation:

$$\left(\frac{F_0}{F}\right) - 1 = K_{sv}[Q]$$

where F_0 is the fluorescence intensity without Cl^-, F is the fluorescence intensity in the presence of various concentrations of Cl^-, [Q] is the concentration of Cl^-, and K_{sv} is the Stern-Volmer constant.

3.2.13 Cytosolic Ca^{2+} imaging

C2C12 cells growing on 35 mm glass-bottom dishes (MatTek) were loaded with mix of Fura-2 AM (5 μM; Invitrogen) and Pluronic F-127 (0.02%; Invitrogen) in culture medium at 37°C for 30 min and then washed with imaging buffer containing (in mM): 145 NaCl, 5 KCl, 1 $CaCl_2$, 1 $MgCl_2$, 10 glucose, 10 HEPES, pH 7.4. Imaging was performed at room temperature on a DMi8 microscope (Leica Microsystems) equipped with a 63×/1.40 NA oil-immersion objective and an OcraFlash 4.0 camera (Hamamatsu). Samples were excited with an Optoscan monochromator (Cairn Research) at 340 nm or 380 nm (300 m-sec exposure); emission was recorded using a Fura-2 filter set (Dc: 410, Em: 510/84; 16-bit, 4×4 binning; AHF Analysentechnik) with the Winfluor software. At the end of each

experiment, R_{max} was achieved by the addition of 1 µM ionomycin. No significant variation of R_{max} was observed between experiments.

3.2.14 Image processing and quantitative analysis

For $DiBAC_4(3)$ and SPQ fluorescence images and Fura-2 ratiometric images, the measurement of mean fluorescence intensities of regions of interest (ROIs) was carried out with the Fiji software (Schindelin *et al.*, 2012). The mean fluorescence intensity of background near the ROI was subtracted. Images of five random fields were analyzed for each sample per experiment. The membrane potential, $[Cl^-]_i$ or 340/380 ratio (Ca^{2+} imaging) from each field per sample were compiled and depicted as mean of n (number of independent experiments) ± standard deviation (S.D.).

cFRET maps were generated using PixFRET plugin (Feige *et al*, 2005) (threshold set to 1, Gaussian blur to 2) with a self-written macro to process movies and were measured by manually drawn ROIs. Since absolute FRET values varied between individual cells, cFRET values of individual cells were normalized to their mean cFRET in isotonic buffer (for buffer change experiments) or their mean cFRET of recorded first 10 min (for differentiation experiments). Normalized cFRET values are depicted as mean of n (number of individual cells) ± S.D.

3.2.15 Statistical analysis

All data are presented as mean ± S.D. *p* values between two groups were determined by a two-tailed Student's *t*-test. For three or more groups, a one-way analysis of variance (ANOVA) with Bonferroni's post-hoc test was performed. *p* values are indicated in all figures according to convention: *, $p < 0.05$; **, $p < 0.01$; ***, $p < 0.001$; and n.s. = not significant.

4. Results

4.1 Pharmacological inhibition of VRAC impairs the differentiation and fusion of C2C12 myoblasts

C2C12 is a mouse myoblastic cell line that can differentiate and fuse into multinucleated myotubes under low-serum conditions (Kubo, 1991). To investigate the putative involvement of VRAC in myogenesis, I first tested the effects of several pharmacological VRAC blockers on myoblast fusion: carbenoxolone (CBX), an effective blocker of VRAC, pannexins and gap junction-forming connexins (Benfenati *et al*, 2009; Ye *et al*, 2009); 5-nitro-2-(3-phenylpropylamino)benzoic acid (NPPB), a conventional Cl^- channel blocker (Okada *et al.*, 2019); 4-(2-butyl-6,7-dichloro-2-cyclopentyl-indan-1-on-5-yl) oxybutyric acid (DCPIB), currently the most effective and selective VRAC antagonist with high sensitivity at micromolar concentrations (Decher *et al*, 2001; Okada *et al.*, 2019). Notably, DCPIB was also reported to block some K^+ channels (Deng *et al*, 2016; Lv *et al*, 2019). Moreover, we included niflumic acid (NFA), a potent blocker of Ca^{2+}-activated Cl^- channels (CaCCs) with moderate to low sensitivity to VRAC, which may only partially inhibit VRAC at the concentrations used (Friard *et al*, 2017; Okada *et al.*, 2019; Sato-Numata *et al*, 2016). C2C12 cells were incubated with various concentrations of drugs in a differentiation medium containing 2% horse serum for 4 days and then stained for nuclei and myosin (a marker of differentiated cells). I used an antibody against myosin that recognizes all myosin heavy chain isoforms. As shown in Figure 4.1, compared to vehicle-treated cultures, the VRAC inhibitors CBX, NPPB, and DCPIB significantly reduced the differentiation and fusion of C2C12 myoblasts in a dose-dependent manner, whereas the CaCC inhibitor NFA did not show any effect. These visual impressions were confirmed when the myotube formation of C2C12 cells was quantified using a fusion index (Figure 4.1).

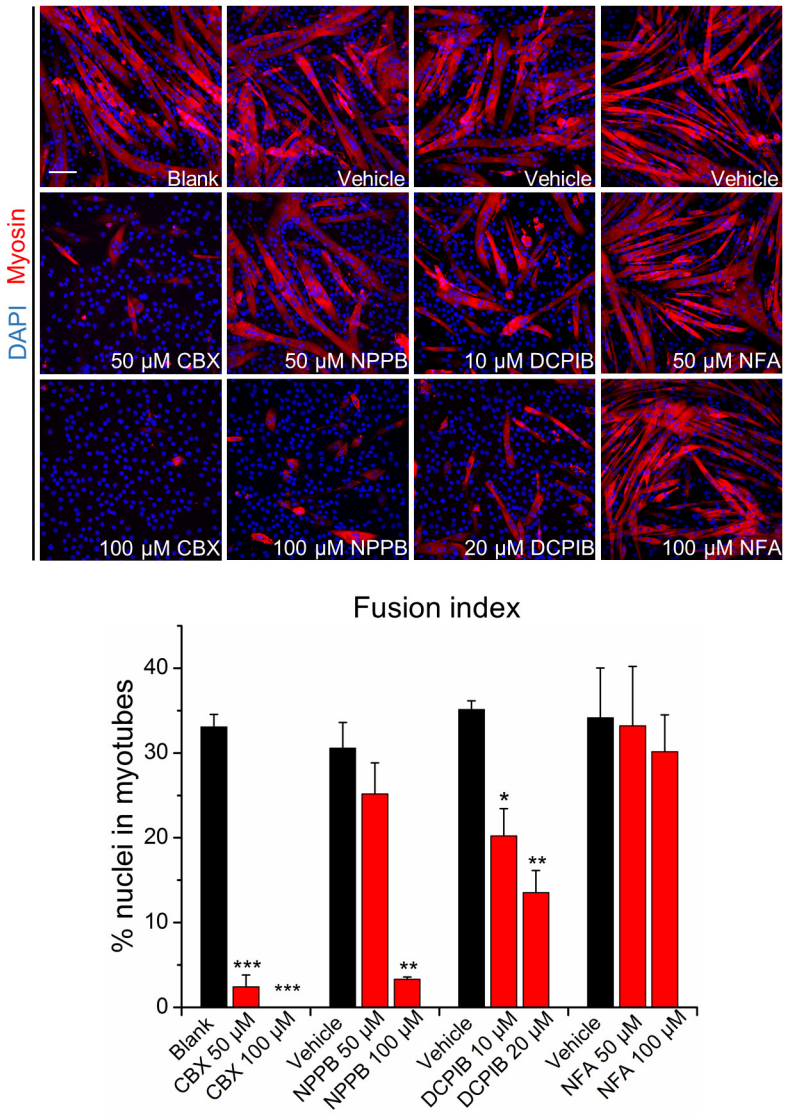

Figure 4.1: VRAC inhibitors impair C2C12 myoblast fusion. Cells were stained with an antibody against myosin (red) and DAPI (nuclei, blue) after 4 days in differentiation medium with indicated concentrations of drugs. The fusion index was calculated as the percentage of nuclei in myotubes (with ≥ 2 nuclei) among all nuclei. Data are presented as mean ± S.D. from three independent experiments. *, $p < 0.05$; **, $p < 0.01$; and ***, $p < 0.001$ compared with the respective controls using one-way ANOVA. Scale bar, 100 µm.

4.2 The expression of LRRC8/VRAC subunits is not upregulated during C2C12 cell differentiation

Since pharmacological data indicate that VRAC plays a role in myoblast differentiation and/or fusion, the next goal was to study its involvement in myogenesis at the molecular biological level. To this end, I first examined the expression profile of the VRAC subunits during myotube formation by Western blotting. This revealed that undifferentiated C2C12

myoblasts expressed all five LRRC8 isoforms (Figure 4.2, *A* and *B*). The expression levels of LRRC8A and LRRC8D did not change during the first 4 days of C2C12 cell differentiation. LRRC8B levels tended to decrease, while LRRC8E levels strongly declined already after 2 days of myoblast exposure to differentiation medium (Figure 4.2*A*). LRRC8C protein seemed to be reduced as well (Figure 4.2*B*), but because the immunodetection was not explicit, I performed quantitative PCR and the results showed that *Lrrc8c* mRNA expression was significantly downregulated after 2 days of cell differentiation (Figure 4.2*C*).

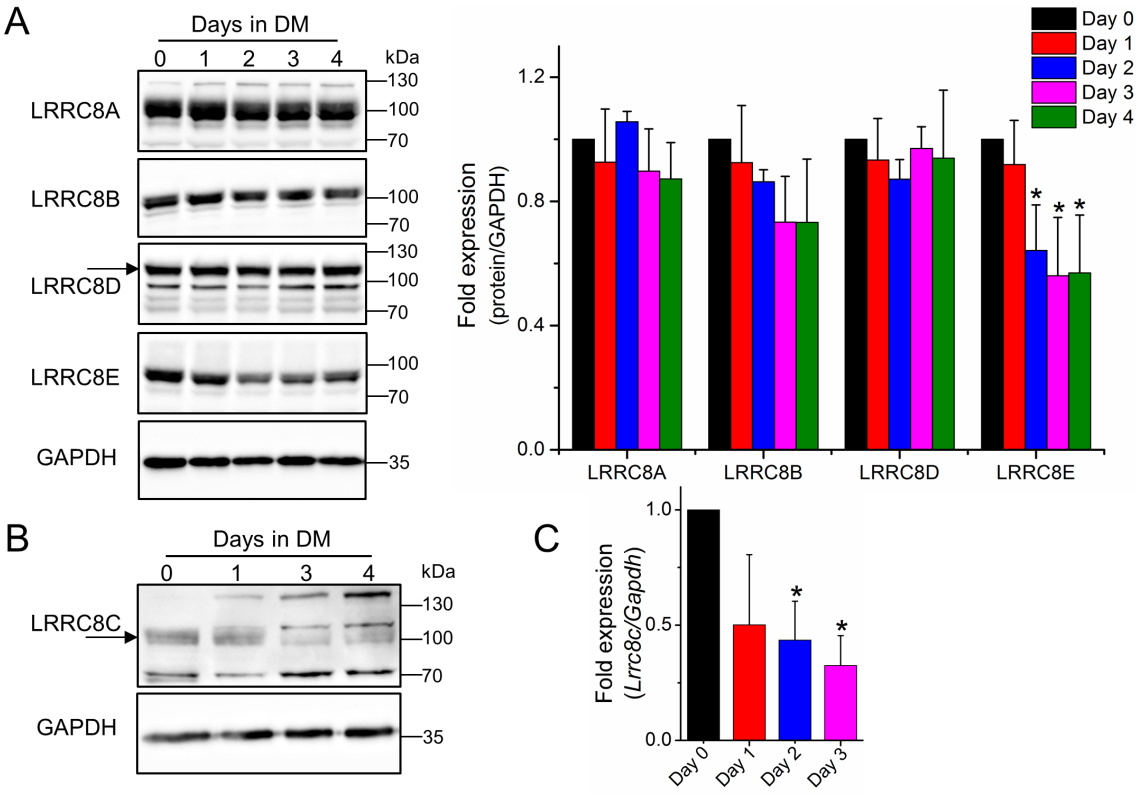

Figure 4.2: Expression profile of LRRC8/VRAC subunits during C2C12 cell differentiation. ***A*,** Western blot analysis (left) and quantification (right) of LRRC8A, LRRC8B, LRRC8D and LRRC8E protein levels. ***B*,** Western blot analysis of LRRC8C. Arrows in (*A*) and (*B*) indicate specific bands as deduced from published knockout controls. ***C*,** Quantitative PCR analysis of *Lrrc8c* mRNA, shown as fold changes compared to Day 0. All data are presented as mean ± S.D. from at least three independent experiments. *, $p < 0.05$ compared with Day 0 using one-way ANOVA. DM, differentiation medium.

4.3 LRRC8A is dispensable for myoblast proliferation but required for normal differentiation

I next used a strategy of inducing post-transcriptional gene silencing through siRNA sequences to clarify the role of the essential VRAC subunit LRRC8A during myotube formation. Two individual siRNAs designed against LRRC8A were transfected into C2C12 myoblasts, while a scrambled siRNA was used as control. Western blotting confirmed a robust knockdown of LRRC8A protein, and siRNA2 was more efficient than siRNA1 (Figure 4.3*A*). Notably, LRRC8A silencing did not impede C2C12 cell growth or viability, as shown by the unaffected dehydrogenase activity (Figure 4.3*B*). Besides, scrambled control for the siRNA did not affect C2C12 differentiation (Figure 4.4) or myotube formation (data not shown). Therefore, I could assess the effect of LRRC8A knockdown on myoblast differentiation and fusion.

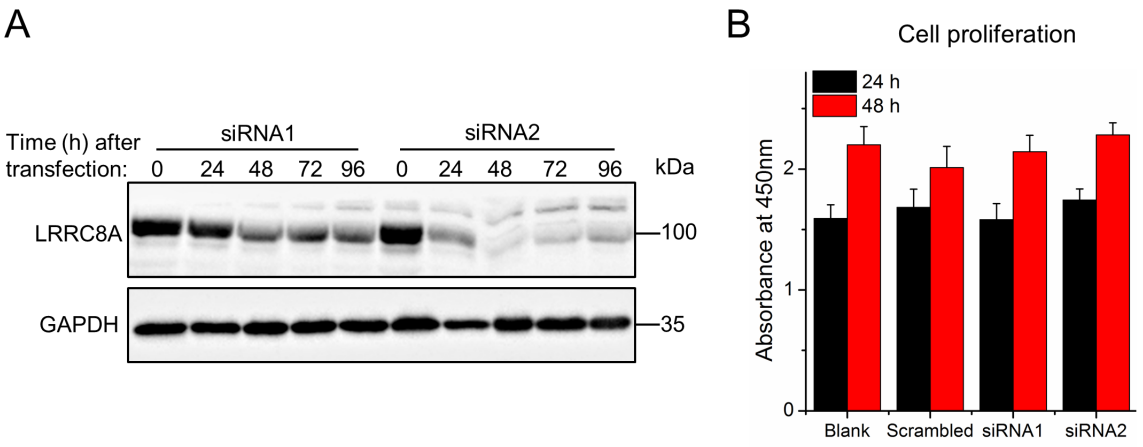

Figure 4.3: LRRC8A knockdown does not affect myoblast proliferation. ***A*****,** Western blot analysis of LRRC8A expression after siRNA transfection. ***B*****,** Quantitative analysis of C2C12 cell proliferation by measuring dehydrogenase activity at the indicated time points after siRNA transfection. Cells were plated at the same initial intensities and incubated overnight before transfection. Data are presented as mean ± S.D. from three independent experiments.

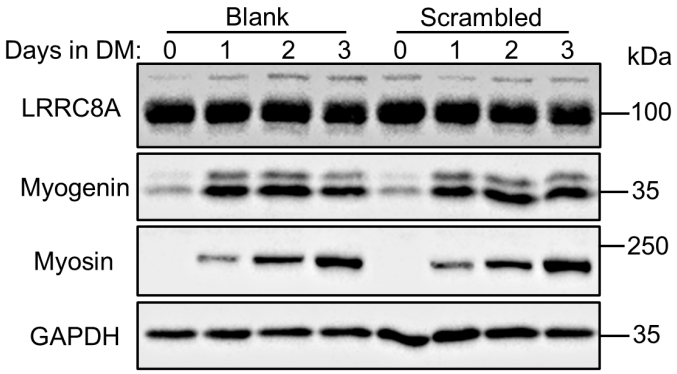

Figure 4.4: Scrambled control for siRNA does not affect C2C12 differentiation. Western blot analysis of LRRC8A, myogenin and myosin. DM, differentiation medium.

Starting 1 day after siRNA transfection, C2C12 cells were induced to differentiate for 3 days. At the beginning of differentiation induction, the amount of LRRC8A protein detected by Western blotting was reduced by ~40 and ~70% in cells treated with siRNA1 and siRNA2, respectively, and further decreased within the observed time of differentiation (Figure 4.5, *A* and *B*). Myogenin is an essential myogenic transcription factor, and we observed its expected upregulation during differentiation. Analysis by quantitative PCR and immunoblotting showed that knockdown of LRRC8A significantly reduced myogenin expression compared with scrambled siRNA (Figure 4.5, *A*, *C* and *E*). Similar results were obtained with the expression of myosin (Figure 4.5, *A* and *D* and Figure 4.6). Furthermore, myotube formation was drastically diminished by LRRC8A silencing (Figure 4.6). The inhibitory effects of siRNA1 and siRNA2 on myoblast differentiation and fusion correlated with their knockdown efficiencies. For example, after 3 days of differentiation, the fusion index reached 34 ± 3% in control cells but only 19 ± 4% in siRNA1-treated cells and 13 ± 3% in siRNA2-treated cells (Figure 4.6). Collectively, these results indicate that LRRC8A is dispensable for myoblast proliferation but critically involved in myogenic commitment.

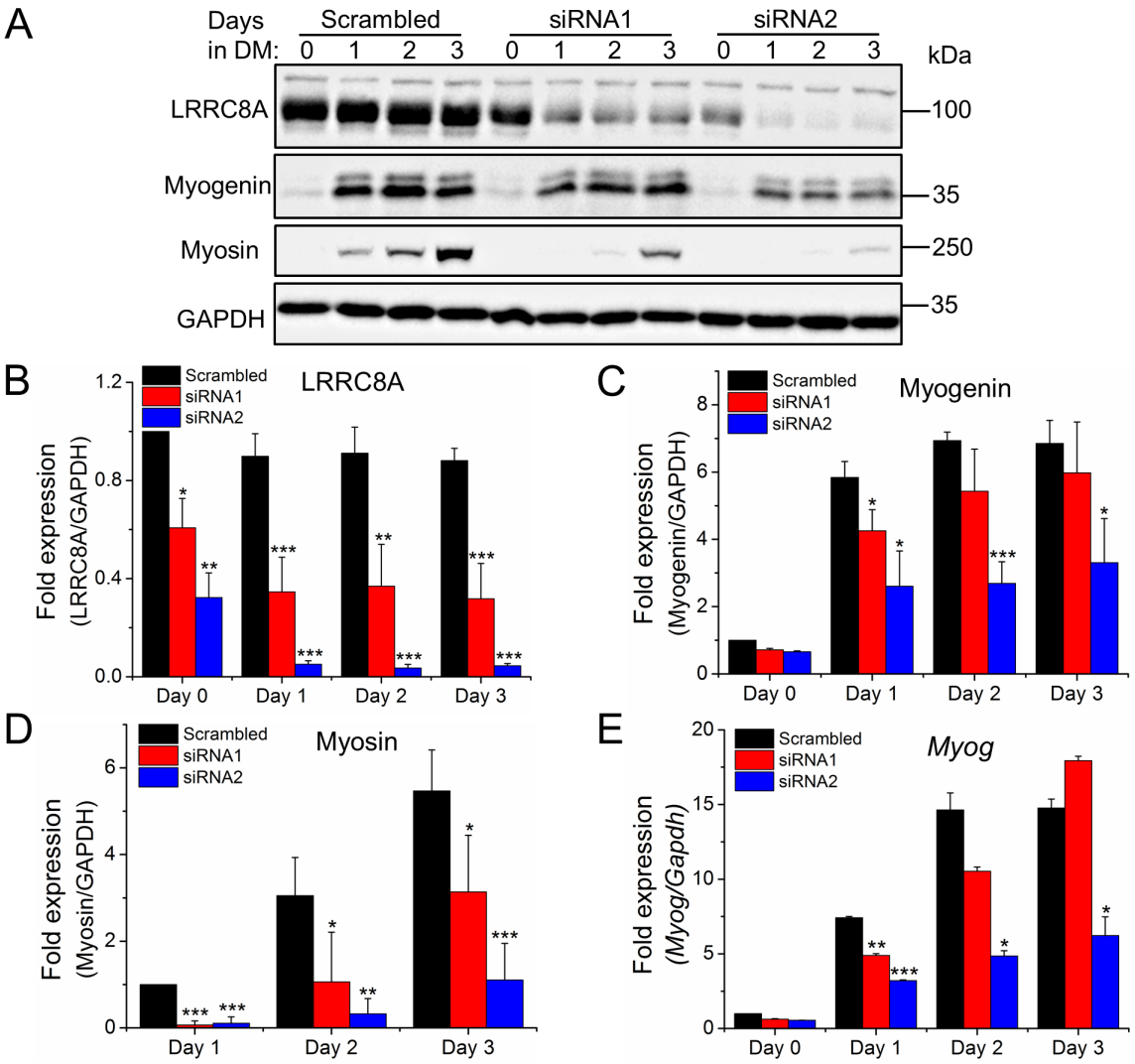

Figure 4.5: LRRC8A knockdown impairs myoblast differentiation. ***A*,** Western blot analysis of LRRC8A, myogenin and myosin. DM, differentiation medium. ***B-D*,** Quantification of Western blot analysis. Fold changes of LRRC8A (*B*) and myogenin (*C*) expression are normalized to Day 0 with scrambled control. Fold changes of myosin (*D*) expression are normalized to Day 1 with scrambled control. ***E*,** Quantitative PCR analysis of *Myogenin* (*Myog*) mRNA on the indicated day of differentiation. Fold changes of *Myog* expression are normalized to Day 0 with scrambled control. All data are presented as mean ± S.D. from at least three independent experiments. *, $p < 0.05$; **, $p < 0.01$; and ***, $p < 0.001$ compared with the respective controls using one-way ANOVA.

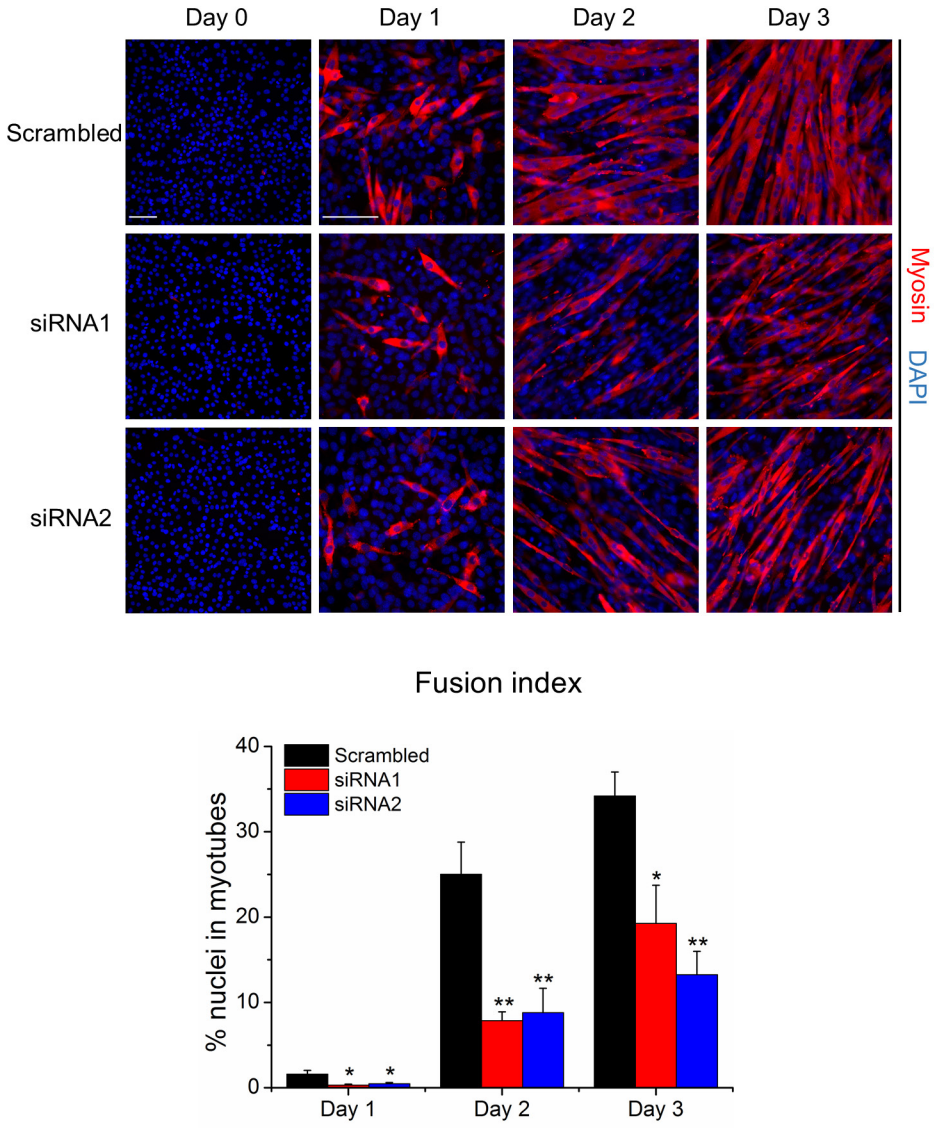

Figure 4.6: LRRC8A knockdown impairs myoblast fusion. C2C12 cells were stained with an anti-myosin antibody (red) and DAPI (nuclei, blue) on the indicated day of differentiation. The fusion index was calculated as the percentage of nuclei in myotubes (with ≥ 2 nuclei) among all nuclei. Data are presented as mean ± S.D. from three independent experiments. *, $p < 0.05$ and **, $p < 0.01$ compared with the respective controls using one-way ANOVA. Scale bars, 100 µm.

4.4 VRAC channel function promotes myoblast differentiation

To further determine the role played by VRAC channel itself during myogenesis, I transiently overexpressed LRRC8A in C2C12 cells. Overexpression of LRRC8A alone, without another LRRC8 isoform, has been shown to rather decrease endogenous VRAC currents (Qiu *et al.*, 2014; Voss *et al.*, 2014). C2C12 myoblasts were incubated for 6 h with plasmid DNA encoding LRRC8A fused to green-fluorescent protein (LRRC8A-GFP)

or GFP alone. When expression of LRRC8A-GFP was already observable 1 day after transfection (Figure 4.7*A*), the cells were induced to differentiate for 2 days and then stained for nuclei and myosin. Quantification of differentiation revealed that more than 20% of GFP-expressing control cells were positive for myosin, while in LRRC8A-GFP-expressing cells, this ratio was significantly reduced to only ~7% (Figure 4.7, *A* and *B*). The inhibitory effect of LRRC8A overexpression on C2C12 myoblast differentiation corroborates the notion that the role of LRRC8A in myogenic commitment indeed lies in its requirement for VRAC activity. Furthermore, the potent VRAC inhibitor DCPIB has recently been shown to bind in the extracellular selectivity filter of VRAC and sterically occlude ion conduction (Kern *et al.*, 2019). Consistent with an important role of VRAC channel function, DCPIB significantly reduced the expression of *Myogenin* mRNA (*Myog*) after 3 days of cell differentiation (Figure 4.7*C*), which is also consistent with its inhibitory effect on myoblast fusion (Figure 4.1).

4.5 VRAC is required for myoblast hyperpolarization and the subsequent increase of intracellular Ca^{2+}

It is well-established that upon induction of differentiation, myoblasts sequentially hyperpolarize due to the activation of two distinct K^+ channels, *ether-à-go-go* (Bijlenga *et al.*, 1998) and Kir2.1 (Fischer-Lougheed *et al.*, 2001; Konig *et al.*, 2004; Liu *et al.*, 1998). This hyperpolarization is completed within the first 6 hours of differentiation (Hinard *et al.*, 2008; Konig *et al.*, 2004) and enhances the driving force for Ca^{2+} (Arnaudeau *et al.*, 2006; Konig *et al.*, 2006), leading to a detectable steady-state increase in intracellular Ca^{2+} concentration ($[Ca^{2+}]_i$) (Bijlenga *et al.*, 2000; Liu *et al.*, 2003). To investigate the mechanism of VRAC involving in myogenic differentiation, I first tested whether VRAC influences the plasma membrane potential. C2C12 myoblasts were loaded with the potentiometric fluorescent probe $DiBAC_4(3)$ (Dall'Asta *et al.*, 1997; Konig *et al.*, 2004) to analyze membrane potential changes. This anionic bis-oxonol dye enters depolarized cells where it binds to intracellular proteins or membranes, thereby exhibiting enhanced fluorescence (Epps *et al*, 1994). Conversely, hyperpolarization is

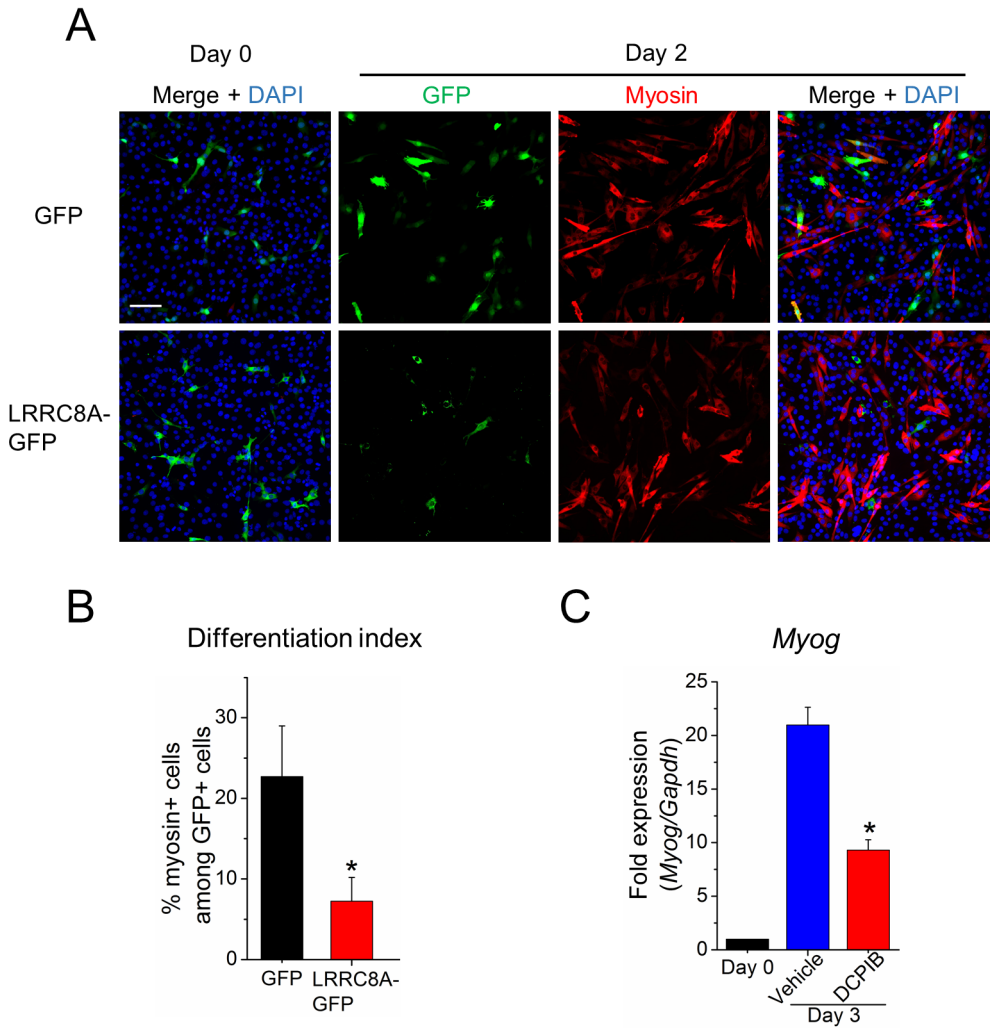

Figure 4.7: Decreased VRAC activity inhibits myoblast differentiation. ***A*,** C2C12 cells transfected with plasmid DNA for GFP or LRRC8A-GFP expression (green) were stained with an anti-myosin antibody (red) and DAPI (nuclei, blue) on the indicated day of differentiation. Scale bar, 100 µm. ***B*,** The differentiation index was calculated as the percentage of myosin$^+$ cells among GFP$^+$ cells. More than 300 GFP$^+$ cells were calculated for each group. ***C*,** Quantitative PCR analysis of myogenin (*Myog*) after 3 days of cell differentiation in the presence of 20 µM DCPIB or of vehicle (DMSO) alone. Fold changes of *Myog* expression are relative to Day 0. All data are presented as mean ± S.D. from three independent experiments. *, $p < 0.05$ compared with the respective controls using a two-tailed unpaired *t*-test.

indicated by decreased fluorescence. Calibration of $DiBAC_4(3)$ fluorescence versus plasma membrane potential for each sample was performed using solutions with different Na^+ concentrations and gramicidin (Figure 4.8*A*). After 6-8 h in differentiation medium, C2C12 myoblasts possessed the normal average resting membrane potential of –80 mV in the presence of vehicle (0.1% DMSO) but only –50 mV and –47 mV in the presence of 20 µM DCPIB and 100 µM NPPB, respectively (Figure 4.8*B*). I also tried to use siRNA.

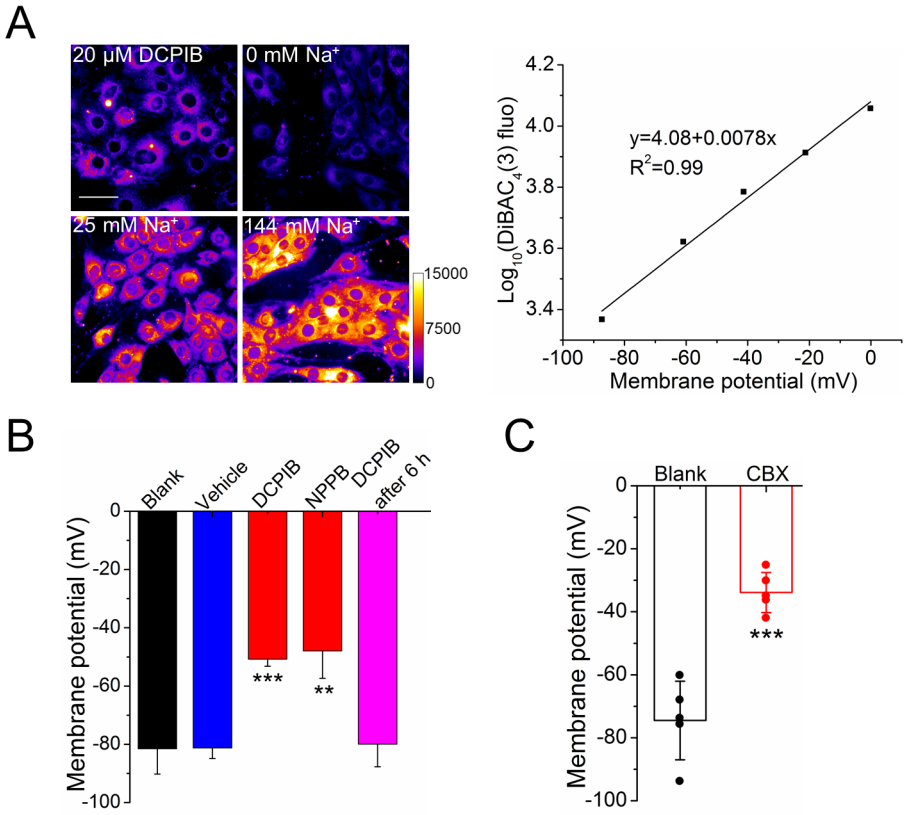

Figure 4.8: VRAC contributes to myoblast hyperpolarization. ***A*,** a representative calibration for measuring the resting membrane potential with the fluorescence probe $DiBAC_4(3)$. *Left*, images of C2C12 cells stained with $DiBAC_4(3)$ after differentiation for 6-8 h with DCPIB. Different external sodium concentrations and gramicidin were used to set the membrane potential. Fluorescence intensities are depicted in color code, as indicated by the calibration bar. Scale bar, 50 µm. *Right*, logarithm of the mean fluorescence intensity plotted against calculated membrane potential from the Nernst equation (see "Methods") and the best linear regression fit, which was used to calculate the membrane potentials in (*B*). ***B*,** Average resting membrane potentials of C2C12 myoblasts measured after 6-8 h in differentiation medium (blank) supplemented with 20 µM DCPIB, 100 µM NPPB or vehicle (DMSO) only; or DCPIB was added after 6 h. ***C*,** Resting membrane potentials of C2C12 cells measured after 20-24 h of differentiation in the presence or absence of 100 µM CBX by whole-cell patch-clamp recording (performed by Thorsten M. Becker from the AG Koch, FU Berlin). Symbols represent values of individual cells. All data are presented as mean ± S.D. from three independent experiments. *, $p < 0.05$; **, $p < 0.01$; and ***, $p < 0.001$ compared with the respective controls using one-way ANOVA (*B*) or a two-tailed unpaired *t*-test (*C*).

Unfortunately, fluorescent aggregates due to the transfection process prevented reliable membrane potential measurements with siRNA-treated cells. Then I collaborated with Dr. Thorsten M. Becker from the lab of Prof. Ursula Koch at the FU to perform whole-cell patch-clamp recording. Consistently, electrophysiological recordings of C2C12 cells after 20-24 h of differentiation showed an average resting membrane potential of −75 mV, which was found to be −34 mV in the presence of 100 µM CBX (Figure 4.8*C*). These data suggest that VRAC inhibition impaired the normal hyperpolarization.

I next determined whether this impinges on the changes of resting $[Ca^{2+}]_i$ during myoblast differentiation. Cytosolic free Ca^{2+} fluctuations were assessed using the ratiometric fluorescent Ca^{2+} indicator Fura-2. As expected, I observed the steady-state increase of $[Ca^{2+}]_i$ in differentiating C2C12 cells (Figure 4.9*A*). In the presence of 20 µM DCPIB, but not of the vehicle DMSO, this increase was abolished (Figure 4.9*A*). It is worth mentioning that the strong effect of DCPIB on the changes of $[Ca^{2+}]_i$ is not due to toxicity, because when DCPIB was removed from the differentiation medium after 24 h, Ca^{2+} levels increased (Figure 4.9*A*), and myotube formation proceeded normally (Figure 4.9*B*). Consistently, VRAC suppression by overexpression of red-fluorescent protein-labelled LRRC8A (LRRC8A-RFP) prevented the increase of $[Ca^{2+}]_i$ (Figure 4.9*C*).

To define more accurately the timing of VRAC activity involved in myoblast differentiation, I applied DCPIB 6 h after induction of differentiation. The addition of DCPIB at this point did not affect the resting membrane potential of C2C12 cells (Figure 4.8*B*) or their differentiation (Figure 4.10). Hence, VRAC activity seemed to be required predominantly during the first 6 h of myoblast differentiation. It is worth recalling that DCPIB was also shown to potently suppress certain K^+ channels that may play a role in maintaining the cellular resting membrane potential (Deng *et al.*, 2016; Lv *et al.*, 2019). The absence of effect of DCPIB added after 6 h excludes the possibility that DCPIB depolarized the membrane through inhibition of these K^+ channels.

Taken together, the results presented so far suggest that the initiation of VRAC activity contributes to the hyperpolarization of myoblasts and the rise in cytosolic Ca^{2+}, thereby supporting myoblast differentiation and fusion.

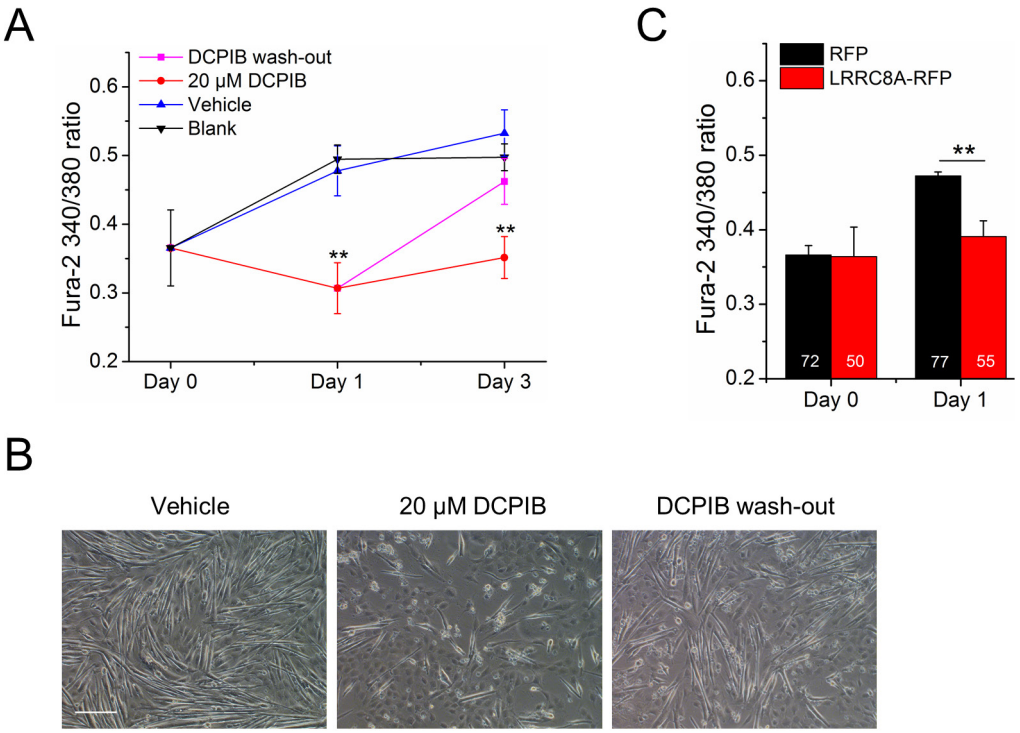

Figure 4.9: VRAC contributes to increased resting $[Ca^{2+}]_i$. ***A*,** Fura-2 ratios in C2C12 cells measured on the indicated day of differentiation in the presence or absence of DCPIB. For DCPIB washout, DCPIB-containing medium was replaced by DCPIB-free medium after 24 h. ***B*,** Differential interference contrast images of C2C12 cells after 3 days in differentiation medium in the presence of DCPIB (for the complete time or only for 24 h in the case of washout) or vehicle (DMSO) only. Scale bar, 200 µm. ***C*,** Fura-2 ratios in C2C12 cells expressing RFP or LRRC8A-RFP on the indicated day of differentiation. Numbers in bars indicate the total number of cells for each group. All data are presented as mean ± S.D. from three independent experiments. **, $p < 0.01$ compared with the respective controls using a two-tailed unpaired *t*-test.

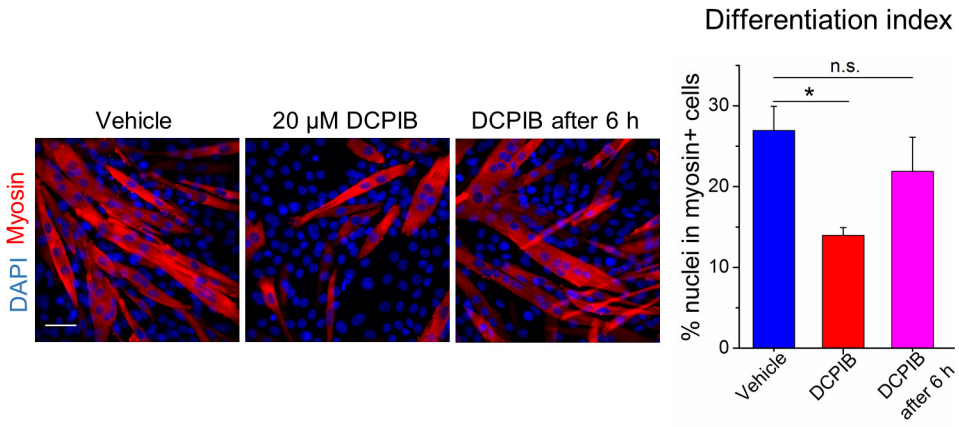

Figure 4.10: Late inhibition of VRAC does not impede myoblast differentiation. C2C12 cells were stained with an anti-myosin antibody (red) and DAPI (nuclei, blue) after 3 days in differentiation medium in the presence of 20 µM DCPIB, vehicle only, or with DCPIB added only 6 h after start of cell differentiation. The differentiation index was calculated as the percentage of nuclei in myosin$^+$ cells among all nuclei. Scale bar, 50 µm. Data are presented as mean ± S.D. from three independent experiments. n.s., not significant. *, $p < 0.05$ compared with control using one-way ANOVA.

4.6 VRAC activation in the early stage of C2C12 myoblast differentiation

Given that I did not detect any upregulation of LRRC8 proteins during myotube formation (Figure 4.2) and VRAC activity appeared to be only required during the first few hours of myoblast differentiation (Figure 4.10), I then aimed at providing direct evidence for transient VRAC activation at the onset of this process. To this end, I used a non-invasive fluorescence resonance energy transfer (FRET) sensor that was previously established in the Stauber lab (König *et al.*, 2019) to monitor VRAC channel activity in C2C12 myoblasts. FRET between two fluorophores is a highly sensitive reporter of changes in proximity and conformation of proteins or molecules (Bykova *et al.*, 2006; Miranda *et al.*, 2013; Zachariassen *et al.*, 2016). Fluorescent proteins were fused to the cytosolic C-terminus of LRRC8 subunits (König *et al.*, 2019); and the proximity of the C-terminal domains within the pore-forming LRRC8 hexamers (Deneka *et al.*, 2018; Kasuya *et al.*, 2018; Kefauver *et al.*, 2018) allows for inter-subunit FRET. VRAC activation with the rearrangement of the C-terminal domains is reflected by a drop in FRET efficiency (König *et al.*, 2019). At first, I co-expressed LRRC8A tagged with mCerulean3 (to serve

as FRET donor) and LRRC8E tagged with Venus (to serve as FRET acceptor) in C2C12 cells and monitored FRET during hypotonic stimulation (by switching from extracellular 340 mOsm to 250 mOsm). As expected, I observed a robust decrease of the corrected FRET (cFRET) value by ~10% within 60 s (Figure 4.11*A*). This indicates that osmotic swelling activates LRRC8A-Cerulean/LRRC8E-Venus-containing VRAC complexes in C2C12 myoblasts.

Next, I tested for iso-osmotic VRAC activation at the onset of myoblast differentiation. Within 2.5 h in isotonic differentiation buffer, cFRET of LRRC8A-Cerulean/LRRC8E-Venus remained almost constant in undifferentiable HeLa cells (Figure 4.11*B*). However, among 9 tested C2C12 myoblasts, 5 of them showed a steady cFRET decrease of ~10% within the first hour of differentiation (Figure 4.11*C* and Figure 4.12). Specifically, the recorded cFRET started to decrease at about 40 min after induction of differentiation and returned to baseline at about 120 min (Figure 4.11*C* and Figure 4.12). It is important to mention that cFRET at 55-64 min differed with $p = 0.032$ between the two populations with or without cFRET decrease. Besides, the presence of these two populations is consistent with the proportion of C2C12 cells typically undergoing differentiation.

These results confirm that VRAC is activated upon induction of myoblast differentiation and its inactivation after 2 h is in agreement with the requirement of VRAC only early in differentiation.

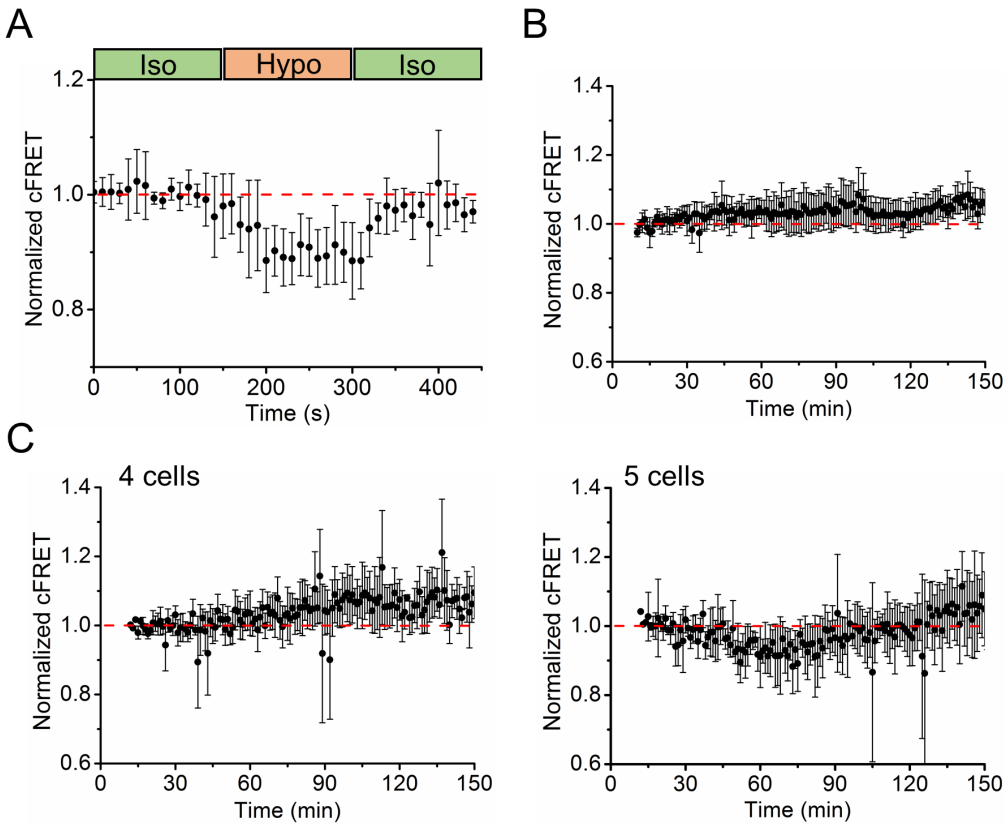

Figure 4.11: VRAC activation at the onset of myoblast differentiation. ***A***, normalized cFRET values during buffer exchange experiments with 50-70% confluent C2C12 cells (n = 3 dishes with 13 cells). Data were acquired in 10 s intervals. Iso, isotonic; Hypo, hypotonic. ***B***, normalized cFRET values during incubation of 80-100% confluent HeLa cells in isotonic differentiation buffer (n = 5, 14 cells). Data were acquired in 1 min intervals. ***C***, normalized cFRET values during incubation of 80-100% confluent C2C12 cells in isotonic differentiation buffer (n = 7, 9 cells). Data were acquired in 1 min intervals. All data are presented as mean ± S.D.

4.7 Myoblast differentiation results in an intracellular chloride decrease that is sensitive to VRAC inhibition

The confirmation of temporary VRAC activation prompted me to explore what it conducts when activated. Depending on the subunit composition of LRRC8 heteromers, VRAC can conduct various organic substances (Lutter *et al.*, 2017; Planells-Cases *et al.*, 2015; Zhou *et al.*, 2020), but all combinations mediate Cl^- conductance (Chen *et al.*, 2019b; Jentsch, 2016; Strange *et al.*, 2019). Therefore, I examined whether VRAC activation during myoblast differentiation results in cytosolic Cl^- changes. I loaded C2C12 cells with the chloride indicator 6-methoxy-*N*-(3-sulfopropyl)quinolinium (SPQ)

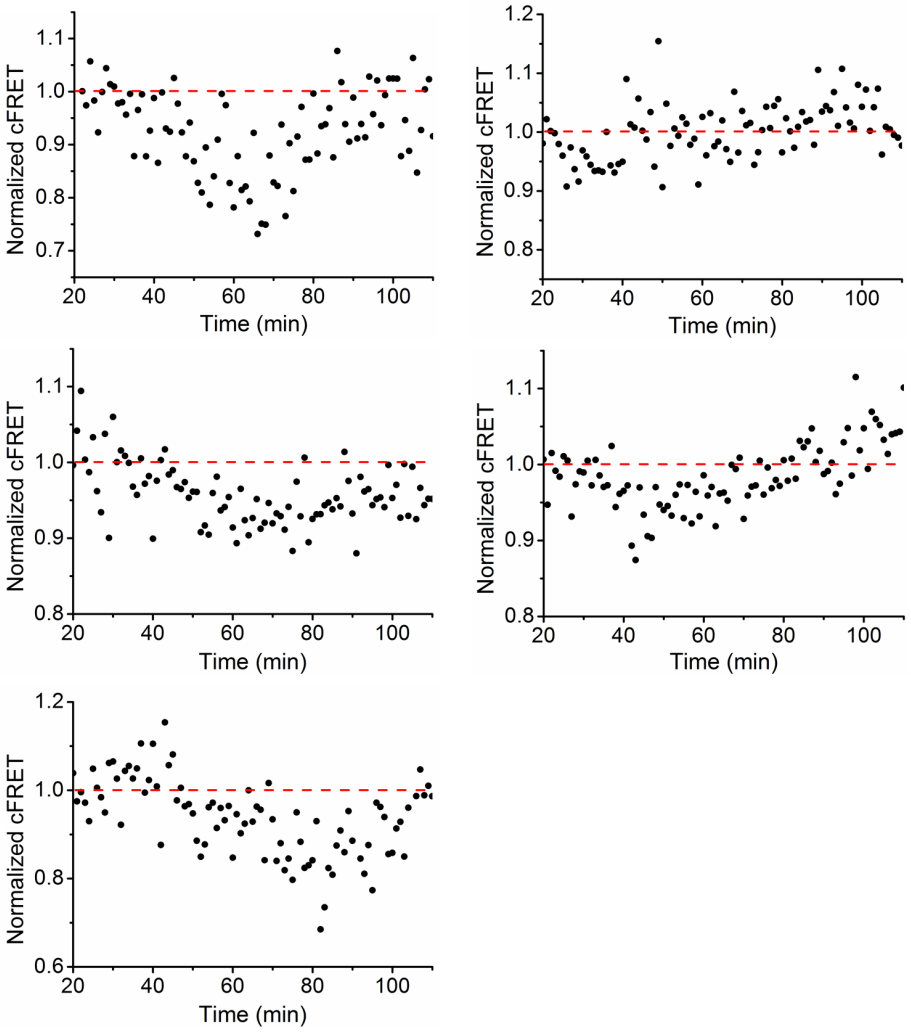

Figure 4.12: VRAC activation during the differentiation of individual myoblasts (the 5 cells in Figure 4.11*C*). Normalized cFRET values during incubation of 80-100% confluent C2C12 cells in isotonic differentiation buffer. Data were acquired in 1 min intervals.

(Diaz *et al.*, 2010; Pilas & Durack, 1997) to analyze intracellular Cl^- concentration ($[Cl^-]_i$) changes in a calibrated, quantitative manner (Figure 4.13*A*). The fluorescence of SPQ is quenched by increasing chloride concentrations. Proliferating, undifferentiated C2C12 myoblasts displayed a high resting $[Cl^-]_i$ of ~82 mM that reduced to ~50 mM after 2.5 h in differentiation medium and remained at 50-60 mM until 48 h (Figure 4.13*B*). This reduction of $[Cl^-]_i$ was prevented when I treated the cells with 100 µM CBX (Fig. 4.13*B*), the VRAC inhibitor that impaired myoblast hyperpolarization (Figure 4.8*C*) and differentiation (Figure 4.1). This suggests that VRAC activity accounts for the release of cytosolic Cl^- during myogenic commitment.

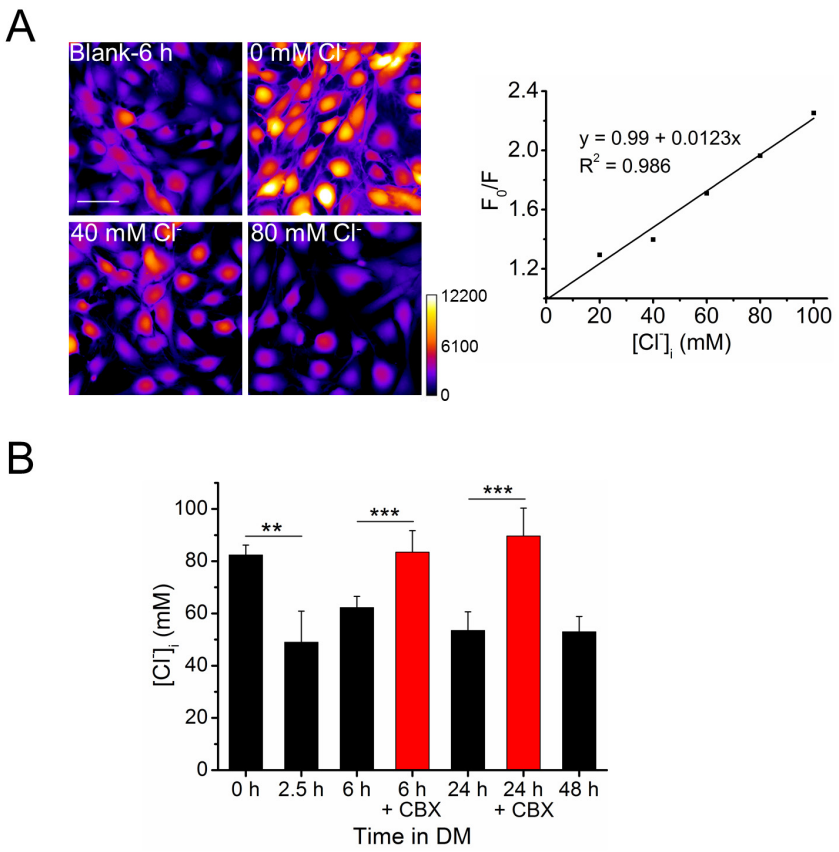

Figure 4.13: Myoblast differentiation is accompanied by an $[Cl^-]_i$ decrease. ***A***, representative calibration for measuring the resting $[Cl^-]_i$ with the fluorescence probe SPQ. *Left*, images of C2C12 cells stained with SPQ after 6 h of differentiation. Nigericin and tributyltin were used to equilibrate intracellular and external Cl^- concentrations. Fluorescence intensities are represented in color code, as shown in the calibration bar. Scale bar, 50 µm. *Right*, Stern-Volmer plot (see "Methods") for the fluorescence of SPQ against Cl^- concentration. The resulting best linear regression fit was used to calculate the $[Cl^-]_i$ in (*B*). ***B***, average $[Cl^-]_i$ of C2C12 myoblasts measured at different time points after induction of differentiation in the presence or absence of 100 µM CBX. DM, differentiation medium. Data are presented as mean ± S.D. from three independent experiments. **, $p < 0.01$ and ***, $p < 0.001$ compared with the respective controls using a two-tailed unpaired *t*-test.

4.8 Intracellular chloride depletion impairs myoblast fusion

To further study the role of an intracellular Cl^- decrease in the process of myogenesis, I tested the effect of Cl^- depletion on myoblast differentiation and/or fusion by using the chloride-reduced differentiation medium. In this medium, KCl and NaCl, which account for 99.5% of the total chloride content, were replaced with potassium gluconate and sodium gluconate. After 6 h in this medium, C2C12 cells possessed a significantly reduced $[Cl^-]_i$ of only ~4 mM (Figure 4.14*A*), whereas the $[Cl^-]_i$ of cells cultured in

normal differentiation medium showed the previously observed decrease (Figure 4.13*B*) to ~58 mM (Figure 4.14*A*). However, I did not observe any difference in either the percentage of myogenin-positive nuclei (Figure 4.14*B*) or total myogenin protein levels (Figure 4.14*C*) between C2C12 cells with normal or reduced [Cl^-] during differentiation. Surprisingly, the expression of myosin was significantly suppressed in Cl^--reduced medium compared with normal medium (Figure 4.14*C*) (protein levels in medium with reduced Cl^- were 51 ± 16 % of control, $p = 1.8\times10^{-4}$, data not shown).

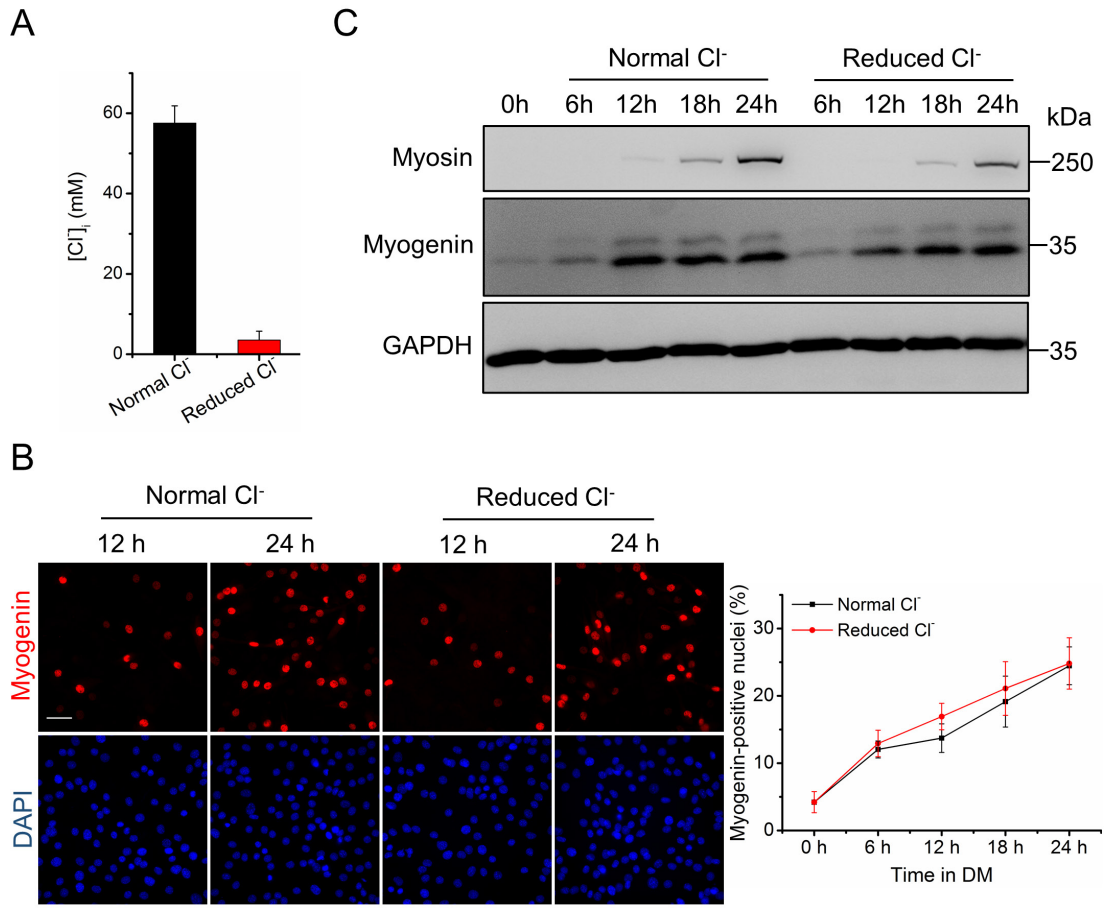

Figure 4.14: Reduced extracellular Cl^- does not affect myoblast differentiation. ***A***, resting $[Cl^-]_i$ of C2C12 cells measured after 6 h of differentiation in normal medium or Cl^--reduced medium. ***B***, C2C12 myoblasts were stained with an anti-myogenin antibody (red) and DAPI (nuclei, blue) at the indicated time of differentiation. DM, differentiation medium. Scale bar, 50 µm. ***C***, Western blot analysis of myogenin and myosin at the indicated time of differentiation. All data are presented as mean ± S.D. from three independent experiments.

Then, I induced C2C12 cells to differentiate for prolonged periods in either normal or Cl^--reduced differentiation medium. 4 days after induction of differentiation, extensive large myotubes were observed in normal medium. In Cl^--reduced medium, however, most C2C12 myoblasts remained elongated thin cells (Figure 4.15*A*). Immunoblot analysis revealed that the ability of myoblasts to express myogenin was not affected in both of the media; however, the expression of myosin was significantly inhibited in Cl^--reduced medium (Figure 4.15*B*). Notably, when I changed the Cl^--reduced medium to normal medium after 2 days of cell differentiation, C2C12 myoblasts were still able to form large myotubes (Figure 4.15*A*). This excludes the possible toxic effect of low external [Cl^-]. Therefore, a drastic reduction in $[Cl^-]_i$ does not potentiate myoblast differentiation but may rather hinder myoblast fusion.

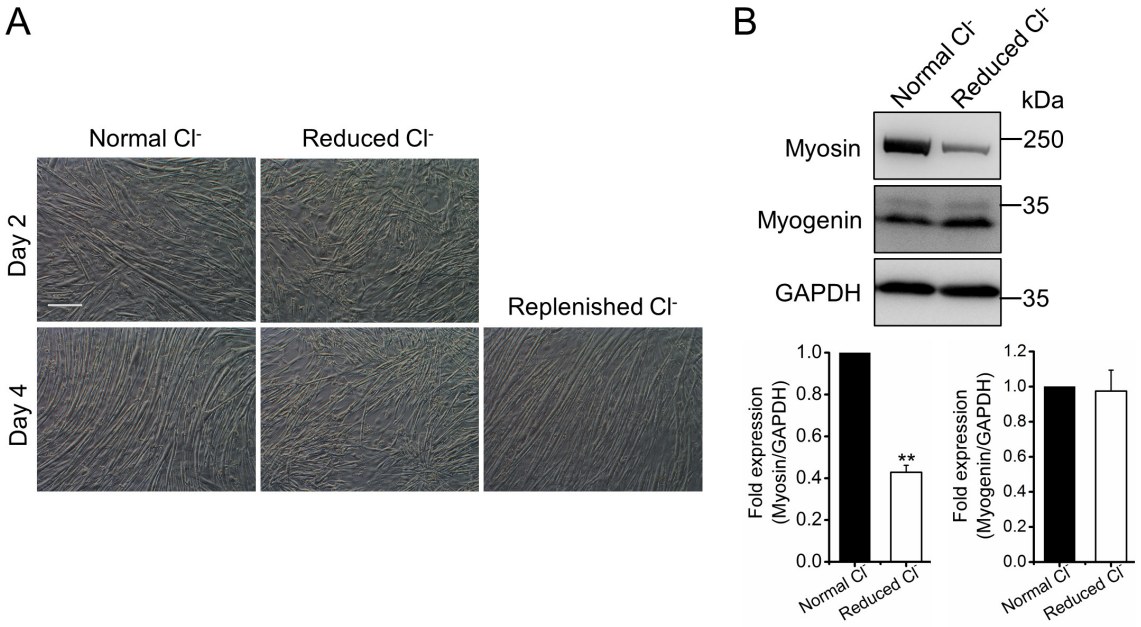

Figure 4.15: Reduced extracellular Cl^- impairs myoblast fusion. ***A***, differential interference contrast images of C2C12 cells on the indicated day of differentiation in normal or Cl^--reduced medium (for 4 days or only for 2 days in the case of washout). Scale bar, 200 µm. ***B***, Western blot analysis and quantification of myogenin and myosin protein levels after 4 days of differentiation in normal or Cl^--reduced medium. Fold changes are relative to normal medium. Data are presented as mean ± S.D. from three independent experiments. **, $p < 0.01$ compared with control using a two-tailed paired *t*-test.

4.9 Effect of VRAC inhibition on osteoblast differentiation of C2C12 cells and 3T3-L1 adipocyte differentiation

Lastly, I investigated whether VRAC plays a more general role in cell differentiation, by assessing the effect of pharmacological VRAC inhibition on two other types of differentiation: osteoblast and adipocyte differentiation.

Recombinant bone morphogenetic protein-2 (BMP-2) stimulation triggers a signaling cascade, which converts the differentiation of C2C12 myoblasts into that of osteoblasts (Katagiri *et al*, 1994; Rauch *et al*, 2002). I induced the osteogenic differentiation of C2C12 cells with 30 nM BMP-2 and stained for extracellular calcium deposits after 8 days. Alizarin red S staining and quantitative analysis showed that compared with control culture, the VRAC inhibitors CBX and DCPIB greatly reduced matrix mineralization (Figure 4.16), indicating that VRAC may play an important role in osteoblast differentiation.

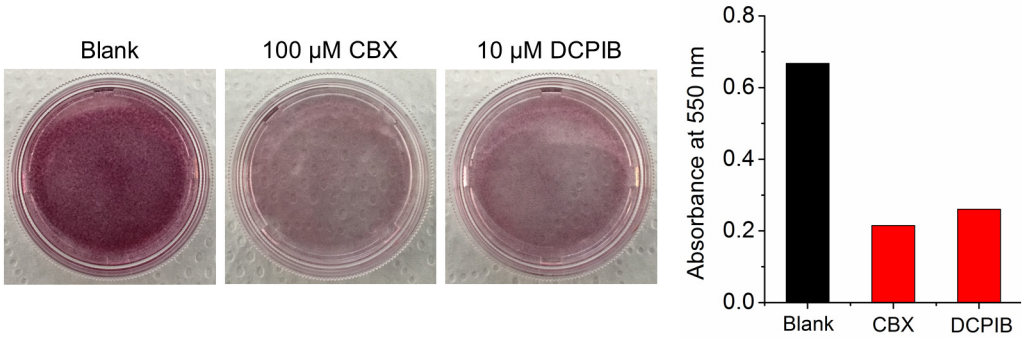

Figure 4.16: VRAC inhibitors suppress osteoblast differentiation of C2C12 cells. Alizarin Red S staining (left) and quantification (right) of C2C12 cells after 8 days in osteogenic differentiation medium with or without drugs. Cetylpyridinium chloride (10%) was used for dye extraction. Data from one trial experiment.

On the other hand, whereas 100 μM CBX significantly reduced the accumulation of triglyceride-containing lipid droplets in 3T3-L1 cells, neither 30 μM DCPIB nor 100 μM NPPB showed any effect, as judged by qualitative and quantitative oil red O staining (Figure 4.17). Notably, DCPIB has been shown to block VRAC currents in adipocytes (Zhang *et al.*, 2017b), while CBX inhibits Pannexin1 (Michalski & Kawate, 2016;

Willebrords *et al*, 2017), which has previously been shown to regulate adipose stromal cell differentiation and fat accumulation *in vivo* (Adamson *et al*, 2015; Lee *et al*, 2018). Therefore, it seems that under the experimental conditions, VRAC channel activity is dispensable for adipocyte differentiation of 3T3-L1 cells.

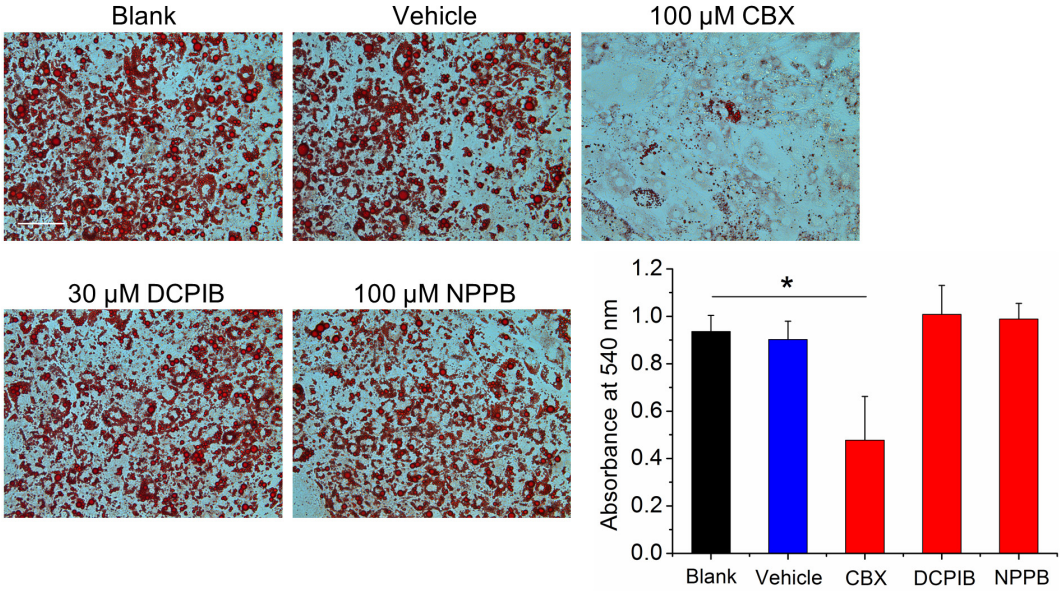

Figure 4.17: Effect of VRAC inhibition on adipogenesis in 3T3-L1 cells. Oil red O staining (left) and quantification (right) after 3T3-L1 adipocyte differentiation experiments with or without drugs. Scale bar, 100 μm. Isopropanol was used for dye extraction. Data are presented as mean ± S.D. from three independent experiments. *, $p < 0.05$ compared with control using a two-tailed unpaired *t*-test.

5. Discussion

5.1 Functional VRAC is required for normal myoblast differentiation

LRRC8A-deficient (*Lrrc8a*$^{-/-}$) mice appear normal at birth, but histological examination revealed significantly thinned skeletal muscle bundles at later ages (Kumar *et al.*, 2014), suggesting that lack of the essential VRAC subunit LRRC8A may lead to dysfunction of myoblast proliferation, differentiation, and/or fusion into multinucleated myotubes. Here, I found that LRRC8A deficiency does not impair the proliferation of C2C12 myoblasts, in agreement with a parallel study in the Stauber lab (Liu & Stauber, 2019). But I uncovered that inhibition of the LRRC8A-containing anion channel VRAC impairs the differentiation and fusion of C2C12 cells. A recently published study by Sah and coworkers (Kumar *et al*, 2020) confirmed my findings. Consistent with my results that knocking down LRRC8A inhibited C2C12 myoblast differentiation and fusion, they reported that LRRC8A (renamed "SWELL1") depletion suppressed the expression of numerous muscle differentiation genes in C2C12 myoblasts and impaired myotube formation of both C2C12 myoblasts and primary satellite cells (Kumar *et al.*, 2020). They also generated skeletal muscle-specific LRRC8A knockout mice by crossing *Lrrc8a*$^{lox/lox}$ mice with *Myf5*-Cre mice. These skeletal muscle-targeted *Lrrc8a* knock-out mice displayed normal muscle mass but significantly decreased myofiber cross-sectional area (Kumar *et al.*, 2020). However, Kumar et al. proposed that the role of LRRC8A in muscle development is due to non-conductive protein-protein interactions (Kumar *et al.*, 2020), rather than VRAC channel activity as found by me. The suggested requirement of LRRC8A-GRB2 physical interaction within the insulin-PI3K-AKT-mTOR pathway, a well-known key regulator of muscle mass and metabolism (Sandri, 2008; Schiaffino *et al*, 2013; Yoon, 2017), is surprising given the normal total skeletal muscle mass of muscle-specific *Lrrc8a*$^{-/-}$ mice (Kumar *et al.*, 2020).

In this work, three main lines of evidence indicate that VRAC conductance contributes to the process of skeletal myogenesis. First, not only pharmacological VRAC inhibitors,

but also VRAC current-suppressing overexpression of LRRC8A (Qiu *et al.*, 2014; Voss *et al.*, 2014), impaired C2C12 myoblast differentiation. Second, the drop in inter-subunit FRET, which mirrors channel opening (König *et al.*, 2019), showed VRAC activity within first two hours of the differentiation process. Third, the observed decrease in $[Cl^-]_i$ during the first hours of differentiation was prevented by the VRAC inhibitor CBX, indicating that the Cl^- efflux is mediated by VRAC. Another clue to explain the discrepancy between studies by me and by Kumar et al. (Kumar *et al.*, 2020) is from *ébouriffé* mice (Lalouette *et al.*, 1996). The spontaneous mouse mutant *ébouriffé* was recently discovered to carry a mutation that truncates the last 15 cytosolic C-terminal leucine-rich repeats of LRRC8A (Platt *et al.*, 2017). Most of the truncated LRRC8A mutants are retained in the ER, so they cannot carry the other LRRC8 subunits (LRRC8B-E) to the plasma membrane (Voss *et al.*, 2014), resulting in drastically reduced, but not completely eliminated, VRAC currents (Platt *et al.*, 2017). Importantly, unlike *Lrrc8a*$^{-/-}$ mice (Kumar *et al.*, 2014) and mice lacking LRRC8A specifically in skeletal muscle (Kumar *et al.*, 2020), *ébouriffé* mice displayed normal striated muscle histology (Platt *et al.*, 2017). This contradicts the notion by Sah and coworkers that LRRC8A modulated insulin-PI3K-AKT signaling via a C-terminal LRR domain-mediated interaction with GRB2 (Kumar *et al.*, 2020; Zhang *et al.*, 2017b). The milder phenotype of *ébouriffé* mice is possibly due to a small residual VRAC current (Behe *et al*, 2017; Platt *et al.*, 2017). In any case, it will be interesting to see how LRRC8A performs both VRAC channel function and protein-protein interactions (if any) during skeletal muscle development.

The molecular mechanism of VRAC activation is still unclear. Experimentally, VRAC is often activated by cell swelling induced by hypotonic stimulation. As cells rarely experience major changes in extracellular osmolarity under normal physiological conditions, cell swelling can be caused by increased intracellular tonicity, such as during transepithelial transport or macromolecular catabolism (Hoffmann *et al.*, 2009; Kang *et al.*, 2018; Lang *et al*, 1998; Stuhlmann *et al.*, 2018). However, multiple pathways seem to exist that can open this channel under isotonic conditions (outlined in section 1.2.2). Furthermore, various intra- and extracellular signaling pathways have been proposed to modulate VRAC activity (Akita & Okada, 2014; Chen *et al.*, 2019b; Okada *et al.*, 2019;

Pedersen *et al.*, 2015; Pedersen *et al.*, 2016). These include the involvement of signaling by integrins (Neveux *et al*, 2010), RhoA (Carton *et al*, 2002), and Ca^{2+} (Hazama & Okada, 1990; Lemonnier *et al*, 2002; Wu *et al*, 1997), which also play important roles in myogenesis (Hindi *et al.*, 2013). Since I uncovered that VRAC is transiently activated within the first hours of myogenic differentiation, a regulatory mechanism of VRAC activity should occur in the very early stage of this process. Intriguingly, the RhoA GTPase is required for the initial myogenic commitment (Wei *et al*, 1998) and must be deactivated before myoblast fusion (Charrasse *et al*, 2006). Store-operated Ca^{2+} channels, key molecules for the hyperpolarization of myoblasts (Darbellay *et al.*, 2009), were shown to strongly regulate VRAC currents in epithelial cells (Lemonnier *et al.*, 2002). The precise mechanism underlying the activation and/or modulation of VRAC during myoblast differentiation remains to be explored.

5.2 LRRC8 proteins may have roles independent of VRAC channel function

VRAC is a plasma membrane channel formed by LRRC8 hetero-hexamers (König & Stauber, 2019; Qiu *et al.*, 2014; Strange *et al.*, 2019; Voss *et al.*, 2014). But as mentioned above, whether LRRC8 proteins carry out functions independent of VRAC deserves further discussion. The LRRC8A protein was first identified in a 17-year-old patient suffering from congenital absence of serum γ-globulins and defective B cell development (Sawada *et al*, 2003). A chromosomal translocation found in this patient led to the heterozygous truncation of LRRC8A (LRRC8A$^{\Delta 91/+35}$), in which the last 91 C-terminal amino acids of LRRC8A were replaced by 35 amino acids encoded by an intron sequence (Sawada *et al.*, 2003). However, the overexpression of LRRC8A$^{\Delta 91/+35}$ had neither dominant-negative nor gain-of-function effect on VRAC currents (Qiu *et al.*, 2014). On the other hand, *Lrrc8a*$^{-/-}$ mice showed only modestly impaired B cell development and B cell function was normal (Kumar *et al.*, 2014). Thus, even if LRRC8A$^{\Delta 91/+35}$ is indeed the cause of the patient's phenotype (Sawada *et al.*, 2003), it does not seem to be related to VRAC channel function.

Before knowing its role as a VRAC subunit, LRRC8C had been identified as a factor for adipocyte differentiation (Tominaga *et al.*, 2004). Its knockdown in 3T3-L1 cells impaired adipocyte differentiation, while its overexpression in NIH-3T3 cells, a cell type that does not usually differentiate into adipocytes, promoted adipogenesis (Tominaga *et al.*, 2004). Consistent with a crucial role in adipogenesis, LRRC8C-deficient mice gained lower body weight and fat content than wild-type mice under a high-fat diet (Hayashi *et al.*, 2011). However, it has been shown that *LRRC8C* disruption does not reduce VRAC currents (Lutter *et al.*, 2017; Voss *et al.*, 2014). Besides, LRRC8C localizes to the ER when expressed alone (Tominaga *et al.*, 2004; Voss *et al.*, 2014), so it seems unlikely that the enhancement of adipocyte differentiation by LRRC8C overexpression is due to its modulation on VRAC properties, such as permeability to organic osmolytes (Lutter *et al.*, 2017; Schober *et al.*, 2017). On the other hand, LRRC8A knockout inhibited adipocyte differentiation of 3T3-F442A cells; and decreased weight gain and lipid content were also observed in mice with adipocyte-specific LRRC8A depletion (Zhang *et al.*, 2017b). These observations indicate that although LRRC8A and LRRC8C are required for adipocyte expansion in the setting of obesity, VRAC channel activity is dispensable. This is in agreement with my data that the VRAC inhibitors DCPIB and NPPB did not affect 3T3-L1 adipocyte differentiation. Furthermore, it was shown that knockdown of LRRC8A inhibits the proliferation and migration of hepatocellular carcinoma cells, while overexpression of LRRC8A significantly induces cell proliferation and migration (Lu *et al.*, 2019). But overexpression of LRRC8A rather decreases VRAC currents like its knockdown (Qiu *et al.*, 2014; Voss *et al.*, 2014). Therefore, it seems that LRRC8 proteins do have roles independent of VRAC channel function.

Intriguingly, two different – mutually exclusive – ways in which the LRRC8A protein participates in PI3K-AKT signaling have been proposed (Kumar *et al.*, 2014; Zhang *et al.*, 2017b). Although it has been established that both the amino and carboxyl termini of LRRC8 proteins are cytoplasmic (Abascal & Zardoya, 2012; Lee *et al.*, 2014; Qiu *et al.*, 2014; Voss *et al.*, 2014), Geha and coworkers suggested that a fraction of LRRC8A is present in the cell membrane with an opposite topology (Kumar *et al.*, 2014; Platt *et al.*, 2017). They proposed that the putative LRRC8A ligand binds to the then extracellular C-

terminal LRR domain, thereby activating the interaction between GRB2 and the proline-rich region in an intracellular loop of LRRC8A, resulting in AKT phosphorylation and thymocyte survival (Kumar *et al.*, 2014). In contrast, Sah and coworkers asserted that LRRC8A interacts with GRB2 through the cytoplasmic LRR domain to regulate insulin-PI3K-AKT2 signaling during adipocyte expansion (Zhang *et al.*, 2017b). Moreover, since its overexpression and siRNA-mediated knockdown led to changes in ER Ca^{2+} dynamics in HEK cells, LRRC8B was proposed to act as a Ca^{2+} release channel in the ER (Ghosh *et al.*, 2017). However, it should be noted that in this study, endogenous LRRC8B was identified in the ER but not in the plasma membrane (Ghosh *et al.*, 2017). This is in contrast with the reported plasma membrane localization of LRRC8B co-expressed with LRRC8A (Voss *et al.*, 2014), which has been confirmed in a recent proteomics study (Orre *et al*, 2019).

Obviously, a lot of extra work is needed to determine whether LRRC8 proteins play physiological and/or pathological roles independent of VRAC in different cells and tissues, and more importantly, to clarify the relationship between VRAC and VRAC-independent functions.

5.3 VRAC promotes myoblast hyperpolarization

Proliferating, undifferentiated myoblasts are very depolarized cells. An early event in the differentiation process of human myoblasts is a hyperpolarization of the resting membrane potential, which involves a two-step mechanism. Firstly, an *ether-à-go-go* K^+ current is expressed and rapidly drives the membrane potential of myoblasts from –8 mV to about –32 mV (Bernheim *et al.*, 1996; Bijlenga *et al.*, 1998; Liu *et al.*, 1998), coinciding with a cell-cycle arrest (Timchenko *et al.*, 2001; Walsh & Perlman, 1997). Subsequently, the activation of an inward-rectifying K^+ channel Kir2.1 further hyperpolarizes myoblasts to approximately –74 mV (Fischer-Lougheed *et al.*, 2001; Liu *et al.*, 1998; Liu *et al.*, 2003). It has been shown that the Kir2.1 current density of human myoblasts reaches its maximum already after six hours of cell differentiation (Hinard *et al.*, 2008; Konig *et al.*, 2004). The hyperpolarized resting membrane potential of about

−75 mV was reported for differentiating C2C12 myoblasts (Pietrangelo *et al.*, 2006), as I also observed here both by a potentiometric fluorescent probe and by electrophysiological recordings (done by Dr. Thorsten M. Becker from the AG Koch, FU Berlin). I found that differentiating myoblasts treated with VRAC inhibitors does not fully hyperpolarize but remain at an intermediate resting potential. Besides, I was able to show temporary VRAC activation within the first two hours of myoblast differentiation. These data determine a function of VRAC before that of Kir2.1. Consistent with a role of VRAC in the early phase of myogenic differentiation, volume-activated Cl^- currents have been shown to drastically decrease during myotube formation of C2C12 cells (Voets *et al*, 1997). I also observed significantly downregulated expression of LRRC8C and LRRC8E after two days of cell differentiation. Correspondingly, the combined disruption of *LRRC8C* and *LRRC8E* robustly reduces VRAC currents (Lutter *et al.*, 2017; Voss *et al.*, 2014).

The anion channel VRAC is associated with membrane depolarization in some familiar situations (Hoffmann *et al.*, 2009; Jentsch, 2016; Nilius & Droogmans, 2001), for example, during pancreatic insulin secretion where its activity triggers the early opening of voltage-dependent Ca^{2+} channels (Kang *et al.*, 2018; Stuhlmann *et al.*, 2018). But I demonstrated here that VRAC contributes to membrane hyperpolarization. How could VRAC be linked with hyperpolarization? I found that proliferating, undifferentiated C2C12 myoblasts possess a surprisingly high, but actually not unprecedented (Kaneko *et al*, 2001; Kim *et al*, 2015), intracellular Cl^- concentration of approximately 80 mM. Under cell culture conditions (external $[Cl^-]$ at around 120 mM), the reversal potential for Cl^- calculated from the Nernst Equation is at approximately −10 mV. During the sequential hyperpolarization of myoblasts from about −10 mV to about −80 mV (Hinard *et al.*, 2008; Konig *et al.*, 2004; Liu *et al.*, 1998; Liu *et al.*, 2003) (myoblasts rested at an intermediate potential when VRAC was inhibited), VRAC will mediate the efflux of Cl^- and cause the observed $[Cl^-]_i$ decrease. Hence, Cl^- conductance by VRAC cannot directly lead to myoblast hyperpolarization. Instead, VRAC may indirectly affect the membrane potential, most likely by regulating the activity of Kir2.1 K^+ channels. It has been shown that Kir2.1 activation during initial myoblast differentiation is not due to new channel synthesis or transport to the plasma membrane, but a tyrosine dephosphorylation (Hinard

et al., 2008). Changes in cytosolic Cl^- may thus control myogenesis by modulating (de)-phosphorylation events. There are several examples where the activity of kinases or phosphatases is dependent on Cl^- (Chen *et al*, 2019a; Hjörleifsson & Ásgeirsson, 2017; Pederson *et al*, 1998; Piala *et al*, 2014). Cytoplasmic Cl^- has also been implicated in other intracellular processes related to cell differentiation, such as endocytic trafficking (Stauber & Jentsch, 2013) and plasma membrane remodeling (He *et al*, 2017). On the other hand, it is also possible that not the actual Cl^- decrease, but the movement of Cl^- is crucial for the hyperpolarization to proceed. In this case, "side-products" of VRAC activity, such as changes in intracellular osmolarity, intracellular pH, membrane tension, or plasma membrane voltage (Hoffmann *et al.*, 2009; Jentsch, 2016), may be important signals.

Emerging evidence supports the necessary role of membrane hyperpolarization in stem cell differentiation (Levin *et al*, 2017; Sundelacruz *et al*, 2009; Vitali *et al*, 2018; Yang & Brackenbury, 2013). Consistent with the notion that VRAC may have a general role in the regulation of cell differentiation, I found that inhibition of VRAC impairs osteogenic differentiation, which also involves both cellular hyperpolarization (Sundelacruz *et al*, 2008) and Kir2.1 activity (Sacco *et al*, 2015). However, as discussed in section 5.2, I conclude that VRAC activity is dispensable for 3T3-L1 adipocyte differentiation. It has been reported that human mesenchymal stem cells undergo hyperpolarization during adipogenic differentiation (Sundelacruz *et al.*, 2008). But 3T3-L1 cells possess a similar plasma membrane potential to primary white fat adipocytes (Bentley *et al*, 2014). Therefore, even if VRAC is not important in "obesogenic" adipogenesis, it cannot be ruled out that VRAC may have functions in the process of cell fate determination from mesenchymal stem cells to adipocytes. It will be interesting to see whether and how VRAC plays a role in cell differentiation processes other than skeletal myogenesis.

5.4 Possible role of intracellular chloride in myoblast fusion

As the most abundant anion in nature, the chloride ion Cl^- has been increasingly recognized as a signaling effector or second messenger in the regulation of various

cellular functions (Duran *et al*, 2010; Stauber & Jentsch, 2013; Valdivieso Á & Santa-Coloma, 2019). I found that despite the significant $[Cl^-]_i$ decrease accompanying myotube formation, an excessive reduction resulted from extracellular Cl^- depletion does not accelerate myoblast differentiation but rather blocks fusion. This suggests that only a moderate decrease in intracellular Cl^- facilitates all steps of myogenesis. Myoblast fusion involves a complex system of regulatory signaling pathways (Hindi *et al.*, 2013; Sampath *et al.*, 2018), which may require a proper intracellular Cl^- content. Intriguingly, it was shown that the Na^+-K^+-2Cl^- cotransporter NKCC1 (a protein that actively transports Na^+, K^+, and Cl^- into cells) is upregulated during myotube formation; and inhibition of it suppresses myoblast fusion and exercise-induced muscle hypertrophy (Mandai *et al.*, 2017). The importance of an efficient Cl^- homeostasis in skeletal muscle is also supported by a chloride channel disease (myotonia congenita) characterized by muscle paralysis and hyperexcitability (Imbrici *et al*, 2015; Tang & Chen, 2011). The role of cytoplasmic Cl^- in different stages of skeletal myogenesis, if any, remains to be explored.

5.5 Conclusions and outlook

In summary, I uncovered an unexpected new role of LRRC8/VRAC channels in myogenic differentiation. I could show that LRRC8/VRAC channels facilitates myoblast differentiation by contributing to membrane hyperpolarization and intracellular Ca^{2+} signals. I identified the activation of VRAC as an early molecular event during myotube formation and an accompanied decrease in intracellular Cl^-. Additionally, I clarified a correlation between $[Cl^-]_i$ and myoblast fusion. My work provides a new perspective for understanding the signal transduction pathways in skeletal myogenesis and highlights the importance of a Cl^- anion and osmolyte channel in cell differentiation.

Future investigations should focus on elucidating the precise mechanism of VRAC activation/modulation and its contribution to membrane hyperpolarization. Furthermore, whether VRAC also transiently activates and promotes myogenic differentiation of satellite cells during muscle regeneration and whether it plays a role in other cell differentiation processes, such as osteogenic differentiation, deserve to be determined.

Apart from the essential subunit LRRC8A, particular attention should be paid to specific LRRC8 subunit compositions. Owing to the recent progress in the establishment of a non-invasive FRET sensor for VRAC activity, it is now possible to monitor temporary activation of these ubiquitously expressed channels during cell physiological processes *in situ*.

References

Abascal F, Zardoya R (2012) LRRC8 proteins share a common ancestor with pannexins, and may form hexameric channels involved in cell-cell communication. *Bioessays* 34: 551-560

Adamson SE, Meher AK, Chiu YH, Sandilos JK, Oberholtzer NP, Walker NN, Hargett SR, Seaman SA, Peirce-Cottler SM, Isakson BE *et al* (2015) Pannexin 1 is required for full activation of insulin-stimulated glucose uptake in adipocytes. *Mol Metab* 4: 610-618

Afzali AM, Ruck T, Herrmann AM, Iking J, Sommer C, Kleinschnitz C, Preubetae C, Stenzel W, Budde T, Wiendl H *et al* (2016) The potassium channels TASK2 and TREK1 regulate functional differentiation of murine skeletal muscle cells. *Am J Physiol Cell Physiol* 311: C583-c595

Akita T, Fedorovich SV, Okada Y (2011) Ca^{2+} nanodomain-mediated component of swelling-induced volume-sensitive outwardly rectifying anion current triggered by autocrine action of ATP in mouse astrocytes. *Cell Physiol Biochem* 28: 1181-1190

Akita T, Okada Y (2014) Characteristics and roles of the volume-sensitive outwardly rectifying (VSOR) anion channel in the central nervous system. *Neuroscience* 275: 211-231

Antigny F, Koenig S, Bernheim L, Frieden M (2013) During post-natal human myogenesis, normal myotube size requires TRPC1- and TRPC4-mediated Ca^{2+} entry. *J Cell Sci* 126: 2525-2533

Antigny F, Konig S, Bernheim L, Frieden M (2014) Inositol 1,4,5 trisphosphate receptor 1 is a key player of human myoblast differentiation. *Cell Calcium* 56: 513-521

Antigny F, Sabourin J, Saüc S, Bernheim L, Koenig S, Frieden M (2017) TRPC1 and TRPC4 channels functionally interact with STIM1L to promote myogenesis and maintain fast repetitive Ca^{2+} release in human myotubes. *Biochim Biophys Acta Mol Cell Res* 1864: 806-813

Araya R, Eckardt D, Maxeiner S, Krüger O, Theis M, Willecke K, Sáez JC (2005) Expression of connexins during differentiation and regeneration of skeletal muscle: functional relevance of connexin43. *J Cell Sci* 118: 27-37

Araya R, Eckardt D, Riquelme MA, Willecke K, Sáez JC (2003) Presence and importance of connexin43 during myogenesis. *Cell Commun Adhes* 10: 451-456

Araya R, Riquelme MA, Brandan E, Sáez JC (2004) The formation of skeletal muscle myotubes requires functional membrane receptors activated by extracellular ATP. *Brain Res Brain Res Rev* 47: 174-188

Arnaudeau S, Holzer N, Konig S, Bader CR, Bernheim L (2006) Calcium sources used by post-natal human myoblasts during initial differentiation. *J Cell Physiol* 208: 435-445

Ashcroft FM, Rorsman P (2013) K_{ATP} channels and islet hormone secretion: new insights and controversies. *Nat Rev Endocrinol* 9: 660-669

Bao J, Perez CJ, Kim J, Zhang H, Murphy CJ, Hamidi T, Jaubert J, Platt CD, Chou J, Deng M *et al* (2018) Deficient LRRC8A-dependent volume-regulated anion channel activity is associated with male infertility in mice. *JCI insight* 3

Behe P, Foote JR, Levine AP, Platt CD, Chou J, Benavides F, Geha RS, Segal AW (2017) The

LRRC8A Mediated "Swell Activated" Chloride Conductance Is Dispensable for Vacuolar Homeostasis in Neutrophils. *Front Pharmacol* 8: 262

Bella J, Hindle KL, McEwan PA, Lovell SC (2008) The leucine-rich repeat structure. *Cell Mol Life Sci* 65: 2307-2333

Benfenati V, Caprini M, Nicchia GP, Rossi A, Dovizio M, Cervetto C, Nobile M, Ferroni S (2009) Carbenoxolone inhibits volume-regulated anion conductance in cultured rat cortical astroglia. *Channels* 3: 323-336

Bentley DC, Pulbutr P, Chan S, Smith PA (2014) Etiology of the membrane potential of rat white fat adipocytes. *Am J Physiol Endocrinol Metab* 307: E161-175

Bentzinger CF, Wang YX, Rudnicki MA (2012) Building muscle: molecular regulation of myogenesis. *Cold Spring Harb Perspect Biol* 4

Bernheim L, Bader CR (2002) Human myoblast differentiation: Ca^{2+} channels are activated by K^+ channels. *News Physiol Sci* 17: 22-26

Bernheim L, Liu JH, Hamann M, Haenggeli CA, Fischer-Lougheed J, Bader CR (1996) Contribution of a non-inactivating potassium current to the resting membrane potential of fusion-competent human myoblasts. *J Physiol* 493 (Pt 1): 129-141

Best L, Brown PD (2009) Studies of the mechanism of activation of the volume-regulated anion channel in rat pancreatic beta-cells. *J Membr Biol* 230: 83-91

Best L, Brown PD, Sener A, Malaisse WJ (2010) Electrical activity in pancreatic islet cells: The VRAC hypothesis. *Islets* 2: 59-64

Bi P, Ramirez-Martinez A, Li H, Cannavino J, McAnally JR, Shelton JM, Sánchez-Ortiz E, Bassel-Duby R, Olson EN (2017) Control of muscle formation by the fusogenic micropeptide myomixer. *Science* 356: 323-327

Bidaud I, Monteil A, Nargeot J, Lory P (2006) Properties and role of voltage-dependent calcium channels during mouse skeletal muscle differentiation. *J Muscle Res Cell Motil* 27: 75-81

Bijlenga P, Liu JH, Espinos E, Haenggeli CA, Fischer-Lougheed J, Bader CR, Bernheim L (2000) T-type a1H Ca^{2+} channels are involved in Ca^{2+} signaling during terminal differentiation (fusion) of human myoblasts. *Proc Natl Acad Sci USA* 97: 7627-7632

Bijlenga P, Occhiodoro T, Liu JH, Bader CR, Bernheim L, Fischer-Lougheed J (1998) An *ether-à-go-go* K^+ current, $I_{h\text{-}eag}$, contributes to the hyperpolarization of human fusion-competent myoblasts. *J Physiol* 512 (Pt 2): 317-323

Bortner CD, Cidlowski JA (1998) A necessary role for cell shrinkage in apoptosis. *Biochem Pharmacol* 56: 1549-1559

Braun T, Gautel M (2011) Transcriptional mechanisms regulating skeletal muscle differentiation, growth and homeostasis. *Nat Rev Mol Cell Biol* 12: 349-361

Brouwers EE, Tibben MM, Rosing H, Hillebrand MJ, Joerger M, Schellens JH, Beijnen JH (2006) Sensitive inductively coupled plasma mass spectrometry assay for the determination of platinum originating from cisplatin, carboplatin, and oxaliplatin in human plasma ultrafiltrate. *J Mass Spectrom* 41: 1186-1194

Buckingham M, Rigby PW (2014) Gene regulatory networks and transcriptional mechanisms that control myogenesis. *Dev Cell* 28: 225-238

Burow P, Klapperstück M, Markwardt F (2015) Activation of ATP secretion via volume-

regulated anion channels by sphingosine-1-phosphate in RAW macrophages. *Pflügers Arch* 467: 1215-1226

Bykova EA, Zhang XD, Chen TY, Zheng J (2006) Large movement in the C terminus of CLC-0 chloride channel during slow gating. *Nat Struct Mol Biol* 13: 1115-1119

Cannon CL, Basavappa S, Strange K (1998) Intracellular ionic strength regulates the volume sensitivity of a swelling-activated anion channel. *Am J Physiol* 275: C416-422

Capó-Aponte JE, Iserovich P, Reinach PS (2005) Characterization of regulatory volume behavior by fluorescence quenching in human corneal epithelial cells. *J Membr Biol* 207: 11-22

Carton I, Trouet D, Hermans D, Barth H, Aktories K, Droogmans G, Jorgensen NK, Hoffmann EK, Nilius B, Eggermont J (2002) RhoA exerts a permissive effect on volume-regulated anion channels in vascular endothelial cells. *Am J Physiol Cell Physiol* 283: C115-125

Chal J, Pourquié O (2017) Making muscle: skeletal myogenesis in vivo and in vitro. *Development* 144: 2104-2122

Charrasse S, Comunale F, Grumbach Y, Poulat F, Blangy A, Gauthier-Rouvière C (2006) RhoA GTPase regulates M-cadherin activity and myoblast fusion. *Mol Biol Cell* 17: 749-759

Chen JC, Lo YF, Lin YW, Lin SH, Huang CL, Cheng CJ (2019a) WNK4 kinase is a physiological intracellular chloride sensor. *Proc Natl Acad Sci USA* 116: 4502-4507

Chen L, König B, Liu T, Pervaiz S, Razzaque YS, Stauber T (2019b) More than just a pressure relief valve: physiological roles of volume-regulated LRRC8 anion channels. *Biol Chem* 400: 1481-1496

Choi H, Ettinger N, Rohrbough J, Dikalova A, Nguyen HN, Lamb FS (2016) LRRC8A channels support TNFα-induced superoxide production by Nox1 which is required for receptor endocytosis. *Free Radic Biol Med* 101: 413-423

Choi JH, Jeong SY, Oh MR, Allen PD, Lee EH (2020) TRPCs: Influential Mediators in Skeletal Muscle. *Cells* 9

Constantin B, Cognard C, Raymond G (1996) Myoblast fusion requires cytosolic calcium elevation but not activation of voltage-dependent calcium channels. *Cell Calcium* 19: 365-374

Cooper TG, Yeung CH, Wagenfeld A, Nieschlag E, Poutanen M, Huhtaniemi I, Sipilä P (2004) Mouse models of infertility due to swollen spermatozoa. *Mol Cell Endocrinol* 216: 55-63

Dall'Asta V, Gatti R, Orlandini G, Rossi PA, Rotoli BM, Sala R, Bussolati O, Gazzola GC (1997) Membrane potential changes visualized in complete growth media through confocal laser scanning microscopy of bis-oxonol-loaded cells. *Exp Cell Res* 231: 260-268

Darbellay B, Arnaudeau S, Ceroni D, Bader CR, Konig S, Bernheim L (2010) Human muscle economy myoblast differentiation and excitation-contraction coupling use the same molecular partners, STIM1 and STIM2. *J Biol Chem* 285: 22437-22447

Darbellay B, Arnaudeau S, König S, Jousset H, Bader C, Demaurex N, Bernheim L (2009) STIM1- and Orai1-dependent store-operated calcium entry regulates human myoblast differentiation. *J Biol Chem* 284: 5370-5380

Decher N, Lang HJ, Nilius B, Bruggemann A, Busch AE, Steinmeyer K (2001) DCPIB is a novel selective blocker of $I_{Cl,swell}$ and prevents swelling-induced shortening of guinea-pig

atrial action potential duration. *Br J Pharmacol* 134: 1467-1479

Deneka D, Sawicka M, Lam AKM, Paulino C, Dutzler R (2018) Structure of a volume-regulated anion channel of the LRRC8 family. *Nature* 558: 254-259

Deng W, Baki L, Baumgarten CM (2010) Endothelin signalling regulates volume-sensitive Cl^- current via NADPH oxidase and mitochondrial reactive oxygen species. *Cardiovasc Res* 88: 93-100

Deng W, Mahajan R, Baumgarten CM, Logothetis DE (2016) The ICl,swell inhibitor DCPIB blocks Kir channels that possess weak affinity for PIP2. *Pflügers Arch* 468: 817-824

Diaz RJ, Hinek A, Wilson GJ (2010) Direct evidence of chloride ion efflux in ischaemic and pharmacological preconditioning of cultured cardiomyocytes. *Cardiovasc Res* 87: 545-551

Donzelli E, Lucchini C, Ballarini E, Scuteri A, Carini F, Tredici G, Miloso M (2011) ERK1 and ERK2 are involved in recruitment and maturation of human mesenchymal stem cells induced to adipogenic differentiation. *J Mol Cell Biol* 3: 123-131

Dunn PJ, Salm EJ, Tomita S (2020) ABC transporters control ATP release through cholesterol-dependent volume-regulated anion channel activity. *J Biol Chem* 295: 5192-5203

Duran C, Thompson CH, Xiao Q, Hartzell HC (2010) Chloride channels: often enigmatic, rarely predictable. *Annu Rev Physiol* 72: 95-121

Elorza-Vidal X, Gaitán-Peñas H, Estévez R (2019) Chloride Channels in Astrocytes: Structure, Roles in Brain Homeostasis and Implications in Disease. *Int J Mol Sci* 20

Emma F, McManus M, Strange K (1997) Intracellular electrolytes regulate the volume set point of the organic osmolyte/anion channel VSOAC. *Am J Physiol* 272: C1766-1775

Epps DE, Wolfe ML, Groppi V (1994) Characterization of the steady-state and dynamic fluorescence properties of the potential-sensitive dye bis-(1,3-dibutylbarbituric acid)trimethine oxonol ($Dibac_4(3)$) in model systems and cells. *Chem Phys Lipids* 69: 137-150

Feige JN, Sage D, Wahli W, Desvergne B, Gelman L (2005) PixFRET, an ImageJ plug-in for FRET calculation that can accommodate variations in spectral bleed-throughs. *Microsc Res Tech* 68: 51-58

Fennelly C, Soker S (2019) Bioelectric Properties of Myogenic Progenitor Cells. *Bioelectricity* 1: 35-45

Fennelly C, Wang Z, Criswell T, Soker S (2016) Sustained Depolarization of the Resting Membrane Potential Regulates Muscle Progenitor Cell Growth and Maintains Stem Cell Properties In Vitro. *Stem Cell Rev Rep* 12: 634-644

Fioretti B, Pietrangelo T, Catacuzzeno L, Franciolini F (2005) Intermediate-conductance Ca^{2+}-activated K^+ channel is expressed in C2C12 myoblasts and is downregulated during myogenesis. *Am J Physiol Cell Physiol* 289: C89-96

Fischer-Lougheed J, Liu JH, Espinos E, Mordasini D, Bader CR, Belin D, Bernheim L (2001) Human myoblast fusion requires expression of functional inward rectifier Kir2.1 channels. *J Cell Biol* 153: 677-686

Formaggio F, Saracino E, Mola MG, Rao SB, Amiry-Moghaddam M, Muccini M, Zamboni R, Nicchia GP, Caprini M, Benfenati V (2019) LRRC8A is essential for swelling-activated chloride current and for regulatory volume decrease in astrocytes. *FASEB J* 33: 101-113

Formigli L, Meacci E, Sassoli C, Squecco R, Nosi D, Chellini F, Naro F, Francini F, Zecchi-Orlandini S (2007) Cytoskeleton/stretch-activated ion channel interaction regulates myogenic differentiation of skeletal myoblasts. *J Cell Physiol* 211: 296-306

Formigli L, Sassoli C, Squecco R, Bini F, Martinesi M, Chellini F, Luciani G, Sbrana F, Zecchi-Orlandini S, Francini F *et al* (2009) Regulation of transient receptor potential canonical channel 1 (TRPC1) by sphingosine 1-phosphate in C2C12 myoblasts and its relevance for a role of mechanotransduction in skeletal muscle differentiation. *J Cell Sci* 122: 1322-1333

Friard J, Corinus A, Cougnon M, Tauc M, Pisani DF, Duranton C, Rubera I (2019) LRRC8/VRAC channels exhibit a noncanonical permeability to glutathione, which modulates epithelial-to-mesenchymal transition (EMT). *Cell Death and Disease* 10: 925

Friard J, Tauc M, Cougnon M, Compan V, Duranton C, Rubera I (2017) Comparative Effects of Chloride Channel Inhibitors on LRRC8/VRAC-Mediated Chloride Conductance. *Front Pharmacol* 8: 328

Gaitán-Peñas H, Gradogna A, Laparra-Cuervo L, Solsona C, Fernández-Dueñas V, Barrallo-Gimeno A, Ciruela F, Lakadamyali M, Pusch M, Estévez R (2016) Investigation of LRRC8-Mediated Volume-Regulated Anion Currents in Xenopus Oocytes. *Biophys J* 111: 1429-1443

Galietta LJ, Haggie PM, Verkman AS (2001) Green fluorescent protein-based halide indicators with improved chloride and iodide affinities. *FEBS Lett* 499: 220-224

Ghosh A, Khandelwal N, Kumar A, Bera AK (2017) Leucine-rich repeat-containing 8B protein is associated with the endoplasmic reticulum Ca^{2+} leak in HEK293 cells. *J Cell Sci* 130: 3818-3828

Gradogna A, Gaitán-Peñas H, Boccaccio A, Estévez R, Pusch M (2017a) Cisplatin activates volume sensitive LRRC8 channel mediated currents in Xenopus oocytes. *Channels* 11: 254-260

Gradogna A, Gavazzo P, Boccaccio A, Pusch M (2017b) Subunit-dependent oxidative stress sensitivity of LRRC8 volume-regulated anion channels. *J Physiol* 595: 6719-6733

Gregory CA, Gunn WG, Peister A, Prockop DJ (2004) An Alizarin red-based assay of mineralization by adherent cells in culture: comparison with cetylpyridinium chloride extraction. *Anal Biochem* 329: 77-84

Grinstein S, Clarke CA, Dupre A, Rothstein A (1982) Volume-induced increase of anion permeability in human lymphocytes. *J Gen Physiol* 80: 801-823

Hayashi T, Nozaki Y, Nishizuka M, Ikawa M, Osada S, Imagawa M (2011) Factor for adipocyte differentiation 158 gene disruption prevents the body weight gain and insulin resistance induced by a high-fat diet. *Biol Pharm Bull* 34: 1257-1263

Hazama A, Okada Y (1988) Ca^{2+} sensitivity of volume-regulatory K^+ and Cl^- channels in cultured human epithelial cells. *J Physiol* 402: 687-702

Hazama A, Okada Y (1990) Involvement of Ca^{2+}-induced Ca^{2+} release in the volume regulation of human epithelial cells exposed to a hypotonic medium. *Biochem Biophys Res Commun* 167: 287-293

He M, Ye W, Wang WJ, Sison ES, Jan YN, Jan LY (2017) Cytoplasmic Cl(-) couples membrane remodeling to epithelial morphogenesis. *Proc Natl Acad Sci USA* 114: E11161-e11169

Hinard V, Belin D, Konig S, Bader CR, Bernheim L (2008) Initiation of human myoblast differentiation via dephosphorylation of Kir2.1 K^+ channels at tyrosine 242. *Development* 135: 859-867

Hindi SM, Tajrishi MM, Kumar A (2013) Signaling mechanisms in mammalian myoblast fusion. *Sci Signal* 6: re2

Hjörleifsson JG, Ásgeirsson B (2017) pH-Dependent Binding of Chloride to a Marine Alkaline Phosphatase Affects the Catalysis, Active Site Stability, and Dimer Equilibrium. *Biochemistry* 56: 5075-5089

Hoffmann EK, Lambert IH, Pedersen SF (2009) Physiology of cell volume regulation in vertebrates. *Physiol Rev* 89: 193-277

Hoffmann EK, Simonsen LO, Lambert IH (1984) Volume-induced increase of K^+ and Cl^- permeabilities in Ehrlich ascites tumor cells. Role of internal Ca^{2+}. *J Membr Biol* 78: 211-222

Hyzinski-García MC, Rudkouskaya A, Mongin AA (2014) LRRC8A protein is indispensable for swelling-activated and ATP-induced release of excitatory amino acids in rat astrocytes. *J Physiol* 592: 4855-4862

Iannotti FA, Barrese V, Formisano L, Miceli F, Taglialatela M (2013) Specification of skeletal muscle differentiation by repressor element-1 silencing transcription factor (REST)-regulated $K_v7.4$ potassium channels. *Mol Biol Cell* 24: 274-284

Iannotti FA, Panza E, Barrese V, Viggiano D, Soldovieri MV, Taglialatela M (2010) Expression, localization, and pharmacological role of K_v7 potassium channels in skeletal muscle proliferation, differentiation, and survival after myotoxic insults. *J Pharmacol Exp Ther* 332: 811-820

Iannotti FA, Silvestri C, Mazzarella E, Martella A, Calvigioni D, Piscitelli F, Ambrosino P, Petrosino S, Czifra G, Biro T *et al* (2014) The endocannabinoid 2-AG controls skeletal muscle cell differentiation via CB1 receptor-dependent inhibition of K_v7 channels. *Proc Natl Acad Sci USA* 111: E2472-2481

Imbrici P, Altamura C, Pessia M, Mantegazza R, Desaphy JF, Camerino DC (2015) ClC-1 chloride channels: state-of-the-art research and future challenges. *Front Cell Neurosci* 9: 156

Ise T, Shimizu T, Lee EL, Inoue H, Kohno K, Okada Y (2005) Roles of volume-sensitive Cl^- channel in cisplatin-induced apoptosis in human epidermoid cancer cells. *J Membr Biol* 205: 139-145

Jackson PS, Morrison R, Strange K (1994) The volume-sensitive organic osmolyte-anion channel VSOAC is regulated by nonhydrolytic ATP binding. *Am J Physiol* 267: C1203-1209

Jentsch TJ (2016) VRACs and other ion channels and transporters in the regulation of cell volume and beyond. *Nat Rev Mol Cell Biol* 17: 293-307

Jentsch TJ, Lutter D, Planells-Cases R, Ullrich F, Voss FK (2016) VRAC: molecular identification as LRRC8 heteromers with differential functions. *Pflügers Arch* 468: 385-393

Jiang X, Sorkin A (2002) Coordinated traffic of Grb2 and Ras during epidermal growth factor

receptor endocytosis visualized in living cells. *Mol Biol Cell* 13: 1522-1535

Jousset H, Frieden M, Demaurex N (2007) STIM1 knockdown reveals that store-operated Ca^{2+} channels located close to sarco/endoplasmic Ca^{2+} ATPases (SERCA) pumps silently refill the endoplasmic reticulum. *J Biol Chem* 282: 11456-11464

Kaneko H, Nakamura T, Lindemann B (2001) Noninvasive measurement of chloride concentration in rat olfactory receptor cells with use of a fluorescent dye. *Am J Physiol Cell Physiol* 280: C1387-1393

Kang C, Xie L, Gunasekar SK, Mishra A, Zhang Y, Pai S, Gao Y, Kumar A, Norris AW, Stephens SB *et al* (2018) SWELL1 is a glucose sensor regulating β-cell excitability and systemic glycaemia. *Nat Commun* 9: 367

Kang JS, Krauss RS (2010) Muscle stem cells in developmental and regenerative myogenesis. *Curr Opin Clin Nutr Metab Care* 13: 243-248

Kasuya G, Nakane T, Yokoyama T, Jia Y, Inoue M, Watanabe K, Nakamura R, Nishizawa T, Kusakizako T, Tsutsumi A *et al* (2018) Cryo-EM structures of the human volume-regulated anion channel LRRC8. *Nat Struct Mol Biol* 25: 797-804

Katagiri T, Yamaguchi A, Komaki M, Abe E, Takahashi N, Ikeda T, Rosen V, Wozney JM, Fujisawa-Sehara A, Suda T (1994) Bone morphogenetic protein-2 converts the differentiation pathway of C2C12 myoblasts into the osteoblast lineage. *J Cell Biol* 127: 1755-1766

Kefauver JM, Saotome K, Dubin AE, Pallesen J, Cottrell CA, Cahalan SM, Qiu Z, Hong G, Crowley CS, Whitwam T *et al* (2018) Structure of the human volume regulated anion channel. *eLife* 7

Kern DM, Oh S, Hite RK, Brohawn SG (2019) Cryo-EM structures of the DCPIB-inhibited volume-regulated anion channel LRRC8A in lipid nanodiscs. *eLife* 8

Kim S, Ma L, Unruh J, McKinney S, Yu CR (2015) Intracellular chloride concentration of the mouse vomeronasal neuron. *BMC Neurosci* 16: 90

Klausen TK, Bergdahl A, Hougaard C, Christophersen P, Pedersen SF, Hoffmann EK (2007) Cell cycle-dependent activity of the volume- and Ca^{2+}-activated anion currents in Ehrlich lettre ascites cells. *J Cell Physiol* 210: 831-842

König B, Hao Y, Schwartz S, Plested AJ, Stauber T (2019) A FRET sensor of C-terminal movement reveals VRAC activation by plasma membrane DAG signaling rather than ionic strength. *eLife* 8

König B, Stauber T (2019) Biophysics and Structure-Function Relationships of LRRC8-Formed Volume-Regulated Anion Channels. *Biophys J* 116: 1185-1193

Konig S, Béguet A, Bader CR, Bernheim L (2006) The calcineurin pathway links hyperpolarization (Kir2.1)-induced Ca^{2+} signals to human myoblast differentiation and fusion. *Development* 133: 3107-3114

Konig S, Hinard V, Arnaudeau S, Holzer N, Potter G, Bader CR, Bernheim L (2004) Membrane hyperpolarization triggers myogenin and myocyte enhancer factor-2 expression during human myoblast differentiation. *J Biol Chem* 279: 28187-28196

Krause RM, Hamann M, Bader CR, Liu JH, Baroffio A, Bernheim L (1995) Activation of nicotinic acetylcholine receptors increases the rate of fusion of cultured human myoblasts.

J Physiol 489 (Pt 3): 779-790

Kubo Y (1991) Comparison of initial stages of muscle differentiation in rat and mouse myoblastic and mouse mesodermal stem cell lines. *J Physiol* 442: 743-759

Kubota K, Kim JY, Sawada A, Tokimasa S, Fujisaki H, Matsuda-Hashii Y, Ozono K, Hara J (2004) LRRC8 involved in B cell development belongs to a novel family of leucine-rich repeat proteins. *FEBS Lett* 564: 147-152

Kumar A, Xie L, Ta CM, Hinton AO, Gunasekar SK, Minerath RA, Shen K, Maurer JM, Grueter CE, Abel ED *et al* (2020) SWELL1 regulates skeletal muscle cell size, intracellular signaling, adiposity and glucose metabolism. *eLife* 9

Kumar L, Chou J, Yee CS, Borzutzky A, Vollmann EH, von Andrian UH, Park SY, Hollander G, Manis JP, Poliani PL *et al* (2014) Leucine-rich repeat containing 8A (LRRC8A) is essential for T lymphocyte development and function. *J Exp Med* 211: 929-942

Kunzelmann K (2016) Ion channels in regulated cell death. *Cell Mol Life Sci* 73: 2387-2403

Kurosaka M, Ogura Y, Funabashi T, Akema T (2016) Involvement of Transient Receptor Potential Cation Channel Vanilloid 1 (TRPV1) in Myoblast Fusion. *J Cell Physiol* 231: 2275-2285

Lalouette A, Lablack A, Guenet JL, Montagutelli X, Segretain D (1996) Male sterility caused by sperm cell-specific structural abnormalities in ebouriffé, a new mutation of the house mouse. *Biol Reprod* 55: 355-363

Lang F, Busch GL, Ritter M, Völkl H, Waldegger S, Gulbins E, Häussinger D (1998) Functional significance of cell volume regulatory mechanisms. *Physiol Rev* 78: 247-306

Lang F, Hoffmann EK (2012) Role of ion transport in control of apoptotic cell death. *Compr Physiol* 2: 2037-2061

Langlois S, Xiang X, Young K, Cowan BJ, Penuela S, Cowan KN (2014) Pannexin 1 and pannexin 3 channels regulate skeletal muscle myoblast proliferation and differentiation. *J Biol Chem* 289: 30717-30731

Lee CC, Freinkman E, Sabatini DM, Ploegh HL (2014) The protein synthesis inhibitor blasticidin s enters mammalian cells via leucine-rich repeat-containing protein 8D. *J Biol Chem* 289: 17124-17131

Lee KH, Park JY, Kim K (2004) NMDA receptor-mediated calcium influx plays an essential role in myoblast fusion. *FEBS Lett* 578: 47-52

Lee VR, Barr KJ, Kelly JJ, Johnston D, Brown CFC, Robb KP, Sayedyahossein S, Huang K, Gros R, Flynn LE *et al* (2018) Pannexin 1 regulates adipose stromal cell differentiation and fat accumulation. *Sci Rep* 8: 16166

Lemonnier L, Prevarskaya N, Shuba Y, Vanden Abeele F, Nilius B, Mazurier J, Skryma R (2002) Ca^{2+} modulation of volume-regulated anion channels: evidence for colocalization with store-operated channels. *FASEB J* 16: 222-224

Levin M, Pezzulo G, Finkelstein JM (2017) Endogenous Bioelectric Signaling Networks: Exploiting Voltage Gradients for Control of Growth and Form. *Annu Rev Biomed Eng* 19: 353-387

Li F, Yin J, Yue T, Liu L, Zhang H (2010) The CLIC5 (chloride intracellular channel 5) involved in C2C12 myoblasts proliferation and differentiation. *Cell Biol Int* 34: 379-384

Li T, Finch EA, Graham V, Zhang ZS, Ding JD, Burch J, Oh-hora M, Rosenberg P (2012) STIM1-Ca^{2+} signaling is required for the hypertrophic growth of skeletal muscle in mice. *Mol Cell Biol* 32: 3009-3017

Liang W, Huang L, Zhao D, He JZ, Sharma P, Liu J, Gramolini AO, Ward ME, Cho HC, Backx PH (2014) Swelling-activated Cl^- currents and intracellular CLC-3 are involved in proliferation of human pulmonary artery smooth muscle cells. *J Hypertens* 32: 318-330

Liem LK, Simard JM, Song Y, Tewari K (1995) The patch clamp technique. *Neurosurgery* 36: 382-392

Liu HT, Akita T, Shimizu T, Sabirov RZ, Okada Y (2009) Bradykinin-induced astrocyte-neuron signalling: glutamate release is mediated by ROS-activated volume-sensitive outwardly rectifying anion channels. *J Physiol* 587: 2197-2209

Liu JH, Bijlenga P, Fischer-Lougheed J, Occhiodoro T, Kaelin A, Bader CR, Bernheim L (1998) Role of an inward rectifier K^+ current and of hyperpolarization in human myoblast fusion. *J Physiol* 510 (Pt 2): 467-476

Liu JH, König S, Michel M, Arnaudeau S, Fischer-Lougheed J, Bader CR, Bernheim L (2003) Acceleration of human myoblast fusion by depolarization: graded Ca^{2+} signals involved. *Development* 130: 3437-3446

Liu T, Stauber T (2019) The Volume-Regulated Anion Channel LRRC8/VRAC Is Dispensable for Cell Proliferation and Migration. *Int J Mol Sci* 20

López JJ, Salido GM, Pariente JA, Rosado JA (2006) Interaction of STIM1 with endogenously expressed human canonical TRP1 upon depletion of intracellular Ca^{2+} stores. *J Biol Chem* 281: 28254-28264

Louis M, Zanou N, Van Schoor M, Gailly P (2008) TRPC1 regulates skeletal myoblast migration and differentiation. *J Cell Sci* 121: 3951-3959

Lu P, Ding Q, Li X, Ji X, Li L, Fan Y, Xia Y, Tian D, Liu M (2019) SWELL1 promotes cell growth and metastasis of hepatocellular carcinoma in vitro and in vivo. *EBioMedicine* 48: 100-116

Lück JC, Puchkov D, Ullrich F, Jentsch TJ (2018) LRRC8/VRAC anion channels are required for late stages of spermatid development in mice. *J Biol Chem* 293: 11796-11808

Luik RM, Wu MM, Buchanan J, Lewis RS (2006) The elementary unit of store-operated Ca^{2+} entry: local activation of CRAC channels by STIM1 at ER-plasma membrane junctions. *J Cell Biol* 174: 815-825

Lutter D, Ullrich F, Lueck JC, Kempa S, Jentsch TJ (2017) Selective transport of neurotransmitters and modulators by distinct volume-regulated LRRC8 anion channels. *J Cell Sci* 130: 1122-1133

Lv J, Liang Y, Zhang S, Lan Q, Xu Z, Wu X, Kang L, Ren J, Cao Y, Wu T *et al* (2019) DCPIB, an Inhibitor of Volume-Regulated Anion Channels, Distinctly Modulates K2P Channels. *ACS Chem Neurosci* 10: 2786-2793

Mandai S, Furukawa S, Kodaka M, Hata Y, Mori T, Nomura N, Ando F, Mori Y, Takahashi D, Yoshizaki Y *et al* (2017) Loop diuretics affect skeletal myoblast differentiation and exercise-induced muscle hypertrophy. *Sci Rep* 7: 46369

Martella E, Bellotti C, Dozza B, Perrone S, Donati D, Lucarelli E (2014) Secreted adiponectin

as a marker to evaluate in vitro the adipogenic differentiation of human mesenchymal stromal cells. *Cytotherapy* 16: 1476-1485

Meacci E, Bini F, Sassoli C, Martinesi M, Squecco R, Chellini F, Zecchi-Orlandini S, Francini F, Formigli L (2010) Functional interaction between TRPC1 channel and connexin-43 protein: a novel pathway underlying S1P action on skeletal myogenesis. *Cell Mol Life Sci* 67: 4269-4285

Meola G, Cardani R (2015) Myotonic dystrophies: An update on clinical aspects, genetic, pathology, and molecular pathomechanisms. *Biochim Biophys Acta* 1852: 594-606

Michalski K, Kawate T (2016) Carbenoxolone inhibits Pannexin1 channels through interactions in the first extracellular loop. *J Gen Physiol* 147: 165-174

Millay DP, O'Rourke JR, Sutherland LB, Bezprozvannaya S, Shelton JM, Bassel-Duby R, Olson EN (2013) Myomaker is a membrane activator of myoblast fusion and muscle formation. *Nature* 499: 301-305

Miranda P, Contreras JE, Plested AJ, Sigworth FJ, Holmgren M, Giraldez T (2013) State-dependent FRET reports calcium- and voltage-dependent gating-ring motions in BK channels. *Proc Natl Acad Sci USA* 110: 5217-5222

Model MA (2018) Methods for cell volume measurement. *Cytometry A* 93: 281-296

Mongin AA (2016) Volume-regulated anion channel--a frenemy within the brain. *Pflügers Arch* 468: 421-441

Mongin AA, Orlov SN (2001) Mechanisms of cell volume regulation and possible nature of the cell volume sensor. *Pathophysiology* 8: 77-88

Nakanishi K, Kakiguchi K, Yonemura S, Nakano A, Morishima N (2015) Transient Ca^{2+} depletion from the endoplasmic reticulum is critical for skeletal myoblast differentiation. *FASEB J* 29: 2137-2149

Neveux I, Doe J, Leblanc N, Valencik ML (2010) Influence of the extracellular matrix and integrins on volume-sensitive osmolyte anion channels in C2C12 myoblasts. *Am J Physiol Cell Physiol* 298: C1006-1017

Nilius B, Droogmans G (2001) Ion channels and their functional role in vascular endothelium. *Physiol Rev* 81: 1415-1459

Nilius B, Eggermont J, Voets T, Buyse G, Manolopoulos V, Droogmans G (1997) Properties of volume-regulated anion channels in mammalian cells. *Prog Biophys Mol Biol* 68: 69-119

Nilius B, Sehrer J, Viana F, De Greef C, Raeymaekers L, Eggermont J, Droogmans G (1994) Volume-activated Cl^- currents in different mammalian non-excitable cell types. *Pflügers Arch* 428: 364-371

Obi S, Nakajima T, Hasegawa T, Nakamura F, Sakuma M, Toyoda S, Tei C, Inoue T (2019) Heat induces myogenic transcription factors of myoblast cells via transient receptor potential vanilloid 1 (Trpv1). *FEBS Open Bio* 9: 101-113

Okada Y (1997) Volume expansion-sensing outward-rectifier Cl^- channel: fresh start to the molecular identity and volume sensor. *Am J Physiol* 273: C755-789

Okada Y, Okada T, Sato-Numata K, Islam MR, Ando-Akatsuka Y, Numata T, Kubo M, Shimizu T, Kurbannazarova RS, Marunaka Y *et al* (2019) Cell Volume-Activated and Volume-Correlated Anion Channels in Mammalian Cells: Their Biophysical, Molecular, and

Pharmacological Properties. *Pharmacol Rev* 71: 49-88

Okada Y, Sato K, Numata T (2009) Pathophysiology and puzzles of the volume-sensitive outwardly rectifying anion channel. *J Physiol* 587: 2141-2149

Okada Y, Shimizu T, Maeno E, Tanabe S, Wang X, Takahashi N (2006) Volume-sensitive chloride channels involved in apoptotic volume decrease and cell death. *J Membr Biol* 209: 21-29

Orre LM, Vesterlund M, Pan Y, Arslan T, Zhu Y, Fernandez Woodbridge A, Frings O, Fredlund E, Lehtiö J (2019) SubCellBarCode: Proteome-wide Mapping of Protein Localization and Relocalization. *Mol Cell* 73: 166-182.e167

Osei-Owusu J, Yang J, Vitery MDC, Qiu Z (2018) Molecular Biology and Physiology of Volume-Regulated Anion Channel (VRAC). *Curr Top Membr* 81: 177-203

Pedersen SF, Klausen TK, Nilius B (2015) The identification of a volume-regulated anion channel: an amazing Odyssey. *Acta physiol* 213: 868-881

Pedersen SF, Okada Y, Nilius B (2016) Biophysics and Physiology of the Volume-Regulated Anion Channel (VRAC)/Volume-Sensitive Outwardly Rectifying Anion Channel (VSOR). *Pflügers Arch* 468: 371-383

Pederson BA, Nordlie MA, Foster JD, Nordlie RC (1998) Effects of ionic strength and chloride ion on activities of the glucose-6-phosphatase system: regulation of the biosynthetic activity of glucose-6-phosphatase by chloride ion inhibition/deinhibition. *Arch Biochem Biophys* 353: 141-151

Petrunkina AM, Harrison RA, Ekhlasi-Hundrieser M, Töpfer-Petersen E (2004) Role of volume-stimulated osmolyte and anion channels in volume regulation by mammalian sperm. *Mol Hum Reprod* 10: 815-823

Piala AT, Moon TM, Akella R, He H, Cobb MH, Goldsmith EJ (2014) Chloride sensing by WNK1 involves inhibition of autophosphorylation. *Sci Signal* 7: ra41

Pietrangelo T, Fioretti B, Mancinelli R, Catacuzzeno L, Franciolini F, Fanò G, Fulle S (2006) Extracellular guanosine-5'-triphosphate modulates myogenesis via intermediate Ca^{2+}-activated K^+ currents in C2C12 mouse cells. *J Physiol* 572: 721-733

Pilas B, Durack G (1997) A flow cytometric method for measurement of intracellular chloride concentration in lymphocytes using the halide-specific probe 6-methoxy-N-(3-sulfopropyl) quinolinium (SPQ). *Cytometry* 28: 316-322

Planells-Cases R, Lutter D, Guyader C, Gerhards NM, Ullrich F, Elger DA, Kucukosmanoglu A, Xu G, Voss FK, Reincke SM *et al* (2015) Subunit composition of VRAC channels determines substrate specificity and cellular resistance to Pt-based anti-cancer drugs. *EMBO J* 34: 2993-3008

Platt CD, Chou J, Houlihan P, Badran YR, Kumar L, Bainter W, Poliani PL, Perez CJ, Dent SYR, Clapham DE *et al* (2017) Leucine-rich repeat containing 8A (LRRC8A)-dependent volume-regulated anion channel activity is dispensable for T-cell development and function. *J Allergy Clin Immunol* 140: 1651-1659.e1651

Porter GA, Jr., Makuck RF, Rivkees SA (2002) Reduction in intracellular calcium levels inhibits myoblast differentiation. *J Biol Chem* 277: 28942-28947

Przybylski RJ, MacBride RG, Kirby AC (1989) Calcium regulation of skeletal myogenesis. I.

Cell content critical to myotube formation. *In Vitro Cell Dev Biol* 25: 830-838

Przybylski RJ, Szigeti V, Davidheiser S, Kirby AC (1994) Calcium regulation of skeletal myogenesis. II. Extracellular and cell surface effects. *Cell Calcium* 15: 132-142

Qiu Z, Dubin AE, Mathur J, Tu B, Reddy K, Miraglia LJ, Reinhardt J, Orth AP, Patapoutian A (2014) SWELL1, a plasma membrane protein, is an essential component of volume-regulated anion channel. *Cell* 157: 447-458

Quinn ME, Goh Q, Kurosaka M, Gamage DG, Petrany MJ, Prasad V, Millay DP (2017) Myomerger induces fusion of non-fusogenic cells and is required for skeletal muscle development. *Nat Commun* 8: 15665

Rauch C, Brunet AC, Deleule J, Farge E (2002) C2C12 myoblast/osteoblast transdifferentiation steps enhanced by epigenetic inhibition of BMP2 endocytosis. *Am J Physiol Cell Physiol* 283: C235-243

Rorsman P, Braun M (2013) Regulation of insulin secretion in human pancreatic islets. *Annu Rev Physiol* 75: 155-179

Rubino S, Bach MD, Schober AL, Lambert IH, Mongin AA (2018) Downregulation of Leucine-Rich Repeat-Containing 8A Limits Proliferation and Increases Sensitivity of Glioblastoma to Temozolomide and Carmustine. *Front Oncol* 8: 142

Rudkouskaya A, Chernoguz A, Haskew-Layton RE, Mongin AA (2008) Two conventional protein kinase C isoforms, alpha and beta I, are involved in the ATP-induced activation of volume-regulated anion channel and glutamate release in cultured astrocytes. *J Neurochem* 105: 2260-2270

Sabirov RZ, Prenen J, Tomita T, Droogmans G, Nilius B (2000) Reduction of ionic strength activates single volume-regulated anion channels (VRAC) in endothelial cells. *Pflügers Arch* 439: 315-320

Sacco S, Giuliano S, Sacconi S, Desnuelle C, Barhanin J, Amri EZ, Bendahhou S (2015) The inward rectifier potassium channel Kir2.1 is required for osteoblastogenesis. *Hum Mol Genet* 24: 471-479

Sampath SC, Sampath SC, Millay DP (2018) Myoblast fusion confusion: the resolution begins. *Skeletal muscle* 8: 3

Sandri M (2008) Signaling in muscle atrophy and hypertrophy. *Physiology* 23: 160-170

Sato-Numata K, Numata T, Inoue R, Okada Y (2016) Distinct pharmacological and molecular properties of the acid-sensitive outwardly rectifying (ASOR) anion channel from those of the volume-sensitive outwardly rectifying (VSOR) anion channel. *Pflügers Arch* 468: 795-803

Sawada A, Takihara Y, Kim JY, Matsuda-Hashii Y, Tokimasa S, Fujisaki H, Kubota K, Endo H, Onodera T, Ohta H *et al* (2003) A congenital mutation of the novel gene LRRC8 causes agammaglobulinemia in humans. *J Clin Invest* 112: 1707-1713

Schiaffino S, Dyar KA, Ciciliot S, Blaauw B, Sandri M (2013) Mechanisms regulating skeletal muscle growth and atrophy. *FEBS J* 280: 4294-4314

Schindelin J, Arganda-Carreras I, Frise E, Kaynig V, Longair M, Pietzsch T, Preibisch S, Rueden C, Saalfeld S, Schmid B *et al* (2012) Fiji: an open-source platform for biological-image analysis. *Nat Methods* 9: 676-682

Schober AL, Wilson CS, Mongin AA (2017) Molecular composition and heterogeneity of the LRRC8-containing swelling-activated osmolyte channels in primary rat astrocytes. *J Physiol* 595: 6939-6951

Schwab A, Fabian A, Hanley PJ, Stock C (2012) Role of ion channels and transporters in cell migration. *Physiol Rev* 92: 1865-1913

Seigneurin-Venin S, Parrish E, Marty I, Rieger F, Romey G, Villaz M, Garcia L (1996) Involvement of the dihydropyridine receptor and internal Ca^{2+} stores in myoblast fusion. *Exp Cell Res* 223: 301-307

Sekar RB, Periasamy A (2003) Fluorescence resonance energy transfer (FRET) microscopy imaging of live cell protein localizations. *J Cell Biol* 160: 629-633

Shimizu T, Numata T, Okada Y (2004) A role of reactive oxygen species in apoptotic activation of volume-sensitive Cl^- channel. *Proc Natl Acad Sci USA* 101: 6770-6773

Sirianant L, Wanitchakool P, Ousingsawat J, Benedetto R, Zormpa A, Cabrita I, Schreiber R, Kunzelmann K (2016) Non-essential contribution of LRRC8A to volume regulation. *Pflügers Arch* 468: 805-816

Spangenburg EE, Bowles DK, Booth FW (2004) Insulin-like growth factor-induced transcriptional activity of the skeletal alpha-actin gene is regulated by signaling mechanisms linked to voltage-gated calcium channels during myoblast differentiation. *Endocrinology* 145: 2054-2063

Stanford CM, Jacobson PA, Eanes ED, Lembke LA, Midura RJ (1995) Rapidly forming apatitic mineral in an osteoblastic cell line (UMR 106-01 BSP). *J Biol Chem* 270: 9420-9428

Stauber T (2015) The volume-regulated anion channel is formed by LRRC8 heteromers - molecular identification and roles in membrane transport and physiology. *Biol Chem* 396: 975-990

Stauber T, Jentsch TJ (2013) Chloride in vesicular trafficking and function. *Annu Rev Physiol* 75: 453-477

Stiber J, Hawkins A, Zhang ZS, Wang S, Burch J, Graham V, Ward CC, Seth M, Finch E, Malouf N *et al* (2008) STIM1 signalling controls store-operated calcium entry required for development and contractile function in skeletal muscle. *Nat Cell Biol* 10: 688-697

Stiber JA, Rosenberg PB (2011) The role of store-operated calcium influx in skeletal muscle signaling. *Cell Calcium* 49: 341-349

Strange K, Yamada T, Denton JS (2019) A 30-year journey from volume-regulated anion currents to molecular structure of the LRRC8 channel. *J Gen Physiol* 151: 100-117

Stroka KM, Jiang H, Chen SH, Tong Z, Wirtz D, Sun SX, Konstantopoulos K (2014) Water permeation drives tumor cell migration in confined microenvironments. *Cell* 157: 611-623

Stuhlmann T, Planells-Cases R, Jentsch TJ (2018) LRRC8/VRAC anion channels enhance β-cell glucose sensing and insulin secretion. *Nat Commun* 9: 1974

Sundelacruz S, Levin M, Kaplan DL (2008) Membrane potential controls adipogenic and osteogenic differentiation of mesenchymal stem cells. *PloS one* 3: e3737

Sundelacruz S, Levin M, Kaplan DL (2009) Role of membrane potential in the regulation of cell proliferation and differentiation. *Stem Cell Rev and Rep* 5: 231-246

Syeda R, Qiu Z, Dubin AE, Murthy SE, Florendo MN, Mason DE, Mathur J, Cahalan SM,

Peters EC, Montal M *et al* (2016) LRRC8 Proteins Form Volume-Regulated Anion Channels that Sense Ionic Strength. *Cell* 164: 499-511

Tajhya RB, Hu X, Tanner MR, Huq R, Kongchan N, Neilson JR, Rodney GG, Horrigan FT, Timchenko LT, Beeton C (2016) Functional KCa1.1 channels are crucial for regulating the proliferation, migration and differentiation of human primary skeletal myoblasts. *Cell Death and Disease* 7: e2426

Tanaka S, Ono Y, Sakamoto K (2017) DCEBIO facilitates myogenic differentiation via intermediate conductance Ca^{2+} activated K^{+} channel activation in C2C12 myoblasts. *J Pharmacol Sci* 133: 276-279

Tang CY, Chen TY (2011) Physiology and pathophysiology of CLC-1: mechanisms of a chloride channel disease, myotonia. *J Biomed Biotechnol* 2011: 685328

Timchenko NA, Iakova P, Cai ZJ, Smith JR, Timchenko LT (2001) Molecular basis for impaired muscle differentiation in myotonic dystrophy. *Mol Cell Biol* 21: 6927-6938

Tominaga K, Kondo C, Kagata T, Hishida T, Nishizuka M, Imagawa M (2004) The novel gene fad158, having a transmembrane domain and leucine-rich repeat, stimulates adipocyte differentiation. *J Biol Chem* 279: 34840-34848

Tu MK, Levin JB, Hamilton AM, Borodinsky LN (2016) Calcium signaling in skeletal muscle development, maintenance and regeneration. *Cell Calcium* 59: 91-97

Valdivieso Á G, Santa-Coloma TA (2019) The chloride anion as a signalling effector. *Biol Rev Camb Philos Soc* 94: 1839-1856

Varela D, Simon F, Riveros A, Jørgensen F, Stutzin A (2004) NAD(P)H oxidase-derived H_2O_2 signals chloride channel activation in cell volume regulation and cell proliferation. *J Biol Chem* 279: 13301-13304

Vitali I, Fièvre S, Telley L, Oberst P, Bariselli S, Frangeul L, Baumann N, McMahon JJ, Klingler E, Bocchi R *et al* (2018) Progenitor Hyperpolarization Regulates the Sequential Generation of Neuronal Subtypes in the Developing Neocortex. *Cell* 174: 1264-1276.e1215

Voets T, Droogmans G, Raskin G, Eggermont J, Nilius B (1999) Reduced intracellular ionic strength as the initial trigger for activation of endothelial volume-regulated anion channels. *Proc Natl Acad Sci USA* 96: 5298-5303

Voets T, Wei L, De Smet P, Van Driessche W, Eggermont J, Droogmans G, Nilius B (1997) Downregulation of volume-activated Cl^{-} currents during muscle differentiation. *Am J Physiol* 272: C667-674

Voss FK, Ullrich F, Münch J, Lazarow K, Lutter D, Mah N, Andrade-Navarro MA, von Kries JP, Stauber T, Jentsch TJ (2014) Identification of LRRC8 heteromers as an essential component of the volume-regulated anion channel VRAC. *Science* 344: 634-638

Walsh K, Perlman H (1997) Cell cycle exit upon myogenic differentiation. *Curr Opin Genet Dev* 7: 597-602

Wang R, Lu Y, Gunasekar S, Zhang Y, Benson CJ, Chapleau MW, Sah R, Abboud FM (2017) The volume-regulated anion channel (LRRC8) in nodose neurons is sensitive to acidic pH. *JCI insight* 2: e90632

Wedhas N, Klamut HJ, Dogra C, Srivastava AK, Mohan S, Kumar A (2005) Inhibition of

mechanosensitive cation channels inhibits myogenic differentiation by suppressing the expression of myogenic regulatory factors and caspase-3 activity. *FASEB J* 19: 1986-1997

Wei-Lapierre L, Carrell EM, Boncompagni S, Protasi F, Dirksen RT (2013) Orai1-dependent calcium entry promotes skeletal muscle growth and limits fatigue. *Nat Commun* 4: 2805

Wei L, Zhou W, Croissant JD, Johansen FE, Prywes R, Balasubramanyam A, Schwartz RJ (1998) RhoA signaling via serum response factor plays an obligatory role in myogenic differentiation. *J Biol Chem* 273: 30287-30294

Willebrords J, Maes M, Crespo Yanguas S, Vinken M (2017) Inhibitors of connexin and pannexin channels as potential therapeutics. *Pharmacol Ther* 180: 144-160

Wilson CS, Bach MD, Ashkavand Z, Norman KR, Martino N, Adam AP, Mongin AA (2019) Metabolic constraints of swelling-activated glutamate release in astrocytes and their implication for ischemic tissue damage. *J Neurochem* 151: 255-272

Wondergem R, Gong W, Monen SH, Dooley SN, Gonce JL, Conner TD, Houser M, Ecay TW, Ferslew KE (2001) Blocking swelling-activated chloride current inhibits mouse liver cell proliferation. *J Physiol* 532: 661-672

Wong R, Chen W, Zhong X, Rutka JT, Feng ZP, Sun HS (2018) Swelling-induced chloride current in glioblastoma proliferation, migration, and invasion. *J Cell Physiol* 233: 363-370

Woo JS, Cho CH, Kim DH, Lee EH (2010) TRPC3 cation channel plays an important role in proliferation and differentiation of skeletal muscle myoblasts. *Exp Mol Med* 42: 614-627

Wu MM, Buchanan J, Luik RM, Lewis RS (2006) Ca^{2+} store depletion causes STIM1 to accumulate in ER regions closely associated with the plasma membrane. *J Cell Biol* 174: 803-813

Wu X, Yang H, Iserovich P, Fischbarg J, Reinach PS (1997) Regulatory volume decrease by SV40-transformed rabbit corneal epithelial cells requires ryanodine-sensitive Ca^{2+}-induced Ca^{2+} release. *J Membr Biol* 158: 127-136

Xie L, Zhang Y, Gunasekar SK, Mishra A, Cao L, Sah R (2017) Induction of adipose and hepatic SWELL1 expression is required for maintaining systemic insulin-sensitivity in obesity. *Channels* 11: 673-677

Xu P, Lu J, Li Z, Yu X, Chen L, Xu T (2006) Aggregation of STIM1 underneath the plasma membrane induces clustering of Orai1. *Biochem Biophys Res Commun* 350: 969-976

Xu Q, Yu L, Liu L, Cheung CF, Li X, Yee SP, Yang XJ, Wu Z (2002) p38 Mitogen-activated protein kinase-, calcium-calmodulin-dependent protein kinase-, and calcineurin-mediated signaling pathways transcriptionally regulate myogenin expression. *Mol Biol Cell* 13: 1940-1952

Xue Y, Li H, Zhang Y, Han X, Zhang G, Li W, Zhang H, Lin Y, Chen P, Sun X *et al* (2018) Natural and synthetic flavonoids, novel blockers of the volume-regulated anion channels, inhibit endothelial cell proliferation. *Pflügers Arch* 470: 1473-1483

Yang J, Vitery MDC, Chen J, Osei-Owusu J, Chu J, Qiu Z (2019) Glutamate-Releasing SWELL1 Channel in Astrocytes Modulates Synaptic Transmission and Promotes Brain Damage in Stroke. *Neuron* 102: 813-827.e816

Yang M, Brackenbury WJ (2013) Membrane potential and cancer progression. *Front Physiol* 4: 185

Yang SN, Shi Y, Yang G, Li Y, Yu J, Berggren PO (2014) Ionic mechanisms in pancreatic β cell signaling. *Cell Mol Life Sci* 71: 4149-4177

Ye ZC, Oberheim N, Kettenmann H, Ransom BR (2009) Pharmacological "cross-inhibition" of connexin hemichannels and swelling activated anion channels. *Glia* 57: 258-269

Yeung CH, Barfield JP, Cooper TG (2006) Physiological volume regulation by spermatozoa. *Mol Cell Endocrinol* 250: 98-105

Yoon MS (2017) mTOR as a Key Regulator in Maintaining Skeletal Muscle Mass. *Front Physiol* 8: 788

Yuan JP, Zeng W, Huang GN, Worley PF, Muallem S (2007) STIM1 heteromultimerizes TRPC channels to determine their function as store-operated channels. *Nat Cell Biol* 9: 636-645

Zachariassen LG, Katchan L, Jensen AG, Pickering DS, Plested AJ, Kristensen AS (2016) Structural rearrangement of the intracellular domains during AMPA receptor activation. *Proc Natl Acad Sci USA* 113: E3950-3959

Zanou N, Schakman O, Louis P, Ruegg UT, Dietrich A, Birnbaumer L, Gailly P (2012) Trpc1 ion channel modulates phosphatidylinositol 3-kinase/Akt pathway during myoblast differentiation and muscle regeneration. *J Biol Chem* 287: 14524-14534

Zhang H, Deng Z, Zhang D, Li H, Zhang L, Niu J, Zuo W, Fu R, Fan L, Ye JH *et al* (2018) High expression of leucine‐rich repeat‐containing 8A is indicative of a worse outcome of colon cancer patients by enhancing cancer cell growth and metastasis. *Oncol Rep* 40: 1275-1286

Zhang J, Lieberman M (1996) Chloride conductance is activated by membrane distention of cultured chick heart cells. *Cardiovasc Res* 32: 168-179

Zhang Q, Vashisht AA, O'Rourke J, Corbel SY, Moran R, Romero A, Miraglia L, Zhang J, Durrant E, Schmedt C *et al* (2017a) The microprotein Minion controls cell fusion and muscle formation. *Nat Commun* 8: 15664

Zhang Y, Xie L, Gunasekar SK, Tong D, Mishra A, Gibson WJ, Wang C, Fidler T, Marthaler B, Klingelhutz A *et al* (2017b) SWELL1 is a regulator of adipocyte size, insulin signalling and glucose homeostasis. *Nat Cell Biol* 19: 504-517

Zhou C, Chen X, Planells-Cases R, Chu J, Wang L, Cao L, Li Z, López-Cayuqueo KI, Xie Y, Ye S *et al* (2020) Transfer of cGAMP into Bystander Cells via LRRC8 Volume-Regulated Anion Channels Augments STING-Mediated Interferon Responses and Anti-viral Immunity. *Immunity* 52: 767-781.e766

Acknowledgements

First, I would like to thank my supervisor Prof. Dr. Tobias Stauber. Thank you for giving me the opportunity to join your group and for always supporting me in the last four years. I am so lucky to have a helpful and friendly supervisor like you. I want to thank the Guangzhou Elite Project for supporting my living expenses in Germany.

I want to thank Dr. Thorsten M. Becker and Prof. Dr. Ursula Koch for collaborating with us in a very productive way. As well I want to thank Prof. Dr. Sigmar Striker for his generous support in the laboratory and for reviewing my thesis.

I am especially grateful to Dr. Xiaoyan Wei, who has taught me a lot about experimental techniques and muscle development. I would like to thank my trusted “teammate” Tianbao Liu for all the support and fun he has given over the past four years.

I thank my lovely colleagues Dr. Lisa von Kleist, Dr. Antje Buttgereit, Dr. Benjamin König, Sumaira Pervaiz, Shroddha Bose, and Hailan He for all their help, encouragement, and support. I thank all the members of AG Stricker, Knaus, Ewers, and Freund for their help and advice.

A special thank you goes to my boyfriend Mr. Wu. You are always there for me when I need you. I also want to thank my parents for always believing in me. Finally, I thank anyone (family, friends, or strangers) who helped me get here.

Wish you all the best.